

# **Phosphorylation of PLPPR3 membrane proteins as signaling integrator at neuronal synapses**

Inaugural-Dissertation  
to obtain the academic degree  
Doctor rerum naturalium (Dr. rer. nat)

Submitted to the Department of Biology, Chemistry, Pharmacy  
of Freie Universität Berlin

By

CRISTINA KROON

2023

The work presented in this thesis was carried out from July 2018 until June 2023 under the supervision of Prof. Dr. Britta Johanna Eickholt at the Institute of Molecular Biology and Biochemistry at Charité Universitätsmedizin, Berlin.

1<sup>st</sup> reviewer: Prof. Dr. Britta Johanna Eickholt

2<sup>nd</sup> reviewer: Prof. Dr. Helge Ewers

Date of disputation: 16.10.2023

# Acknowledgements

---

The work presented here would not have been possible without the unwavering support of many people. I would like to express my gratitude to all those involved. First and foremost, I thank my supervisor Britta Eickholt for the opportunity to work on this project, and Prof. Dr. Helge Ewers for acting as my second reviewer.

I am extremely grateful to Britta for the opportunity to work in this lab and on this project. Working on PLPPR3 has not always been easy, but it has taught me enormously. Thank you for the excitement you bring into the meetings, and for always reminding us to keep having fun. I have enjoyed doing science and learning about science. It has truly been a privilege to be able to work in such a safe, stable and nice environment. You have provided me opportunities to take part in conferences, scientific exchanges and courses that enabled me to learn, see and experience so much, and I have never taken this for granted. You have distinguished yourself as one of the truly caring supervisors, and I appreciate and admire this.

I thank Patricia and Till for always finding time for scientific questions and discussions. You have both helped me enormously. I thank Joachim for teaching me everything I needed to know, from when I first started the project up until to this moment – I would have been lost without you. I thank my teammate Shannon for always being so positive, supportive and persevering – it has helped me a lot through the years and it has been nice to share this journey with you. I thank our Greek team George and Alex for the amazing scientific collaboration – and two wonderful retreats in Greece – in these past 5 years. I learned a lot from you. I thank Robert for being so helpful and so enthusiastic with my project. Bench time would have been much more dull without our discussions! I have gotten a lot of support from everyone mentioned here, but most importantly, I have had so much fun too!

I thank our technicians Kerstin Schlawe, Kristin Lehmann and Katrin Büttner for keeping the lab running, providing the neurons and cell lines, and cloning. It has been an enormous contribution towards this work. Furthermore, I thank Marieluise Kirchner and Kathrin Textoris-Taube for the mass spectrometry analyses presented in this work. I thank Timothy Zolnik and Niclas Gimber for collaborating with me at the final stages of this project.

Finally, I thank my family and friends – especially Alex, Yaya and Evvi – for providing some balance in the crazy journey towards this degree. Ja minu suurim tänu kuulub sinule, Karel, et hoiad ja toetad mind. Sa aitad luua tasakaalu ja hingerahu, ning ilma sinuta oleks olnud kordades raskem. Aitäh, et oled minu kõrval.

## Declaration of authenticity

---

Herewith I certify that I have prepared and written my thesis independently and that I have not used any sources and aids other than those indicated by me. I have not submitted this thesis in any other examination procedure or at another university.

Berlin, 29.06.2023

Cristina Kroon

# Table of contents

---

Summary

Zusammenfassung

|   |    |
|---|----|
| 1. Introduction .....   | 1  |
| 1.1. Overview of neuronal morphogenesis .....   | 1  |
| 1.2. Neuronal morphogenesis is regulated by cell-intrinsic and extrinsic factors.....                             | 4  |
| 1.3. Filopodia are important precursor structures in neuronal development.....                                    | 6  |
| 1.4. Phospholipid phosphatase-related proteins regulate neuronal morphogenesis by inducing filopodia .....        | 7  |
| 1.5. Cellular signaling regulation by protein phosphorylation .....   | 10 |
| 1.6. Objectives of this thesis.....   | 14 |
| 2. PLPPR3 is a highly phosphorylated protein.....   | 15 |
| 2.1. Prediction tools propose numerous phosphorylation sites in the intracellular domain of PLPPR3.....           | 15 |
| 2.2. The distal C-terminus of PLPPR3 is phosphorylated in dependence of localization to the plasma membrane ..... | 18 |
| 2.3. Setting up PhosTag SDS-PAGE for the analysis of PLPPR3 variants .....  | 19 |
| 2.4. PLPPR3 intracellular domain harbors 26 high-confidence phosphorylation sites....                             | 23 |
| 2.5. Discussion and outlook .....   | 28 |
| 3. PLPPR3 S351 is a PKA phosphorylation site .....  | 31 |
| 3.1. PKA phosphorylates PLPPR3 at S351 .....  | 31 |
| 3.2. Other phosphorylation events in the intracellular domain of PLPPR3.....                                      | 34 |
| 3.3. Discussion and outlook .....   | 35 |
| 4. Generation and validation of PLPPR3 pS351-specific antibody.....   | 38 |
| 4.1. Validation for western blot .....  | 38 |
| 4.2. Validation for immunocytochemistry .....   | 40 |
| 4.3. Validation for immunohistochemistry .....  | 45 |
| 4.4. Discussion and outlook .....   | 46 |
| 5. Functional studies .....   | 47 |

|       |   |    |
|-------|---|----|
| 5.1.  | Phosphorylation of PLPPR3 S351 can be triggered in primary neurons and in acute brain slices..... | 47 |
| 5.2.  | Phosphorylation of S351 does not regulate filopodia or axonal branch formation ...                | 48 |
| 5.3.  | PLPPR3 pS351 mediates its binding to BASP1.....   | 51 |
| 5.4.  | PLPPR3 and BASP1 co-localize in clusters along axons .....  | 54 |
| 5.5.  | PLPPR3 and PLPPR3 pS351 are enriched in synaptosomes.....   | 56 |
| 5.6.  | Discussion and outlook .....  | 57 |
| 6.    | Appendix .....  | 60 |
| 6.1.  | Validation of BASP1 antibodies.....   | 60 |
| 7.    | General discussion.....   | 64 |
| 7.1.  | PLPPR3 is a highly phosphorylated protein.....  | 64 |
| 7.2.  | Possible roles for BASP1-PLPPR3 protein complex at the synapse.....                               | 66 |
| 7.3.  | Do PLPPR3 and BASP1 play a role in synaptic transmission?.....                                    | 71 |
| 7.4.  | Conclusion .....  | 71 |
| 8.    | Materials and methods .....   | 73 |
| 8.1.  | Antibodies .....  | 73 |
| 8.2.  | Animal procedures .....   | 75 |
| 8.3.  | Cell line culturing and transfection.....   | 76 |
| 8.4.  | Primary neuronal culture and transfection .....   | 76 |
| 8.5.  | Acute brain slice preparation .....   | 77 |
| 8.6.  | Cloning.....  | 77 |
| 8.7.  | Treatments: Forskolin, 8-Br-cAMP, H89, PMA, DMSO .....  | 81 |
| 8.8.  | Cell and tissue lysis, total protein concentration measurement.....                               | 81 |
| 8.9.  | Lambda phosphatase treatment.....   | 82 |
| 8.10. | <i>In vitro</i> phosphorylation assay .....   | 82 |
| 8.11. | Co-immunoprecipitation .....  | 83 |
| 8.12. | SDS-PAGE, PhosTag SDS-PAGE and western blotting.....  | 83 |
| 8.13. | Quantification of western blot band intensities.....  | 84 |
| 8.14. | Purification of PLPPR3 ICD constructs.....  | 84 |

|   |     |
|---|-----|
| 8.15. Affinity chromatography to identify binding partners .....          | 85  |
| 8.16. Mass spectrometry analysis .....                                    | 85  |
| 8.17. Immunofluorescent labelling.....                                    | 87  |
| 8.18. Filopodia density measurements.....                                 | 88  |
| 8.19. Axonal branch density measurements.....                             | 88  |
| 8.20. Preparation of crude synaptosomes .....                             | 89  |
| 8.21. Microscopy .....  | 89  |
| 8.22. Prediction of phosphorylation sites and conservation analysis ..... | 90  |
| 8.23. Statistics and data visualization.....                              | 90  |
| 9. References.....  | 91  |
| 10. List of publications .....  | 118 |

## Summary

---

Neuronal branching and synaptogenesis are developmental processes that ensure the complex yet precise connectivity of billions of neurons in the brain. These processes rely on the integration of cell extrinsic and intrinsic factors that determine growth. Phospholipid-phosphatase related protein 3 (PLPPR3) belongs to a family of transmembrane proteins, which are highly expressed in neuronal development and regulate critical growth processes in neurons. Prior work in the lab established a crucial function of PLPPR3 in controlling axon branching through the induction of axonal filopodia. However, at the start of this PhD project, little information was available regarding the signaling events regulating PLPPR3 function.

The work presented here establishes PLPPR3 as a highly phosphorylated protein with unique signaling integration property during neuronal development. I identify 26 high-confidence phosphorylation sites in the intracellular domain of PLPPR3 using mass spectrometry. My experiments show that the phosphorylation state of PLPPR3 is dependent on its proximity to the plasma membrane, as half of these phosphorylation events occur only in a membrane-attached variant of the PLPPR3 intracellular domain (chapter 2). I identify PLPPR3 S351 as a *bona fide* phosphorylation site of protein kinase A (PKA), and provide evidence that the intracellular domain is also a substrate for protein kinase C (PKC) and glycogen synthase kinase 3 (GSK3) (chapter 3). I generated a phospho-specific antibody for PLPPR3 S351 and validated its use in western blot experiments (chapter 4). Phosphorylation levels of S351 mimic the developmentally-regulated expression of PLPPR3, however, my experiments suggest that this phosphorylation event does not regulate filopodia formation, the well-described function of PLPPR3 during early development. Instead, phosphorylation at S351 modulates binding to BASP1, a growth-associated protein implicated in axonal development and regeneration. Characterization of PLPPR3 and BASP1 co-localization indicates their distinct enrichment in presynaptic compartments (chapter 5). Furthermore, this work includes validation data of six BASP1 antibodies (Appendix, chapter 6). Finally, I provide theoretical framework of PLPPR3 phosphorylation-based signal integration, and working models of PLPPR3-BASP1 based synapse formation (chapter 7).

In summary, this doctoral thesis identified phosphorylation events in the intracellular domain of PLPPR3, uncovered a specific PKA-dependent signaling event at S351, and a novel interaction partner of PLPPR3 at neuronal synapses. Taken together, these data expand our knowledge of PLPPR3 in neuronal development.

# Zusammenfassung

---

Neuronale Verzweigung und Synaptogenese sind Entwicklungsprozesse, die die komplexe und dennoch präzise Konnektivität von Milliarden von Neuronen im Gehirn sicherstellen. Diese Entwicklungsprozesse beruhen auf der Integration zellextrinsischer und intrinsischer Faktoren, die das Wachstum bestimmen. Das Phospholipid-Phosphatase-verwandte Protein 3 (PLPPR3) gehört zu einer Familie von Transmembranproteinen, die in der neuronalen Entwicklung stark exprimiert werden und kritische Wachstumsprozesse in Neuronen regulieren. Frühere Arbeiten im Labor haben eine entscheidende Funktion von PLPPR3 bei der Steuerung der Axonverzweigung durch die Induktion axonaler Filopodien nachgewiesen. Zu Beginn dieses Doktoratsprojekts waren jedoch nur wenige Informationen über die Signalmechanismen verfügbar, die die PLPPR3-Funktion regulieren.

Die hier vorgestellte Arbeit etabliert PLPPR3 als hoch phosphoryliertes Protein und schlägt es als Signalintegrator vor. Ich identifiziere mithilfe der Massenspektrometrie 26 hochzuverlässige Phosphorylierungsstellen in der intrazellulären Domäne von PLPPR3. Meine Experimente zeigen, dass der Phosphorylierungszustand von PLPPR3 von seiner Nähe zur Plasmamembran abhängt, da die Hälfte dieser Phosphorylierungsereignisse nur in der membrangebundenen intrazellulären Domäne vorhanden ist (Kapitel 2). Ich identifiziere PLPPR3 S351 als eine Phosphorylierungsstelle der Proteinkinase A (PKA) und liefere den Beweis, dass die intrazelluläre Domäne auch ein Substrat für Proteinkinase C (PKC) und Glykogensynthasekinase 3 (GSK3) ist (Kapitel 3). Ich habe einen phosphospezifischen Antikörper für PLPPR3 S351 generiert und seine Verwendung in western blot Experimenten validiert (Kapitel 4). Die Phosphorylierungsniveaus von S351 ahmen die entwicklungsregulierte Expression von PLPPR3 nach. Meine Experimente legen jedoch nahe, dass dieses Phosphorylierungsereignis nicht die Bildung von Filopodien reguliert, die gut beschriebene Funktion von PLPPR3 während der frühen Entwicklung. Stattdessen moduliert die Phosphorylierung an S351 die Bindung an BASP1, ein wachstumsassoziiertes Protein, das an der Entwicklung und Regeneration von Axonen beteiligt ist. Die Charakterisierung der Co-Lokalisierung von PLPPR3 und BASP1 zeigt deren deutliche Anreicherung in präsynaptischen Kompartimenten (Kapitel 5). Darüber hinaus umfasst diese Arbeit Validierungsdaten von sechs BASP1-Antikörpern (Anhang, Kapitel 6). Abschließend stelle ich einen theoretischen Rahmen für die auf PLPPR3-Phosphorylierung basierende Signalintegration und Arbeitsmodelle für die auf PLPPR3-BASP1 basierende Synapsenbildung bereit (Kapitel 7).

Zusammenfassend identifiziert diese Doktorarbeit Phosphorylierungsereignisse in der intrazellulären Domäne von PLPPR3, deckt ein spezifisches PKA-abhängiges Signalereignis

bei S351 und einen neuen Interaktionspartner von PLPPR3 an neuronalen Synapsen auf. Zusammengenommen erweitern diese Daten unser Wissen über PLPPR3 in der neuronalen Entwicklung.

# 1. Introduction

---

Human brain is an incredibly complex organ. Our neocortex consists of approximately 16 billion neurons, each of which can make thousands to tens of thousands of synapses.<sup>1</sup> Even by the lowest estimate, this brings the total number of synapses in the human neocortex to an astounding 620 trillion.<sup>1</sup> The staggering number of connections enables remarkable cognitive abilities, some of which, such as language, reasoning, planning and inner speech, are considered uniquely human traits.<sup>2</sup>

The smallest functional unit of the nervous system is a neuron. Neurons have specialized in conveying electrical and chemical signals, allowing us to receive and integrate information from the outside world, and respond to it by executing voluntary movements. The electrical activity of neurons is supported by their polarized shape with physiologically distinct compartments: a soma surrounded by numerous dendrites and a single axon.<sup>3</sup> The polarized shape determines unidirectional flow of signals: from dendrites, which receive and integrate input, to the axon that relays signal to other cells.

Orchestrating the development of a brain which consists of billions of neurons making trillions of connections is a daunting task. To achieve this, cells have evolved elaborate control mechanisms at single cell and population levels.

## 1.1. Overview of neuronal morphogenesis

During corticogenesis, glutamatergic neurons migrate from the place they are born in the ventricular zone to their final position in the cerebral cortex. Cortical development proceeds in an inside-out fashion: neurons destined to populate the deeper layers are born first, while neurons that come to populate the uppermost layer are generated last.<sup>4-6</sup> Younger neurons migrate past earlier born neurons, thus generating the laminar structure of the cortex.<sup>7</sup> During this migration, neurons undergo polarization: the leading processes, oriented towards the cortical plate, specify into dendrites, while the trailing process is destined to become the axon.<sup>8,9</sup> Once they have reached their final position in the cortex, both dendrites and axons undergo branching and establish synapses.<sup>10-14</sup>

Cell culture has been a useful model to study neuronal morphogenesis, because dissociated primary neurons undergo similar stages of development in a cell culture dish that are comparable to those seen *in vivo* (Figure 1).<sup>15,16</sup> Upon plating, neurons initially form lamellipodia and filopodia around the cell body, which constitutes stage 1 of neuronal morphogenesis. In the second stage of development, approximately 1-1.5 days *in vitro*, neurons extend immature neurites. At stage three, typically after 2 days *in vitro*, neurons “break the symmetry” and become polarized: one of the minor processes grows rapidly and forms the

axon. In the fourth stage of development, from around four days *in vitro* onwards, the other small processes around the cell body develop into dendrites, and both the axon and dendrites arborize. Finally, at around two weeks in culture, neurons have established complex connectivity with mature synapses.

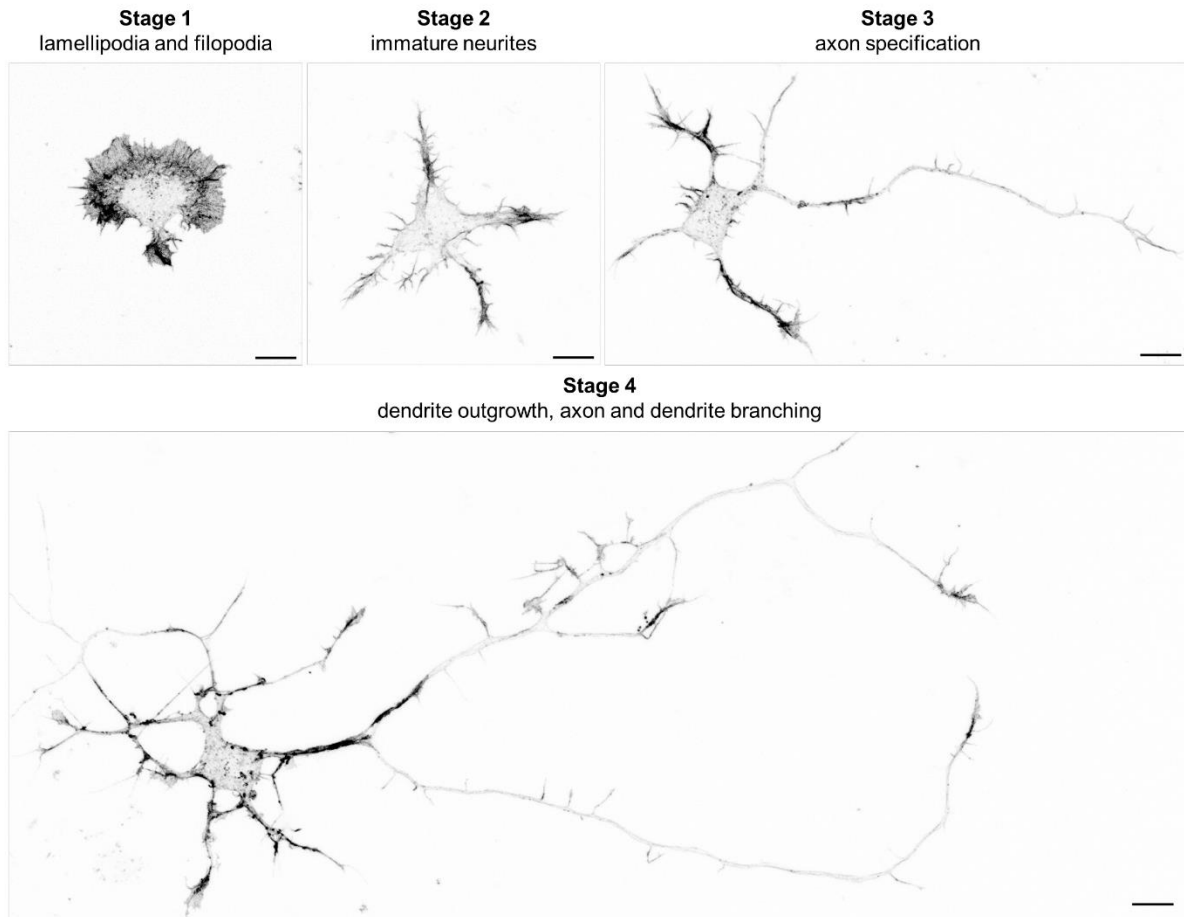


*Figure 1. Morphogenesis of primary neurons in vitro follows through a similar program as neurons in vivo. Shortly after plating the neurons form lamellipodia and filopodia around the cell body. In stage 2 of development they begin to extend multiple immature neurites. Stage 3 is defined by axon specification: the neurons establish polarity as one neurite undergoes growth spurt and becomes the axon. In stage 4 the dendrites start to develop and both dendrites and the axon arborize. Developmental stages adapted from Dotti et al. (1988) and Polleux & Snider (2010). Scale bar 10  $\mu$ m.*

In order to achieve the intricate connectivity with trillions of synapses, both dendrites and the axon branch extensively. Branching significantly increases the complexity of the information that can be processed by a single neuron: dendritic branches mediate the convergence of signals from different inputs, while axonal branches allow for the divergence of information into multiple brain areas. As the majority of synapses are located on axon and dendrite branches, total surface area of arbors is intricately connected with reception, integration, and transmission of information.<sup>17</sup> Branching is not a random process - neurons exert tight regulation over when and where to branch in order to make connections with their correct

targets, and in executing these behaviors, axons and dendrites face unique decisions. Dendrites typically arborize within one cortical layer or column, close to the cell body, in order to integrate signals from multiple inputs.<sup>18</sup> In contrast, axons use multiple modes of branching.<sup>19</sup> Similar to dendrites, axons use terminal branching to innervate multiple targets once they have reached their target area. Some axons branch only once, by bifurcation, generating two daughter branches that grow away from each other as seen in the central sensory projections in the spinal cord.<sup>20</sup> However, by far the most common mode of branching for axons is collateral or interstitial branching, where the axons branch far away from the nerve terminals and project to areas different from the main axon.<sup>21</sup> Thus, both axons and axonal branches have to grow long distances and find their correct targets in the brain. Therefore, axonal growth and branching are tightly coupled to navigation through extracellular space, called axon guidance.

Axon guidance relies on the specialized structures, growth cones, at the tip of elongating axons and branches.<sup>22</sup> Growth cones sense the surrounding environment and use extracellular cues to navigate to their correct targets.<sup>23</sup> As axons reach their intended targets, they make synapses. In fact, axon guidance and synaptogenesis share common mechanisms.<sup>24</sup> Axon pathfinding relies on extracellular cues that activate cell surface receptors, leading to activation of intracellular signaling pathways that order the growth cone to move towards or away from the cue. Similarly, interaction between an axon and another cell triggers the formation of synapses. Furthermore, both rely on dynamic structures called filopodia that probe the surrounding space in their decision-making. Finally, there are guidance molecules that govern both axon pathfinding and synapse formation. Perhaps not surprisingly, synapse formation in turn, is tightly coupled to axonal branching: new branches preferentially form near mature synapses and new synapses preferentially form on new branches. Conversely, mature synapses retain branches, while immature synapses lead to branch retraction.<sup>19</sup>

Axons are guided to their correct targets by extracellular cues. The best-studied guidance cue-receptor pairs include ephrins with their EPH receptors,<sup>25</sup> semaphorins with their plexin and neuropilin receptors,<sup>26,27</sup> slits and ROBO receptors,<sup>28</sup> and netrins with their DCC, UNC5 and neogenin receptors.<sup>29</sup> In majority of studied *in vivo* settings, ephrin-EPH, semaphorin-plexin and slit-ROBO pairs mediate repulsion, while netrin can mediate attraction via DCC and neogenin receptor, and repulsion via UNC5 receptor.<sup>30</sup> Beyond guidance cues, classical morphogens, such as Sonic Hedgehog,<sup>31</sup> WNT<sup>32</sup> and BMP have been shown to regulate axon guidance using signaling pathways that differ from their canonical morphogenetic functions.<sup>33</sup> Finally, growth factors, such as FGF, VEGF, BDNF and others guide axons during neuronal development.<sup>34-36</sup>

It has been proposed that many chemotropic molecules that regulate growth cone guidance also regulate branch formation.<sup>37</sup> Indeed, known guidance cues such as Netrin-1, ephrins, semaphorins or Slit proteins have been shown to regulate neuronal branching.<sup>38,39</sup> Axonal and dendritic branching is regulated by neurotropic factors such as BDNF<sup>40,41</sup> and NGF.<sup>42</sup> Furthermore, branching is influenced by neuronal activity.<sup>43</sup> Dendrites have been shown to preferentially grow into regions with available presynaptic elements.<sup>44</sup> Increasing overall neuronal activity directly promotes axonal branching while silencing neuronal activity suppresses it.<sup>45</sup> Neuronal activity can also indirectly affect branching, as evidenced by seizure-mediated changes in Neuritin gene expression, which mediates axon branch formation.<sup>46</sup> Finally, adhesion to other cells or the extracellular matrix can promote or inhibit neurite branching.<sup>47-55</sup>

Evidently, strict control of branching morphogenesis is essential to establish appropriate circuitry and failure to do so leads to various disorders. Autism spectrum disorder, Rett syndrome, schizophrenia and Down syndrome are all characterized by decreased dendritic branching at the cellular level.<sup>56</sup> Excessive axonal branching has been identified in autism spectrum disorder and epilepsy.<sup>57-61</sup> Aberrant axonal branching is also involved in pathophysiology of amyotrophic lateral sclerosis.<sup>62</sup> Therefore, understanding regulation of neuronal branching will deepen our knowledge of the development and etiology of these disorders. Finally, in cases of neurological injury, loss of function is often caused by disruption of axonal connectivity. Advancing our understanding of axonal growth programs will aid in developing effective treatment strategies to restore connectivity.

## **1.2. Neuronal morphogenesis is regulated by cell-intrinsic and extrinsic factors**

Neuronal morphogenesis is determined by cell intrinsic and cell extrinsic factors. All cells have an intrinsic capacity to grow, driven by developmentally regulated gene expression and growth-related signaling pathways. This intrinsic potential for growth is modulated by extracellular factors that lead to asymmetrical activation of growth-related signaling pathways and thereby guide the direction of growth. While gradients of extracellular cues are indispensable for achieving the correct connectivity in the brain, neurons are nevertheless able to polarize, branch and make synapses in cell culture models where extracellular factors are distributed uniformly or missing entirely. Thus, primary neuronal culture models have significantly advanced our understanding of cell-intrinsic growth.

The central player in cell-intrinsic growth signaling is the phosphoinositide 3-kinase (PI3K), which controls various aspects of neuronal morphogenesis, such as axon specification, elongation and branching.<sup>63-65</sup> During axon specification one of the multiple small neurites

breaks the symmetry of an immature neuron by undergoing a rapid growth spurt (see Figure 1). This polarization is enabled by asymmetric localization of PI3K to the neurite destined to become the axon, where a local accumulation of phosphatidylinositol 3,4,5-trisphosphate (PIP<sub>3</sub>) ensues through phosphorylation of phosphatidylinositol 4,5-bisphosphate (PIP<sub>2</sub>). The second messenger PIP<sub>3</sub> activates two pathways leading to axon specification. Through triggering the subsequent phosphorylations of kinases AKT and GSK3β, it leads to microtubule polymerization and axon outgrowth via effectors such as TAU, CRMP-2 and MAP1B.<sup>66–68</sup> Axon elongation has been shown to utilize the same signaling pathway via GSK3β to effectors CRMP-2 and APC.<sup>67,69</sup> Alternatively, locally accumulated PIP<sub>3</sub> activates the CDC42-RAP1B-PAR complex-RAC1 positive feedback loop which controls axon formation through actin filaments and actin-binding proteins.<sup>70</sup> Localized PI3K activity also controls filopodia formation<sup>42</sup> and axon branch formation.<sup>65</sup>

Another well-established second messenger in axon morphogenesis is the cyclic adenosine monophosphate, or cAMP. During early development, cAMP accumulates in one of the neurites of an unpolarized neuron, where it acts as an early signal for axon specification.<sup>71</sup> At the same time, there is a local accumulation of cyclic guanosine monophosphate (cGMP) in the other neurites, which suppresses these from becoming the axon. Intriguingly, increase of cAMP leads to decrease of cGMP within one neurite, and vice versa, providing a mechanism of how neurons form only a single axon and multiple dendrites. Accumulation of cAMP activates protein kinase A (PKA), which triggers a series of downstream signaling events that ultimately converge on microtubule-associated proteins that support neurite elongation.<sup>71</sup> Another downstream effector of cAMP is the guanine-nucleotide-exchange factor EPAC, which can activate RAP1B and thus provides a complementary cAMP-dependent pathway to axon formation.<sup>72</sup> Beyond axon specification, PKA and EPAC control distinct aspects of axonal morphogenesis which is regulated by temporal cAMP dynamics: short-term intracellular elevation of cAMP leads to axonal branching via PKA, while long-term elevation of cAMP leads to axon elongation via EPAC.<sup>73</sup>

Intracellular growth pathways are stimulated by extracellular cues. Gradients of chemotropic or neurotropic factors trigger asymmetric activation of intracellular signaling and thereby guide directed growth. The PI3K signaling pathway controlling axon morphogenesis is activated by neurotrophins nerve growth factor (NGF), brain derived neurotrophic factor (BDNF) and neurotrophin 3 (NT-3),<sup>67,69,74,75</sup> and insulin like growth factor (IGF).<sup>76–80</sup> BDNF also activates cAMP signaling in axonal development.<sup>81</sup> Another well-established activator of cAMP is the guidance molecule netrin-1.<sup>29</sup>

### 1.3. Filopodia are important precursor structures in neuronal development

Neuronal processes are assembled from their dynamic structural elements, together known as the cytoskeleton. The cytoskeleton is composed of intermediate filaments, filamentous actin and microtubules, which undergo reorganization in response to extracellular and intracellular cues. The rearrangement of the cytoskeleton is primarily orchestrated by actin-binding and microtubule-associated proteins, as well as proteins that cross-link actin to microtubules. Dynamic changes in the cytoskeleton provide the protrusive activity required to establish the polarized shape of neurons.

Filopodia are important precursor structures in neuronal development. They are small, finger-like F-actin based protrusions that appear early in non-polarized neurons (see Figure 1), where they regulate numerous aspects of neuronal development, such as early differentiation, migration and synapse formation.<sup>82</sup> This variety of functions is achieved by different types of filopodial dynamics. On the one hand, transient filopodia serve as exploratory sensors that aid in decision making, such as in growth cone pathfinding. On the other hand, stabilization of selected filopodia leads to the formation of neuronal processes, such as neurites,<sup>83,84</sup> axonal and dendritic branches<sup>85-88</sup> and dendritic spines.<sup>89</sup> Therefore, filopodia are absolutely essential for neuronal morphogenesis.

Because of their significance, for decades people have tried to understand how filopodia formation is regulated. Filopodia formation is driven by polymerization of actin, which is mediated by actin-binding proteins and controlled by signaling proteins small GTPases. The Rho GTPases CDC42 and RIF are established regulators of filopodia formation, which control distinct pathways.<sup>90-92</sup> CDC42 generates filopodia through interaction with WASP/N-WASP, which leads to the recruitment and activation of the actin nucleator ARP2/3. Activated ARP2/3 generates a branched actin network, which can be reorganized to generate bundled actin to form filopodia.<sup>93</sup> Alternatively, by activating formin mDIA2, CDC42 can directly induce the formation of straight actin filaments.<sup>94</sup> Finally, CDC42 can induce filopodia through forming a complex with the adaptor protein IRSp53 and the anti-capping protein MENA, initiating actin filament assembly.<sup>95</sup> The Rho GTPase RIF utilizes a pathway independent of the abovementioned effectors, and instead recruits mDIA1 to induce filopodia.<sup>96</sup>

The transformation of dynamic filopodia into stable neurites or branches requires invasion by microtubules. It has been shown that both dynamic and stable microtubules are able to form neurites, either by directly polymerizing into filopodia<sup>83</sup> or by translocation of the preassembled microtubules.<sup>97</sup> Microtubule-associated proteins, such as MAP1B, MAP2 and TAU, which polymerize and stabilize microtubules, are necessary for the outgrowth and elongation of neurites and the axon.<sup>98</sup> Proteins that can bind both actin and microtubules, such as MAP2,

drebrin and others, provide a link between the two essential components of the cytoskeleton for neurite growth.<sup>98</sup>

#### **1.4. Phospholipid phosphatase-related proteins regulate neuronal morphogenesis by inducing filopodia**

Phospholipid phosphatase-related proteins (PLPPRs, previously also known as plasticity related genes or PRGs) are a unique family of five proteins associated with filopodia formation.<sup>99</sup> All PLPPRs share highly conserved six transmembrane domains and much less conserved intracellular domains of different lengths (Figure 2). They share this topology with phospholipid phosphatases (PLPPs), their evolutionary cousins, which dephosphorylate bioactive lipids such as LPA (Figure 2A).<sup>100</sup> However, PLPPRs have not retained the enzymatic ability due to mutations in the respective catalytic residues (Figure 2B).<sup>99,101</sup> Instead, PLPPRs have evolved into a distinct family of proteins.

The best studied function of PLPPRs is filopodia formation. With the exception of the less-studied PLPPR2, all PLPPRs induce filopodia formation in non-neuronal cells as well as primary neurons.<sup>99</sup> Through filopodia induction, PLPPRs play a role in dendrite and axon branching as well as dendritic spine formation.<sup>88,103–105</sup> The molecular mechanism of PLPPR-based filopodia formation is not clear, however, current evidence suggests that PLPPRs do not utilize the classical small GTPase signaling pathways – CDC42, RIF and their downstream effectors – to make filopodia.<sup>99</sup> Some evidence supports the possibility that PLPPRs may sequester and stabilize membrane phosphoinositides. We have recently shown that PLPPR3, previously also known as PRG2, directly interacts with the phosphatase PTEN and inhibits its activity.<sup>88</sup> We demonstrated that PLPPR3 localizes in nanoclusters along the axonal membrane at a time when neurons undergo branching. Our data suggests that PLPPR3 stabilizes membrane PI(3,4,5)P<sub>3</sub> through local inhibition of PTEN (Figure 3). Interestingly, also PLPPR1 has been shown to directly interact with PTEN.<sup>106</sup> Furthermore, PLPPR3 and PLPPR5 can directly bind PIPs (our own unpublished data).<sup>103</sup> Therefore, current working model suggests that PLPPRs may sequester phosphoinositides at the plasma membrane and thereby induce downstream signaling cascades leading to filopodia formation.

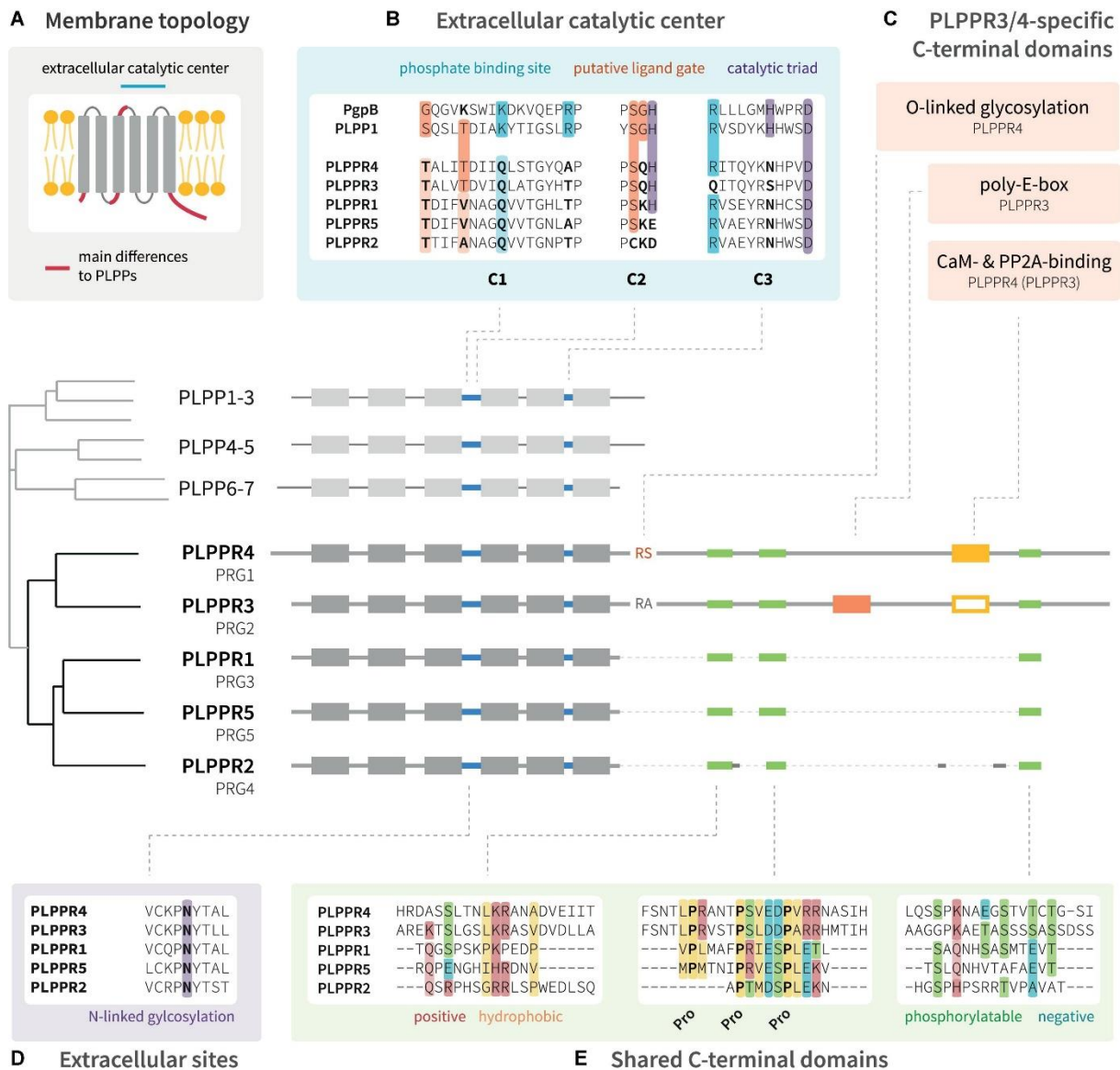


**Figure 2. Structural domains of PLPPR family proteins.** (A) PLPPRs and PLPPs share similar topology with highly conserved six transmembrane domains and non-conserved intracellular N- and C-terminal domains. The site of extracellular catalytic centre is indicated with blue line. (B) Compared to PLPPs, PLPPRs have mutations in several critical residues in the catalytic centre and therefore do not dephosphorylate bioactive lipids. PgpB is a bacterial lipid phosphatase for which structure has recently been resolved.<sup>102</sup> (C) PLPPR3 and 4 have several distinct features in their intracellular domains: PLPPR4 has an O-linked glycosylation site at S347, while PLPPR3 has a 20 amino acid-long stretch of glutamic acids, called the polyE box. PLPPR4 binds calmodulin (CaM) and protein phosphatase 2A (PP2A) via sites that are also present in PLPPR3, but not yet validated. (D,E) Conserved sites between all PLPPRs include an extracellular N-linked glycosylation site, plus a short sequence of hydrophobic and charged amino acids, a proline motif, and a cluster of phosphorylatable residues in the intracellular domain. From Fuchs et al. (2022).<sup>99</sup>

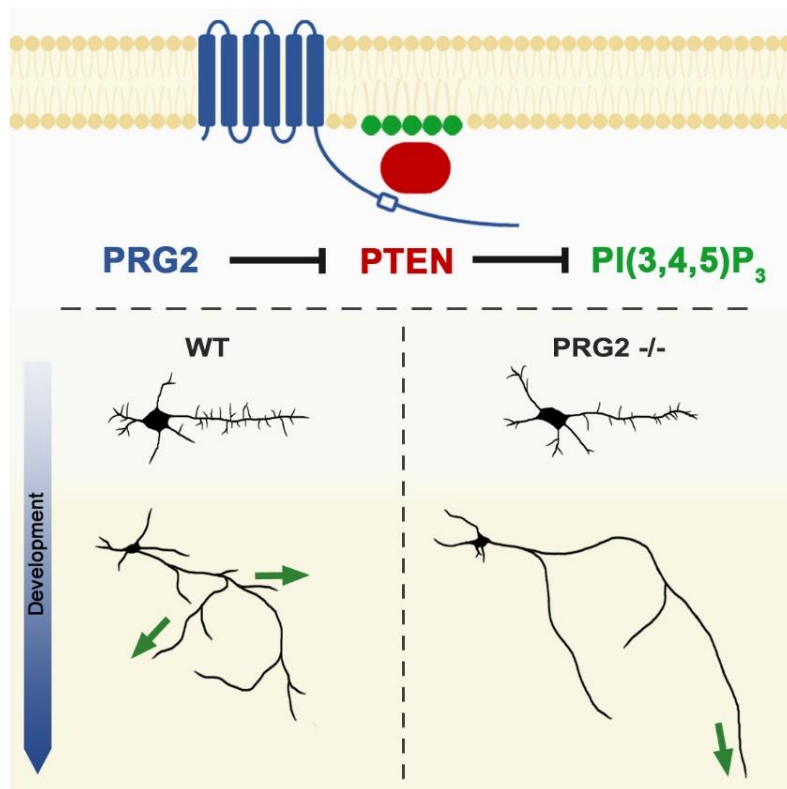


Figure 3. Working model of PLPPR3/PRG2-based filopodia and axon branch formation. PLPPR3 binds the ubiquitous phosphatase PTEN at the plasma membrane and inhibits its phosphatase activity, thus potentiating  $PIP_3$  accumulation and the downstream PI3K- $PIP_3$ -AKT signaling cascade leading to filopodia initiation. Loss of PLPPR3 leads to fewer filopodia and axonal branches. The overall growth capacity is not inhibited and instead directed to the primary axon. From Brosig & Fuchs et al. (2019).

Although almost all of the PLPPR family members appear to induce filopodia and share highly conserved transmembrane domains (Figure 2), there is compelling evidence that the filopodia-inducing function of PLPPRs may reside in the intracellular domain. Indeed, expression of truncated PLPPR variants lacking the intracellular domain fails to induce filopodia,<sup>103,104,107,108</sup> while the isolated intracellular domain of PLPPR1 can induce filopodia formation but only when inserted to the plasma membrane via a myristoylation tag.<sup>106,108</sup> The intracellular domains of PLPPRs differ considerably between the family members, yet share some common motifs. PLPPR4 and PLPPR3 have a long intracellular tail of approximately 400 amino acids, while PLPPR1, 2 and 5 have a short, approximately 50 amino acid long intracellular domain. The intracellular domains are intrinsically disordered, and therefore much less conserved between the family members than the ordered transmembrane domains. However, there are three regions with high sequence similarity: a motif of positively charged and hydrophobic amino acids proximal to the plasma membrane, a proline-rich motif and a stretch of phosphorylatable amino acids in the distal C-terminus (Figure 2E).<sup>99</sup> It is likely that these shared domains mediate the PLPPR-based filopodia formation. In an agreement with that, experimental data indicates that PLPPR3 and PLPPR5 intracellular domains bind phosphoinositides (our own unpublished data).<sup>103</sup>

Currently, little is known regarding the signaling mechanisms that regulate PLPPRs. On the one hand, as membrane proteins PLPPRs could be directly regulated by extracellular signals. On the other hand, their intrinsically disordered intracellular domain is highly accessible to

(multivalent) interactions as well as post-translational modifications, making them ideally suited to act as scaffolds for signaling complexes.<sup>109</sup> To date, few interaction partners and regulatory modifications have been identified. Most notably, PLPPR4 interacts with calmodulin and protein phosphatase 2A,<sup>104,110</sup> and this sequence is also conserved in PLPPR3 (Figure 2C). Besides an O-linked glycosylation site at PLPPR4 S347,<sup>111</sup> no post-translational modifications have been described for PLPPRs, although many family members share possible modification sites (Figure 2D, E). Thus, regulation of PLPPRs remains an unexplored territory.

### **1.5. Cellular signaling regulation by protein phosphorylation**

Cellular morphogenesis relies on the cell's ability to integrate extracellular and intracellular signals and respond to them in a spatially and timely regulated manner. Cells have evolved elaborate signal transduction mechanisms, such as scaffolding, liquid-liquid phase separation and post-translational modifications, to regulate these responses.<sup>112,113</sup> Post-translational modifications represent a rapid and reversible way of modulating the activity of the target protein with relatively small energetic cost.<sup>114</sup> To date, more than 200 post-translational modifications have been described, among which phosphorylation is the most pervasive, well-understood and involved in almost every cellular process.<sup>114</sup>

Phosphorylation is the transfer of a phosphate group from ATP to a target protein (Figure 4). In eukaryotic cells, this modification most commonly happens on serine, threonine and tyrosine residues and is catalyzed by kinases. Importantly, phosphorylation is reversible: the phosphoryl group can be removed from the substrate by phosphatases. Phosphorylation adds a negative charge to the protein, altering their binding properties or conformation,<sup>115,116</sup> which leads to changes in subcellular localization, protein turnover, enzymatic or transcriptional activity, or cross-talk with other post-translational modifications.<sup>117</sup> Thus, phosphorylation provides a molecular switch that alters the behavior of its target in a very small timescale.

The significance of phosphorylation as a cellular mechanism is illustrated by the fact that almost 2% of the entire human genome encodes for kinases, and to date more than 500 kinases have been identified.<sup>118</sup> An additional 250 phosphatases provide the balancing act by mediating dephosphorylation.<sup>119</sup> More than 2/3 of all human proteins have been shown to be phosphoproteins, however, it is believed that around 90% of all proteins may undergo this type of post-translational modification.<sup>117</sup> Modern phosphoproteomic approaches have enabled the unbiased identification of phosphorylation sites and as of 2022, almost 300 000 non-redundant phosphorylation sites have been listed on PhosphoSitePlus ([www.phosphosite.org](http://www.phosphosite.org)), a website that provides information on post-translational modifications.<sup>120</sup> A further 760 000 phosphorylation sites are predicted by Kinexus PhosphoNET database ([www.phosphonet.ca](http://www.phosphonet.ca)).<sup>117</sup> Although a large number of phosphorylation sites have been

identified, we currently know the function and kinase of less than 5% of those.<sup>121</sup> Thus, phosphorylation represents a huge opportunity to expand our knowledge of protein function and signaling.

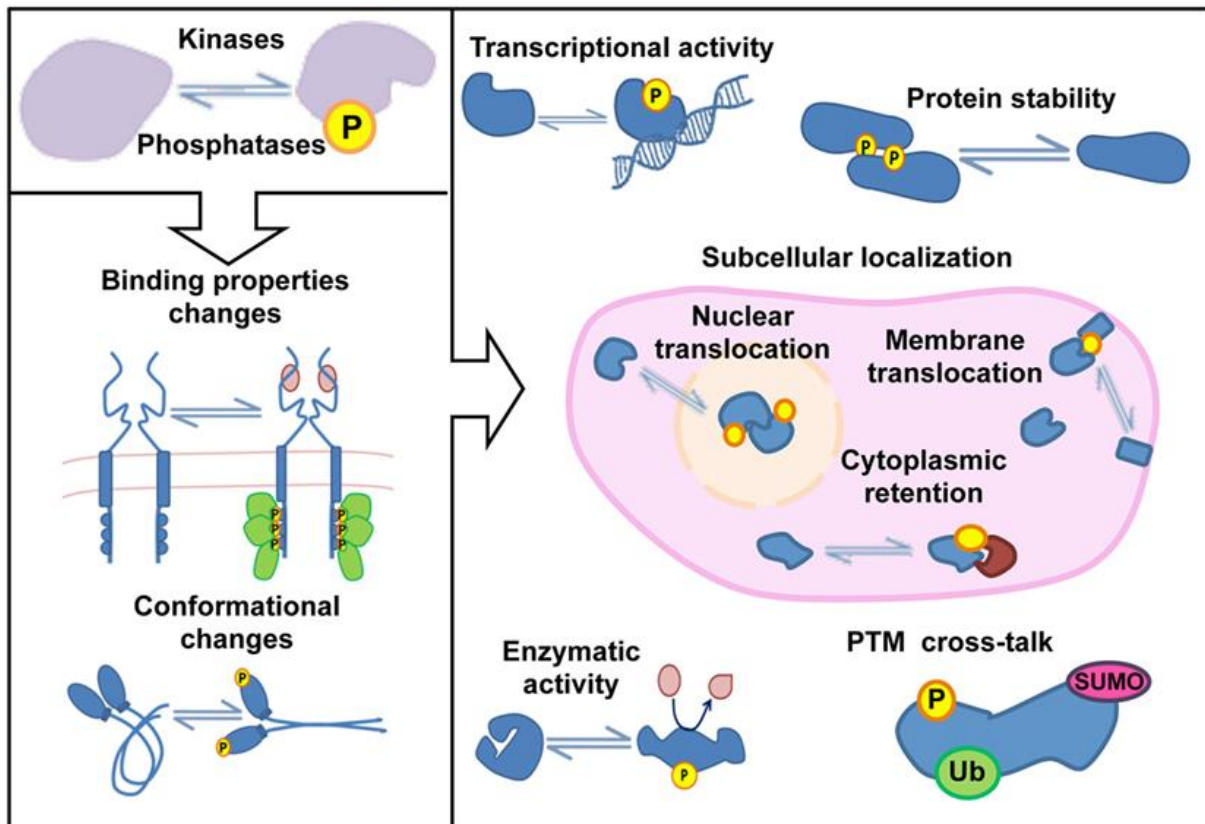


Figure 4. Phosphorylation-induced changes and associated mechanisms in proteins. Kinases catalyze the addition of a phosphoryl group to a target protein, while phosphatases catalyze the removal of it. Phosphorylation induces changes in protein conformation, or serves as a docking site for protein-protein interactions, thereby regulating protein's subcellular localization, enzymatic or transcriptional activity, protein stability or cross-talk with other post-translational modifications. From Alvarez-Salamero et al. (2017).<sup>116</sup>

The majority of phosphorylation sites are found in intrinsically disordered regions.<sup>122</sup> Intrinsically disordered domains are regions with distinct amino acid compositions which prevent them from folding into stable tertiary structures. Instead the protein adopts a multitude of distinct conformations to mediate its biological functions. Within disordered regions, polar and charged amino acids and repetitive motifs are overrepresented, while hydrophobic amino acids are underrepresented.<sup>123</sup> The disordered domains expose, at least transiently, their entire primary amino acid sequence for binding, enabling protein-protein interactions as well as modifications by kinases and other enzymes.<sup>124</sup> This makes intrinsically disordered proteins and proteins with disordered domains uniquely suited to act as signaling hubs. Indeed, disordered domains are overrepresented in cell-signaling and cancer-associated proteins.<sup>125</sup>

The rapid and reversible nature of phosphorylation is employed in signal transduction pathways. The growth signaling pathways summarized above all rely on phosphorylation, and often involve multiple kinases phosphorylating discrete and overlapping sets of target proteins. As an example, the CRMP-2-dependent axon initiation and outgrowth relies on signal transduction from PI3K through the kinases PDK1 and AKT to the inhibitory phosphorylation of GSK3 $\beta$  at serine 9.<sup>67</sup> However, serine 9 can also be phosphorylated by PKA,<sup>126</sup> thereby allowing for the convergence of the PI3K-AKT-GSK3 $\beta$  and the cAMP-PKA signaling pathways. Thus, phosphorylation-dependent signal transduction creates a highly connected network of control points that determine the outcome.

Ultimately, the growth-related signaling pathways converge on cytoskeletal effector proteins that control directed growth. Many kinases play important roles in neuronal morphogenesis. Axonal outgrowth induced by GSK3 $\beta$ -mediated phosphorylation of microtubule-associated proteins CRMP-2, MAP1B and TAU has already been discussed in a previous chapter. GSK3 $\beta$  additionally regulates MAP1B locally in axonal filopodia where it controls early stages of branching.<sup>127</sup> Phosphorylation of the actin-binding protein Drebrin by CDK5 enables its F-actin bundling activity at the base of growth cone filopodia and leads to neuritogenesis.<sup>128</sup> Phosphorylation of cortactin by protein kinase C (PKC) decreases its actin-bundling activity and filopodia formation.<sup>129</sup> Similarly, PKC phosphorylation of GAP43 stabilizes actin filaments and in this way affects axonal outgrowth.<sup>130,131</sup> The role of PKA-dependent phosphorylation of ENA/VASP proteins in filopodia formation has been extensively described.<sup>132–134</sup> PKA induced filopodia formation contributes to axonal branching, although the exact substrates are yet to be determined.<sup>73</sup> Thus, specific phosphorylation events provide a molecular switch that enable cells to undergo directed growth.

As it follows, aberrant phosphorylation can lead to many disease states. Due to the role of signaling cascades in cellular growth and differentiation, deregulation of phosphorylation is strongly associated with various types of cancer. For example AKT, the central node of the PI3K signaling pathway, is highly oncogenic and frequently deregulated in numerous human cancers.<sup>135</sup> Blocking kinase activity is one of the most promising targets in cancer therapeutics.<sup>136</sup> Indeed, as of 2018, 37 kinase inhibitors, including AKT inhibitors were FDA approved in the treatment of cancer, and about 150 kinase-related drugs were undergoing clinical trials.<sup>137</sup> Aberrant phosphorylation is also associated with many neurodegenerative diseases, particularly those characterized by protein aggregates, as it makes some proteins more prone to form aggregates. Aggregations of hyperphosphorylated TDP-43 have been reported in patients with frontotemporal lobar degeneration with ubiquitinated inclusions and amyotrophic lateral sclerosis.<sup>138</sup> Hyperphosphorylation of TAU and the resulting neurofibrillary tangles have long been considered a hallmark of Alzheimer's disease.<sup>139</sup> However, recently a

view emerges that the difference between normal and disease TAU lies not in the number of phosphorylations, but rather in its specific signature.<sup>140</sup> In any case, targeting TAU phosphorylation is currently one of the main avenues in the effort to treat Alzheimer's disease.<sup>141</sup>

## 1.6. Objectives of this thesis

Phosphorylation is an important regulatory mechanism in cells that allows to control signaling in a time and space constrained manner. Phosphorylation has been shown to regulate numerous physiological and pathological cellular processes, and is a promising target for therapeutic interventions. PLPPR3 is an axonal transmembrane protein that facilitates axon branch formation by initiating precursor structures, filopodia. At the start of this project, preliminary data indicated that PLPPR3 is a phosphoprotein, however, no study had investigated the regulation of PLPPR3 function by phosphorylation.

Therefore, I set out to investigate the phosphorylation of PLPPR3 and its role in PLPPR3 function. To this end, I used phospho-mass spectrometry analysis to identify phosphorylation sites in the intracellular domain of PLPPR3 (chapter 2). I used *in vitro* phosphorylation assay to elucidate kinases that target PLPPR3, and site-directed mutagenesis to uncover specific phosphorylation sites (chapter 3). I tested the function of the identified phosphorylation event in filopodia formation in cell lines and axon branching in primary neurons, and used affinity chromatography in combination with mass spectrometry to uncover a novel phospho-mediated binding partner of PLPPR3 (chapter 5). I characterized the localization of PLPPR3 and its interaction partner BASP1 in presynaptic compartments using immunocytochemistry and western blot of biochemical synaptosomal preparations (chapter 5). Additionally, I generated and validated a phospho-specific antibody to further study this phosphorylation event (chapter 4), and tested multiple antibodies for specificity towards BASP1 (Appendix).

## 2. PLPPR3 is a highly phosphorylated protein

---

The basic architecture of biological membranes is organized by lipids, but it is the lipid-embedded membrane proteins that provide its most important functional properties.<sup>142</sup> Membrane channels mediate transport between the extracellular and intracellular space, such as the movement of ions that underlies electrical activity of neurons. Membrane receptors bind extracellular ligands that trigger signaling cascades fundamental to communication between cells. In many instances, membrane proteins are subject to reversible phosphorylation, which regulates their function. At the start of my PhD, preliminary data in our lab indicated that PLPPR3 is phosphorylated. Therefore, I set out to investigate the phosphorylation events that occur in and may regulate PLPPR3 function. To this end, I first explored the possible phosphorylation sites and the kinases that target them by using a phosphorylation prediction tool.

### **2.1. Prediction tools propose numerous phosphorylation sites in the intracellular domain of PLPPR3**

Computational methods based on sequence analysis have provided prediction tools that can be used to narrow down on likely kinase-substrate pairs. Kinases typically target substrates with specific sequence characteristics, such as charge or hydrophobicity, which are complementary to the kinase's own active site and enable efficient interaction with the substrate.<sup>143</sup> Some kinases, such as the serine/threonine kinase CDK2, are "proline-directed", meaning they favour interaction with a substrate motif that has a proline at the +1 position relative to the phosphorylatable serine or threonine. Other kinases, such as CK1 or GSK3, favour binding to primed substrates, i.e motifs that already contain a phosphorylated amino acid. Although heavily biased towards the best understood kinases, prediction tools provide a good starting point in the analysis of phosphorylation events. Thus, at the start of my PhD project, I used a prediction tool to analyze the primary sequence of PLPPR3 for possible phosphorylation sites.

The topology of PLPPR3 consists of six transmembrane domains, extra-and intracellular loops, a short N-terminal and a long C-terminal intracellular domain (see Figure 2). The transmembrane domains and extracellular loops cannot be targeted by kinases that reside in the cytosol. While the intracellular loops and the N-terminal domain contain a few predicted phosphorylation sites (data not shown), I focused on the long intracellular domain as the most likely region for phosphorylation. To this end, I used the NetPhos 3.1 server (<https://services.healthtech.dtu.dk/services/NetPhos-3.1/>) to predict phosphorylation sites in the 433-amino acid long intracellular domain of PLPPR3 (aa 283-716). Using a stringent probability of >0.75, the intracellular domain is predicted to have 39 phosphorylation sites

(Table 1). Phosphorylation sites are predicted in almost all regions of the intracellular domain, with the notable exception of the region flanking the polyE box, a unique stretch of 20 glutamic acids found in PLPPR3 (aa 439-458; see Figure 2). The most commonly predicted kinases included PKC (11 sites), CDC2 (6), PKA (4) and CDK5 (4). I used PhosphoSitePlus (<https://www.phosphosite.org/>) to examine whether any phosphorylation sites had been reported for PLPPR3 in high-throughput proteomic discovery mass spectrometry studies. Twelve phosphorylation sites have previously been identified in samples of human and mouse origin, ranging from healthy brain tissue to various cancer tissues and cell lines (Table 1). Taken together, these data indicate that the intracellular domain of PLPPR3 harbors numerous phosphorylation sites.

*Table 1. Predicted phosphorylation sites with respective kinases in the intracellular domain of PLPPR3. Prediction of phosphorylated serine, threonine and tyrosine residues was performed on the primary amino acid sequence of the intracellular domain (amino acids 283-716). Phosphorylation sites with prediction scores >0.75 were included. Phosphorylated residues are marked in bold. Predicted phosphosites which have previously been reported in high-throughput proteomic discovery mass spectrometry (MS) studies are marked with "+". \* from human and mouse samples. Source: <https://services.healthtech.dtu.dk/services/NetPhos-3.1/> and <https://www.phosphosite.org/>*

| Nr | Site | Sequence           | Proposed kinase | Reported in proteomic discovery MS?* |
|----|------|--------------------|-----------------|--------------------------------------|
| 1  | T293 | EKVPT <b>P</b> APA | p38MAPK         |                                      |
| 2  | T305 | LRALTQ <b>R</b> GH | PKC             |                                      |
| 3  | Y313 | HESMY <b>Q</b> QNK | unsp            |                                      |
| 4  | S318 | QQN <b>K</b> SVSTD | CDC2            |                                      |
| 5  | S320 | NK <b>S</b> VSTDEL | CKII            | +                                    |
| 6  | T342 | AREKT <b>S</b> LGS | unsp            |                                      |
| 7  | S343 | REKT <b>S</b> LGSL | unsp            |                                      |
| 8  | S346 | TSLG <b>S</b> LKRA | PKC             | +                                    |
| 9  | S351 | LKR <b>A</b> SVDVD | PKA             | +                                    |
| 10 | S379 | LPRV <b>S</b> TPSL | PKA             | +                                    |
| 11 | T380 | PRV <b>S</b> TPSLD | CDK5            | +                                    |
| 12 | S382 | V <b>S</b> TPSLDDP | unsp            | +                                    |

|    |      |           |                        |   |
|----|------|-----------|------------------------|---|
| 13 | T392 | RRHMTIHVP | unsp                   | + |
| 14 | S413 | WKQKSLEGR | unsp                   |   |
| 15 | S464 | PVPPSLYPT | CDC2, PKA              |   |
| 16 | S505 | GAGLSPKSS | PKC, p38MAPK           | + |
| 17 | S508 | LSPKSSSSS | unsp                   |   |
| 18 | S511 | KSSSSSVRA | PKC, CDC2              |   |
| 19 | S512 | SSSSSVRAK | PKC                    |   |
| 20 | S563 | ETASSSSAS | PKC, CDC2              | + |
| 21 | S564 | TASSSSASS | unsp                   |   |
| 22 | S565 | ASSSSASSD | unsp                   |   |
| 23 | S567 | SSSASSDSS | PKC                    |   |
| 24 | S568 | SSASSDSSQ | CDC2                   |   |
| 25 | S571 | SSDSSQYRS | PKC, DNAPK, ATM        |   |
| 26 | S575 | SQYRSPSDR | CDK5, GSK3             |   |
| 27 | S577 | YRSPSDRDS | RSK                    |   |
| 28 | S581 | SDRDSASIV | PKA                    |   |
| 29 | T604 | SAGSTPWEW | CDK5                   |   |
| 30 | S618 | EGEGSYELG | CKII, DNAPK            |   |
| 31 | Y619 | GEGSYELGD | unsp                   | + |
| 32 | S631 | GFRSSCKQP | PKC                    |   |
| 33 | S641 | MGPGSPVSD | p38MAPK, CDK5,<br>GSK3 | + |
| 34 | S644 | GSPVSDVDQ | CKII                   | + |
| 35 | S681 | LGAGSREST | unsp                   |   |
| 36 | S684 | GSRESTLRR | PKC                    |   |
| 37 | T685 | SRESTLRRQ | PKC                    |   |

|    |      |           |      |
|----|------|-----------|------|
| 38 | S704 | AEAESYYRR | CDC2 |
| 39 | Y706 | AESYYRRMQ | unsp |

## 2.2. The distal C-terminus of PLPPR3 is phosphorylated in dependence of localization to the plasma membrane

Prediction analysis proposes that both the plasma membrane proximal as well as the distal C-terminus harbor a high density of phosphorylation sites. To investigate this experimentally, I expressed multiple truncated variants of PLPPR3 in cell lines and analyzed them by western blot. All PLPPR3 variants used in this study are summarized in Figure 5.

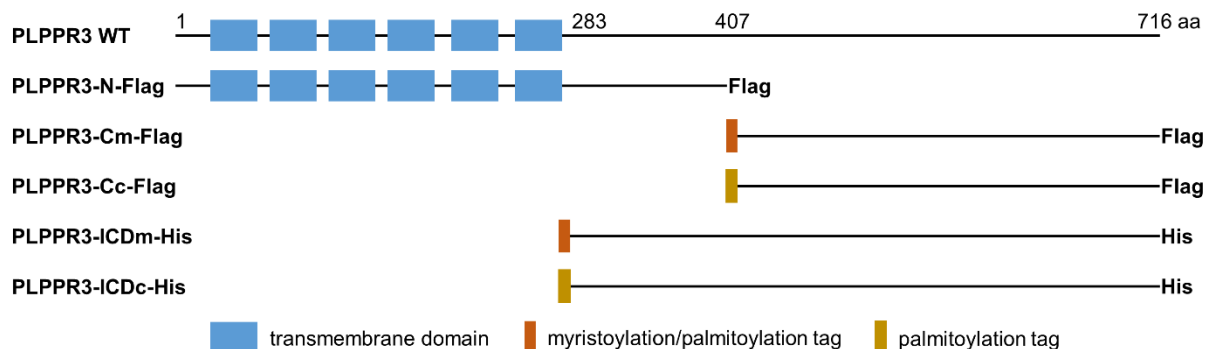


Figure 5. Graphic overview of PLPPR3 variants used in this study. Native PLPPR3 protein consists of six transmembrane domains and a long intracellular domain. PLPPR3-N-Flag consists of the transmembrane domains and the membrane proximal intracellular domain, while PLPPR3-C-Flag consists of the distal intracellular domain. PLPPR3-ICD-His constructs include the entire intracellular domain. Myristoylation/palmitoylation tag is used to attach the intracellular domain variants to the plasma membrane. Palmitoylation tag alone is not sufficient to stably attach the intracellular domain to the plasma membrane, making these variants primarily cytosolic. WT – wild type, aa – amino acid, m – membrane, c – cytosolic.

In the absence of phospho-specific antibodies, it is a common procedure to assess protein phosphorylation status by SDS-PAGE. Many proteins show phosphorylation-dependent mobility shift in the SDS-PAGE, which has been shown to be due to decreased binding of SDS.<sup>144</sup> In order to study the phosphorylation status of the intracellular domain of PLPPR3, I made use of the protein variants previously generated in the lab (Figure 6A, see also Figure 5). The first PLPPR3 variant consists of the N-terminal half of the protein, encompassing the six transmembrane domains and a short 123 amino acid fragment of the membrane proximal intracellular domain (PLPPR3-N-Flag; aa 1-407)<sup>88</sup>; the second PLPPR3 variant consists of distal intracellular domain (PLPPR3-Cm-Flag; aa 408-716) with a membrane-attachment sequence, whilst the third variant consists of the distal intracellular domain with a mutated membrane attachment sequence, rendering it cytosolic (PLPPR3-Cc-Flag; aa 408-716).

PLPPR3-Cm-Flag bears the membrane-targeting sequence of FYN (MGCVQCKDKEA),<sup>145</sup> where the glycine is co-translationally myristoylated and the cysteines post-translationally palmitoylated, thereby mimicking the protein's native subcellular localization in the plasma membrane. In PLPPR3-Cc-Flag the glycine is mutated to alanine, leaving the protein primarily cytosolic as palmitoylation alone is not enough to stably attach the protein to the plasma membrane.

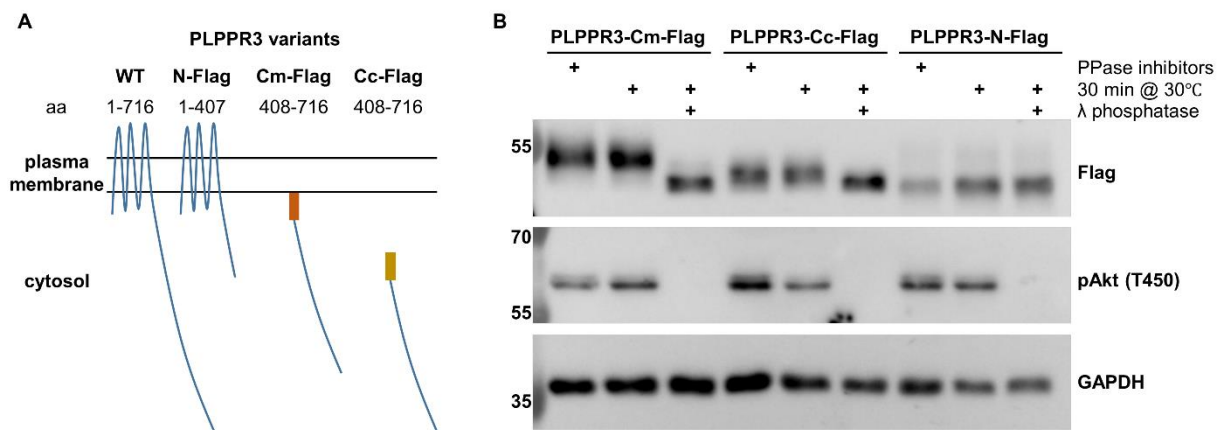


Figure 6. PLPPR3 distal intracellular domain is phosphorylated in dependence of proximity to the plasma membrane. (A) Graphic representation of PLPPR3 variants used in this experiment. Blue: PLPPR3, orange: membrane-targeting sequence, gold: mutated membrane-targeting sequence, aa: amino acid. (B) Representative western blot of mobility shift of the PLPPR3 mutants after phosphatase treatment. PLPPR3 variants were expressed in N1E-cells, lysed in the presence or absence of phosphatase inhibitors and treated with Lambda phosphatase. Phosphatase-treated samples annotate the migration height of the unphosphorylated PLPPR3 band.

I expressed all PLPPR3 variants in N1E-115 cells, where they show distinct localization patterns (data not shown). Following cell lysis, I treated the samples with Lambda phosphatase to non-selectively remove all phosphorylations before analysis by SDS-PAGE and western blot. Control blot for phosphorylated Akt (pAkt T450) shows that the phosphatase treatment had indeed successfully removed its phosphorylation (Figure 6B). Interestingly, the membrane-targeted PLPPR3-Cm-Flag showed a major mobility shift after phosphatase treatment, which was far more pronounced than the band shift obtained following phosphatase treatment of cytosolic PLPPR3-Cc-Flag. PLPPR3-N-Flag did not show a band shift after phosphatase treatment, however, this sequence contains only a short intracellular domain, which may explain low(er) levels of phosphorylation of this variant. Taken together, these data suggest the presence of phosphorylation events in the distal intracellular domain.

### 2.3. Setting up PhosTag SDS-PAGE for the analysis of PLPPR3 variants

In order to investigate the phosphorylation status of the PLPPR3 intracellular domain further, I made use of the PhosTag SDS-PAGE. PhosTag is a phosphate-binding molecule that, with the help of a divalent metal ion, allows the separation of proteins in an acrylamide gel based

on their level of phosphorylation and not just their molecular weight (Figure 7).<sup>146</sup> Moreover, it has been shown that PhosTag can separate proteins with the same number of phosphorylations that are on different residues.<sup>147</sup> Therefore, it can be a powerful tool to study the overall phosphorylation pattern of proteins, or specific phosphorylation events in the absence of phospho-specific antibodies.

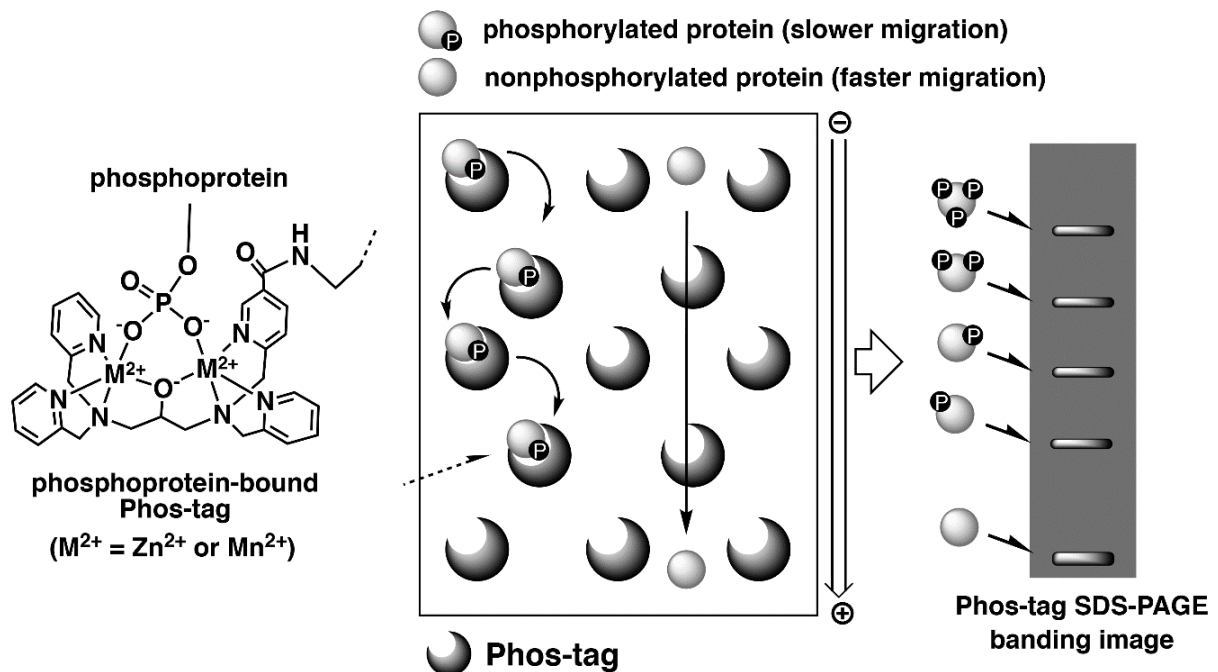


Figure 7. Working principle of PhosTag SDS-PAGE. PhosTag molecule binds phosphate groups of phosphoproteins with the help of divalent metal ions in acrylamide gels and hinders their movement in the gel, allowing the separation of proteins based on their phosphorylation level. PhosTag is also able to separate proteins with the same number of phospho-groups that are on different amino acid residues. Graph from <https://labchem-wako.fujifilm.com/us/category/lifescience/proteomics/phostag/index.html> retrieved on 20.04.2023.

There are three critical decisions in the optimization of PhosTag SDS-PAGE. The system crucially depends on the divalent metal ion, as well as the concentrations of acrylamide and the PhosTag. PhosTag molecule uses divalent metal ions  $Mn^{2+}$  or  $Zn^{2+}$  to trap phospho-groups and slow their migration in the gel.<sup>146</sup> The  $Zn^{2+}$ -based PhosTag has improved resolving capabilities compared to  $Mn^{2+}$ -based gels,<sup>148</sup> while the  $Mn^{2+}$  has the advantage of using regular Laemmli buffer system. Proteins, also unphosphorylated proteins, migrate slower in the PhosTag gel than in the regular SDS-PAGE, therefore, typically lower percentage of acrylamide is used than for the regular SDS-PAGE. Finally, the specific PhosTag concentration will determine how well the phosphorylated forms of protein will be separated. There is a delicate interplay between acrylamide and PhosTag concentrations that allow for sufficient migration as well as for separation of phosphorylated variants of a protein, which has to be established experimentally. Therefore, I set out to optimize the PhosTag SDS-PAGE for PLPPR3.

PLPPR3 truncation mutants vary between ~46-60 kDa in size and separated well on 10% SDS-PAGE. For PhosTag SDS-PAGE I decided to use 8% acrylamide, which is the manufacturer's recommendation for proteins <60 kDa. I tested increasing concentrations of PhosTag in combination with  $Mn^{2+}$  and  $Zn^{2+}$  ions to determine the optimal separation conditions for PLPPR3-Cm-Flag, which showed a dephosphorylation-dependent band shift on regular SDS-PAGE (see Figure 6B). I used protein lysates from PLPPR3-Cm-expressing N1E-115 cells. In order to differentiate phosphorylated forms from unphosphorylated forms, I again made use of Lambda phosphatase-treated control. Dephosphorylated proteins are expected to migrate as one band in PhosTag SDS-PAGE. Due to the working principle of the PhosTag method, protein ladders do not give meaningful information in these gels, and they may cause distortion of protein bands (see PhosTag SDS-PAGE guidebook, available at [http://www.bujnochem.com/wp-content/uploads/2019/09/FUJIFILM-Wako\\_Phos-tag-R.pdf](http://www.bujnochem.com/wp-content/uploads/2019/09/FUJIFILM-Wako_Phos-tag-R.pdf)). Thus, they have been omitted.

As expected, there was an intricate interaction of PhosTag concentration with the metal ion in the gel separation capability. Both 20 and 50  $\mu M$   $Mn^{2+}$  PhosTag gels caused the separation of five distinct phosphorylation bands; however, bands were slightly further apart and better defined on the 50  $\mu M$  PhosTag gel (Figure 8A). At 100  $\mu M$ ,  $Mn^{2+}$  PhosTag led to worse separation with only three phosphorylation bands. 50 and 100  $\mu M$   $Zn^{2+}$  PhosTag gels had comparable separation properties, with 50  $\mu M$   $Zn^{2+}$  gel resulting in better defined bands. Surprisingly, 20  $\mu M$   $Zn^{2+}$  gel had the worst separation properties with only two visible phosphorylation bands.

Curiously, also the phosphatase-treated sample separated into two to three distinct Flag-positive bands. It is possible that the 30 minute treatment was not enough to remove all of the phosphate groups in the sample, or that PLPPR3 C-terminus contains phosphorylation sites that are not accessible to phosphatases. However, based on current experiments the identity of those bands remains elusive and for simplicity, the lowest band will be referred to as the unphosphorylated protein. Furthermore, these experiments do not establish the resolution of PLPPR3 phosphorylation bands. Whether each band represents an individual phosphorylation event or combination of phosphorylation events is not known. Thus, I concluded that the most optimal PhosTag concentration for truncated PLPPR3 variants is 50  $\mu M$ . While  $Mn^{2+}$  gels appeared generally superior to  $Zn^{2+}$  gels, the difference between 50  $\mu M$   $Mn^{2+}$  and  $Zn^{2+}$  gels is minimal and therefore both can be considered suitable for studying the phosphorylation of PLPPR3 variants.

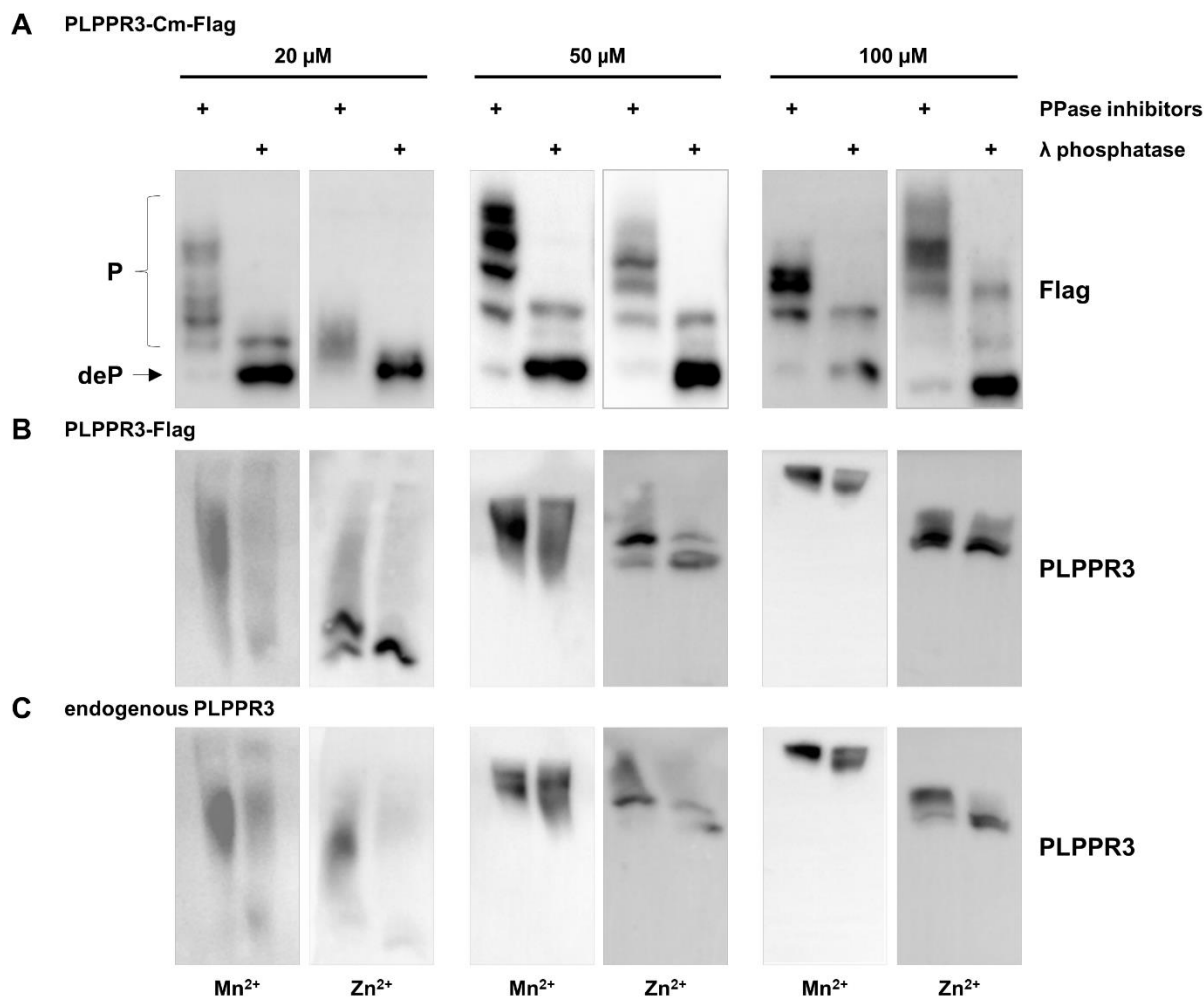


Figure 8. Optimization of PhosTag western blot for the analysis of PLPPR3 phosphorylation. Comparison of representative blots from Mn<sup>2+</sup> and Zn<sup>2+</sup> gels with increasing concentration of PhosTag in the separation of (A) PLPPR3-Cm-Flag, (B) full-length PLPPR3-Flag and (C) endogenous PLPPR3 phosphorylated forms. In (A) and (B), cell lysates from N1E-115 cells expressing PLPPR3 variants were analyzed. In (C), protein lysates from DIV5 primary hippocampal neurons were used. Samples in (A) were separated on an 8% gel, in (B) and (C) 6% gels were used. Phosphatase-treated samples annotate the migration height of the unphosphorylated PLPPR3 band.

I also tested the PhosTag system on full-length recombinant PLPPR3-Flag (Figure 8B) and native PLPPR3 from neuronal lysates (Figure 8C). I used 6% acrylamide gels, as the full-length PLPPR3 is approximately 70 kDa. Unfortunately, neither the Mn<sup>2+</sup> nor Zn<sup>2+</sup>-based gels allowed for a good separation of these full-length proteins in any concentration tested. In both cases, increased concentrations of PhosTag led to poorer mobility of protein in the gel as evidenced by the upward shift of protein bands. In Mn<sup>2+</sup> based gels the proteins smeared, while in Zn<sup>2+</sup>-based gels the protein did not separate beyond two distinct bands. Noticeably, in most cases there was little difference between phosphorylated and dephosphorylated sample, suggesting that poor separation is due to properties of the full-length protein and not phosphorylation status.

In conclusion, I successfully employed the PhosTag system to separate multiple truncated PLPPR3 phosphorylated forms by SDS-PAGE. Therefore, this method can potentially be useful to study individual phosphorylation events. Unfortunately, I could not define conditions to sufficiently resolve full-length recombinant and endogenous PLPPR3 phospho-forms. Thus, a limitation of this approach is that it cannot be used to study endogenous phosphorylation signaling.

#### 2.4. PLPPR3 intracellular domain harbors 26 high-confidence phosphorylation sites

I next used the optimized PhosTag gel system to closer investigate the phosphorylation status of the N- and C-terminal variants of PLPPR3 showed in Figure 6. Similar to the experiments presented in the previous section, truncated PLPPR3 variants were expressed in N1E-115 cells and protein lysates were separated on 8% 50  $\mu$ M  $Mn^{2+}$  PhosTag gel. Lambda phosphatase treatment was used as control to obtain non-phosphorylated protein. PhosTag western blot showed that the membrane-bound PLPPR3-Cm-Flag is present in exclusively phosphorylated state under steady-state conditions, as indicated by four distinct phospho-bands and absence of an unphosphorylated protein band (Figure 9).

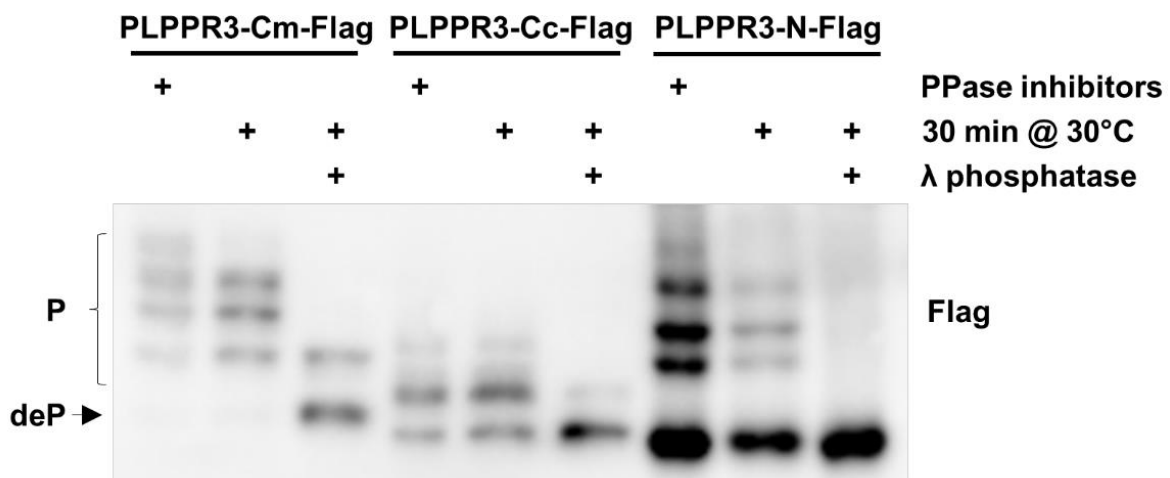


Figure 9. PLPPR3 intracellular domain is phosphorylated in membrane proximal as well as distal part. Proximity to the plasma membrane controls phosphorylation level of PLPPR3 C-terminus. Protein lysates from N1E-115 cells were separated on 8% 50  $\mu$ M  $Mn^{2+}$  PhosTag SDS-PAGE and analyzed by western blot. Phosphatase-treated samples annotate the migration height of the unphosphorylated PLPPR3 band.

In contrast, the steady-state cytosolic PLPPR3-Cc-Flag has three phospho-bands and a notable unphosphorylated protein band. Surprisingly, PLPPR3-N-Flag, which did not show a band shift on a regular SDS-PAGE after phosphatase treatment (see Figure 6B), also separated into four distinct phospho-bands, in addition to a prominent unphosphorylated

protein band. These results indicate that there are phosphorylation events in the membrane proximal as well as distal part of the PLPPR3 intracellular domain.

In order to study the phosphorylation of the entire PLPPR3 intracellular domain, I generated membrane-targeted and cytosolic intracellular domain variants using the same strategy as described in Figure 6A. I tagged the PLPPR3 intracellular domain (aa 284-716) with membrane-attachment (PLPPR3-ICDm-His) or mutated membrane-attachment sequence of FYN (PLPPR3-ICDc-His) (Figure 10A). In order to confirm the correct subcellular localization of PLPPR3-ICDm-His and PLPPR3-ICDc-His, I co-expressed these constructs in N1E-115 cells with membrane-targeted GFP. Immunolabeling confirmed the anticipated co-localization of PLPPR3-ICDm-His with GFP signal at the plasma membrane (Figure 10B), while PLPPR3-ICDc-His showed little overlay with GFP and localized primarily to the cytosol.

Finally, I analyzed these constructs by 8% 50  $\mu\text{M}$   $\text{Mn}^{2+}$  PhosTag SDS-PAGE. Similarly to membrane-bound distal C-terminus, also membrane-bound intracellular domain is entirely present in a phosphorylated state in N1E-115 cells under steady-state conditions (Figure 10C). Similar to the cytosolic distal C-terminus, also the cytosolic intracellular domain has fewer higher-order phosphorylation bands and a prominent unphosphorylated band under steady-state conditions. Unfortunately, when compared to the shorter PLPPR3 variants shown in Figure 9, the intracellular domain does not separate in clear, well-defined bands on 8% 50  $\mu\text{M}$   $\text{Mn}^{2+}$  PhosTag SDS-PAGE, making it impossible to assess the total number of phosphorylation bands. In conclusion, these results from figures 6B, 9 and 10C suggest that membrane association alters the phosphorylation state of the PLPPR3 intracellular domain.

The identification that the phosphorylation status of the PLPPR3 intracellular domain depends on the association with the plasma membrane may indicate the presence of dynamically regulated phosphorylation sites linked to signaling events at the plasma membrane. I decided to employ this insight in a mass spectrometry approach to identify the phosphorylation sites. I collaborated with my colleague Shannon Bareesel to purify PLPPR3-ICDm-His and PLPPR3-ICDc-His for phospho-mass spectrometry analysis (Figure 11A). We initially aimed to use N1E-115 cells as most “neuron-like cells”, but overexpression of PLPPR3 constructs in these cells did not yield sufficient protein (data not shown). We instead used HEK293T cells, which are ideal for protein purification approaches due to high yield of recombinant protein. We purified PLPPR3-ICDm-His out of the membrane fraction, and PLPPR3-ICDc-His out of the cytosolic fraction via the His tag. Lambda phosphatase treatment was used as a control to validate phosphorylated residues. Phospho-mass spectrometry analysis was performed by Dr. Marieluisse Kirchner (Proteomics Core Facility, Berlin Institute of Health).

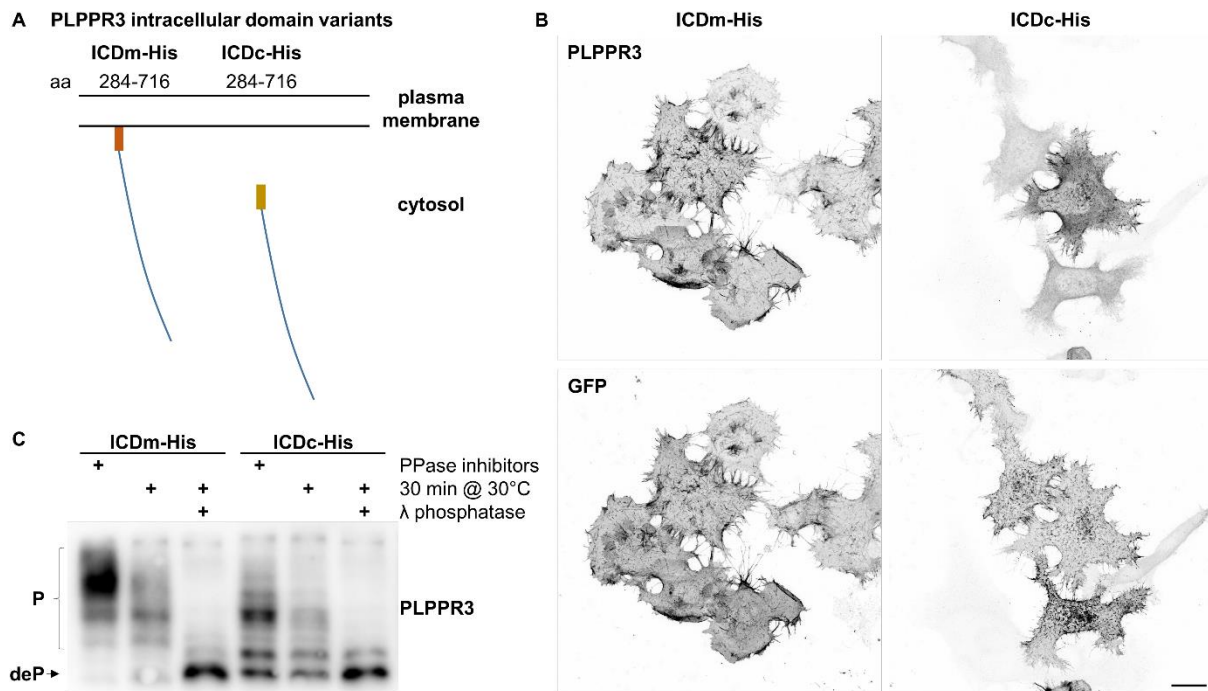


*Figure 10. PLPPR3 intracellular domain is phosphorylated in dependence of proximity to the plasma membrane. (A) Graphic representation of PLPPR3 intracellular domain constructs. aa – amino acid. PLPPR3-ICDm has a membrane anchor and localizes to the plasma membrane, while PLPPR3-ICDc has a mutated membrane anchor, leaving the protein primarily cytosolic. (B) Subcellular localization of PLPPR3 intracellular domain constructs. N1E-115 cells expressing PLPPR3-ICDm-His or PLPPR3-ICDc-His and farnesylated GFP as a membrane marker were immunolabelled for PLPPR3 and GFP. Scale bar 10  $\mu$ m. (C) PLPPR3-ICDm is present in cells in an entirely phosphorylated form, while PLPPR3-ICDc exists in phosphorylated and unphosphorylated forms. Protein lysates from N1E-115 cells were separated on 8% 50  $\mu$ M  $Mn^{2+}$  PhosTag SDS-PAGE and analysed by western blot. Phosphatase-treated samples annotate the migration height of the unphosphorylated PLPPR3 band.*

Our phospho-mass spectrometry analysis consisted of two measurements with two biological replicates in the first and three biological replicates in the second run. Sequence coverage was 88% in the first and 97% in the second run, and the uncovered sequence comprised primarily of the polyE box (Figure 11B). Surprisingly, we found that the intracellular domain of PLPPR3 harbors a total of 26 high-confidence phosphorylation sites, 13 of which were unique to the membrane-targeted intracellular domain (Table 2). Interestingly, the 13 phosphorylation sites that are found in both cytosolic and membrane-bound PLPPR3, have previously been identified in tissues in high throughput mass spectrometry studies, while almost none of the sites found in membrane-tagged PLPPR3 intracellular domain have been reported before (compare with Table 1).

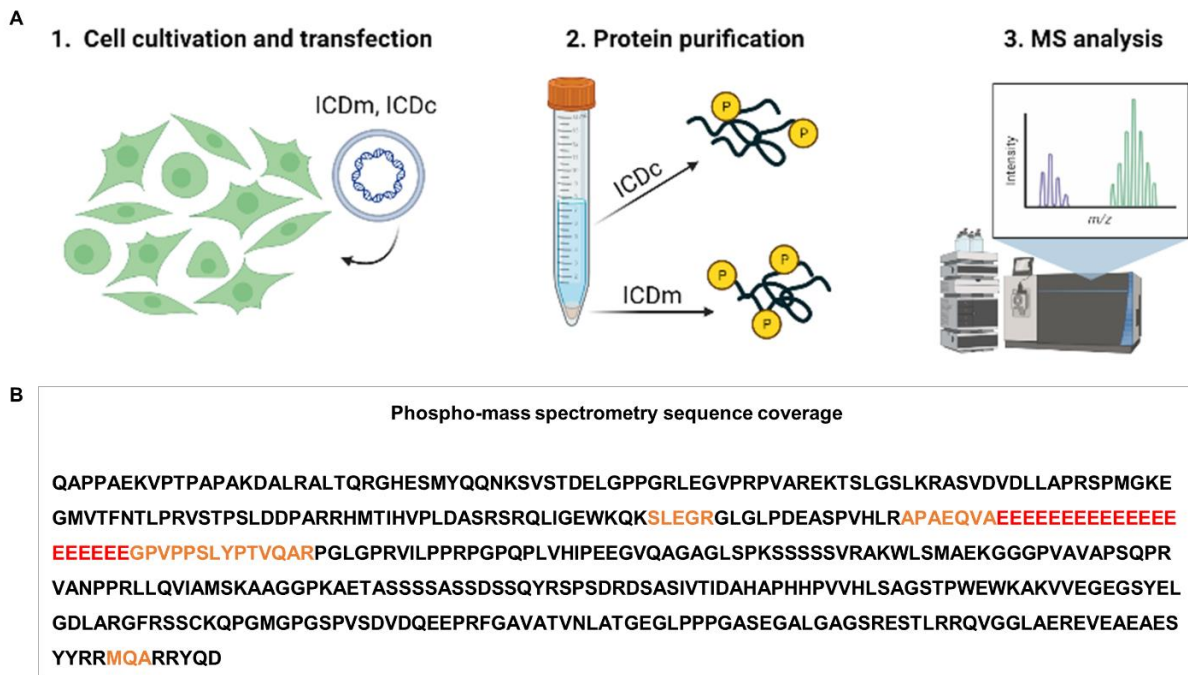


Figure 11. Phospho-mass spectrometry analysis to identify phosphorylation sites in the intracellular domain of PLPPR3. (A) Experimental workflow. Created with BioRender.com. (B) Sequence coverage from two independent mass spectrometry analyses. Black: covered sequence, orange: missing sequence from first run, red: missing sequence from first and second run.

Although western blot and PhosTag western blot experiments suggested that it is the distal C-terminus that is most phosphorylated, mass spectrometry analysis established that the highest density of phosphorylation events are found in the part proximal to the plasma membrane, where a stretch of 123 amino acids showed 15 phosphorylated residues. This part of the intracellular domain is also part of the PLPPR3-N-Flag variant. The remainder of the C-terminus, corresponding to the 308 amino acid long PLPPR3-Cm/Cc-Flag, exhibits 11 phosphorylated residues. One residue that was identified as a phosphorylation site – S641 – appeared completely resistant to dephosphorylation, however, based on set criteria we are confident it is indeed a phosphorylation site. Taken together, these results show that PLPPR3 intracellular domain is highly phosphorylated.

With the advent of mass spectrometry approaches becoming more accessible, a huge number of phosphorylation sites have been identified in the past few decades, however, only a small fraction of sites have been functionally validated. This has led many in the field to propose that a vast number of phosphorylation sites may in fact be unfunctional.<sup>149</sup> Conservation of phosphorylatable residues and their flanking regions across species has been proposed as a criteria to assess potentially functional phosphorylation sites.<sup>150</sup> To explore the conservation of PLPPR3 phosphorylation sites, I analyzed sequence alignments from six species: mouse (*Mus musculus*), human (*Homo sapiens*), zebrafish (*Danio rerio*), tropical clawed frog (*Xenopus*

*tropicalis*), rhesus monkey (*Macaca mulatta*) and chicken (*Gallus gallus*). Curiously, 15 residues identified as phosphorylation sites were conserved across evolutionarily distant species. Another seven residues were conserved in 5/6 analyzed species. Only one residue, T293, was completely non-conserved and uniquely present in mouse. Taken together, these data support the view of numerous functional phosphorylation events in the intracellular domain of PLPPR3.

Table 2. List of high-confidence phosphorylation sites identified in the PLPPR3 intracellular domain by mass spectrometry and analysis of their conservation across species. Phosphorylated residue is marked in red. ICDm: membrane-tagged intracellular domain, ICDC: cytosolic intracellular domain. Conservation of the phosphorylatable residue was analyzed by sequence alignment across six species: mouse (*Mus musculus*), human (*Homo sapiens*), zebrafish (*Danio rerio*), tropical clawed frog (*Xenopus tropicalis*), rhesus monkey (*Macaca mulatta*) and chicken (*Gallus gallus*). Phosphorylation sites conserved across all analyzed species are marked with “+”, non-conserved sites are marked with “-”, for the rest the exact ratio of conserved/total is given. COBAL tool was used for conservation analysis (<https://www.ncbi.nlm.nih.gov/tools/cobalt/cobalt.cgi?CMD=Web>)

| Nr | Site | Sequence            | Identified in ICDm | Identified in ICDC | Unique to ICDm | Conservation across species |
|----|------|---------------------|--------------------|--------------------|----------------|-----------------------------|
| 1  | T293 | EKVPT <b>T</b> PAPA | +                  |                    | +              | -                           |
| 2  | S311 | RGHE <b>S</b> MYQQ  | +                  |                    | +              | 5/6                         |
| 3  | S318 | QQNK <b>S</b> VSTD  | +                  |                    | +              | +                           |
| 4  | S320 | NKSV <b>S</b> TDEL  | +                  | +                  |                | +                           |
| 5  | T321 | KSV <b>S</b> TDELG  |                    | +                  |                | 5/6                         |
| 6  | S343 | REKT <b>S</b> LGSL  | +                  |                    | +              | +                           |
| 7  | S346 | TSLG <b>S</b> LKRA  | +                  | +                  |                | +                           |
| 8  | S351 | LKRAS <b>S</b> VDVD | +                  | +                  |                | +                           |
| 9  | S361 | LAPR <b>S</b> PMGK  | +                  | +                  |                | +                           |
| 10 | S372 | MVTF <b>S</b> NTLP  | +                  |                    | +              | +                           |
| 11 | T374 | TFSN <b>T</b> LPRV  | +                  | +                  |                | +                           |
| 12 | T380 | PRV <b>S</b> TPSLD  | +                  |                    | +              | 3/6                         |
| 13 | S382 | VSTP <b>S</b> LDDP  | +                  |                    | +              | 5/6                         |
| 14 | T392 | RRHM <b>T</b> IHVP  | +                  | +                  |                | +                           |

|    |      |                     |   |   |   |     |
|----|------|---------------------|---|---|---|-----|
| 15 | S400 | PLDA <b>S</b> RSRQ  | + |   | + | 5/6 |
| 16 | S426 | PDEA <b>S</b> PVHL  | + | + |   | 3/6 |
| 17 | S505 | GAGL <b>S</b> PKSS  | + | + |   | 5/6 |
| 18 | T560 | PKAET <b>S</b> ASSS | + |   | + | 5/6 |
| 19 | S564 | TASS <b>S</b> SASS  | + |   | + | +   |
| 20 | S565 | ASS <b>S</b> ASSD   | + |   | + | 4/6 |
| 21 | S568 | SSA <b>S</b> DSSQ   | + | + |   | +   |
| 22 | S570 | ASSD <b>S</b> SQYR  | + |   | + | 5/6 |
| 23 | S575 | SQYR <b>S</b> PSDR  | + | + |   | +   |
| 24 | S641 | MGP <b>S</b> SPVSD  | + | + |   | +   |
| 25 | S644 | GSPV <b>S</b> DVDQ  | + | + |   | +   |
| 26 | S681 | LGAG <b>S</b> REST  | + |   | + | +   |

## 2.5. Discussion and outlook

Results presented in this section establish that PLPPR3 intracellular domain is highly phosphorylated, harboring 26 high-confidence phosphorylation sites within 433 amino acid residues. The high number of phosphorylation sites suggests that while PhosTag SDS-PAGE allowed me to resolve up to four distinct phosphorylation bands in PLPPR3-N and C-terminal half, separation was not enough to reach single site resolution. Further optimization or truncation of PLPPR3 variants could be a possibility to improve resolution.

Curiously, both PhosTag and mass spectrometry analyses point to the existence of a phosphatase-resistant phosphorylation site in the intracellular domain, which is likely residue S641. As false discovery rate in our mass spectrometry analysis was 1%, we cannot completely exclude the possibility that this phospho-site is a false positive. However, based on spectra analyses, occurrences and mass error, the identification of PLPPR3 phosphorylation at S641 was very robust. Moreover, S641 has been found to be phosphorylated in tissue before (Table 1), adding confidence that this is a true phosphorylation site. Both the PLPPR3-Cm-Flag as well as the PLPPR3-Cc-Flag, but not the PLPPR3-N-Flag show a double band after phosphatase treatment, lending support to the possibility that this band reflects S641. Phosphatase-resistant phosphorylation sites have been reported before in TAU and

CRMP2.<sup>151</sup> Interestingly, these sites were phosphorylated by CDK5, which is one of the kinases predicted for PLPPR3 S641.

There are 11 phosphorylation sites that overlap between the membrane-tagged and cytosolic PLPPR3 intracellular domain. These are also the sites that have been reported in discovery mass spectrometry studies in brain tissue before, hinting at their likely relevance to the function of the protein. The overlap in membrane-tagged and cytosolic intracellular domain may be explained by their partial overlap in (plasma) membrane compartments. Dual modification by myristoylation and palmitoylation determines stable plasma membrane localization, as is seen for PLPPR3-ICDm in figure 10B and as has been shown for the non-receptor tyrosine kinase FYN, after which the membrane anchor is modeled.<sup>152</sup> On the other hand, palmitoylation alone is sufficient in localizing proteins to the plasma membrane, however, this association is not stable.<sup>153</sup> Therefore, a fraction of the primarily cytosolic PLPPR3-ICDc can be expected to be found at the plasma membrane, as is also seen in figure 10B. Thus, it is likely that PLPPR3-ICDm and PLPPR3-ICDc may both be targeted by the same kinases at the plasma membrane.

All but one phosphosite found uniquely in the membrane-bound PLPPR3-ICDm-His have never been reported before. It is possible that stable membrane anchoring by two fatty acid modifications enabled the detection of phosphorylation sites that are more transient in nature and therefore difficult to detect in tissue, where native proteins are dynamically trafficked between subcellular compartments. However, it should be kept in mind that as HEK293 cells are immortalized and tumorigenic,<sup>154</sup> they may have abnormal signaling activity causing aberrant phosphorylation. Therefore, future experiments could test the functionality of these phosphorylation sites in neurons.

The high density of phosphorylation sites in PLPPR3 intracellular domain overall raises a question on the functionality of these sites. Many in the field have proposed that in a crowded cell environment, numerous non-functional phosphorylation events may arise due to random encounters between promiscuous kinases and highly similar kinase recognition motifs.<sup>149</sup> This may be especially true in disordered regions, which are highly accessible to kinases. Arguably, phosphorylation sites with an important function would be under evolutionary constraint, and indeed, validated functional phospho-sites have been shown to be significantly better conserved than phospho-sites with no known function.<sup>155,156</sup> Thus, it is generally proposed that conserved phosphorylation sites should be given a priority in the quest for regulatory functions. Analysis of sequence alignments showed that almost all PLPPR3 phosphorylated residues show high conservation across species, thus suggesting that the intracellular domain likely harbors numerous functional phosphorylation events. However, in addition to the precise phosphorylated residue, also the conservation of the kinase recognition motif is relevant.

Indeed, while there are regions that are highly conserved in the PLPPR3 intracellular domain (data not shown), most notably the stretch covering amino acids 343-377, many of the conserved phosphorylatable residues are embedded in less conserved sequence motifs which could interfere with kinase recognition. Thus, while conservation analysis provides support for the possibility of numerous functional phosphorylation sites in the PLPPR3 intracellular domain, only low-throughput validation can prove or disprove the functionality of these sites.

In summary, results presented in this section offer a starting point for future studies into PLPPR3 regulation by phosphorylation. The PhosTag assay as well as the newly generated intracellular domain constructs will be excellent tools to characterize PLPPR3 phosphorylation further, while the list of identified phosphorylation sites with additional data on conservation and predicted kinases will guide future research questions.

### 3. PLPPR3 S351 is a PKA phosphorylation site

---

Experiments in the previous section establish that PLPPR3 intracellular domain is phosphorylated at multiple sites. Online prediction tools that analyze sequence motifs recognized by specific kinases propose that PLPPR3 could be phosphorylated by multiple well-studied kinases, such as CDK5, GSK3, PKA and PKC (Table 1). I next set out to directly test whether any of those kinases phosphorylates PLPPR3.

#### 3.1. PKA phosphorylates PLPPR3 at S351

I tested multiple predicted kinases in an *in vitro* phosphorylation assay, focusing on those previously described in the regulation of axonal development.<sup>132,157–159</sup> To this end, I made use of the PLPPR3 intracellular domain purified from *E. coli* in collaboration with my colleague Fatih Ipek. Although bacteria express many serine/threonine kinases that show homology to eukaryotic kinases,<sup>160</sup> recombinant eukaryotic proteins produced in bacteria are typically unphosphorylated. I tested this assumption in my PhosTag assay and confirmed that indeed the bacterially purified PLPPR3 intracellular domain was minimally phosphorylated (Figure 12A). Next, I phosphorylated the intracellular domain with commercially available purified kinases. Control sample treated with H<sub>2</sub>O separated into multiple phosphorylation bands, likely due to slight differences in gel electrophoresis time (Figure 12B) compared to figure 12A. Furthermore, the most prominent band in the control sample was the uppermost band. To check for possible protein degradation, I added a Lambda phosphatase control to another replicate, which confirmed that the lowermost band is the unphosphorylated band and not degraded protein (data not shown). Curiously, I found a prominent shift towards higher PLPPR3 phosphorylation state with PKA. While GSK3 $\beta$  alone did not appear to phosphorylate PLPPR3, phosphorylation with PKA followed by addition of GSK3 $\beta$  had an added effect on phosphorylation levels. This suggests that PKA may act as a priming kinase for GSK3 $\beta$  in the phosphorylation of PLPPR3 intracellular domain, as has been described for other GSK3 substrates, such as TAU.<sup>161</sup> In contrast, neither CDK5 nor FYNA had an effect on PLPPR3 phosphorylation. These results indicate that PKA, and likely GSK3 $\beta$  can phosphorylate PLPPR3 intracellular domain *in vitro*.

PKA is an interesting candidate kinase for PLPPR3, as extensive literature links PKA activity as important signaling mediator in neuronal morphogenesis, including the generation of neuronal filopodia<sup>132,134,162</sup> and the control of axon branching.<sup>73,163</sup> Thus, I next tested whether PKA can also induce PLPPR3 phosphorylation in cells. PKA preferentially phosphorylates substrate motifs with basic residues, particularly motifs exhibiting two arginines at P-6 and P-3, or at P-3 and P-2 positions, and a hydrophobic amino acid at P+1 position, where P is the phosphorylated serine or threonine.<sup>164–166</sup> Prediction tools propose four residues in the

PLPPR3 intracellular domain that could be targeted by PKA (see Table 1), however, only two of them were identified as true phosphorylation sites in our phospho-mass spectrometry analysis (see Table 2). These potential sites – S351 and S379 – are found in the membrane-proximal part of the intracellular domain (see graphic illustration of constructs in Figure 5).

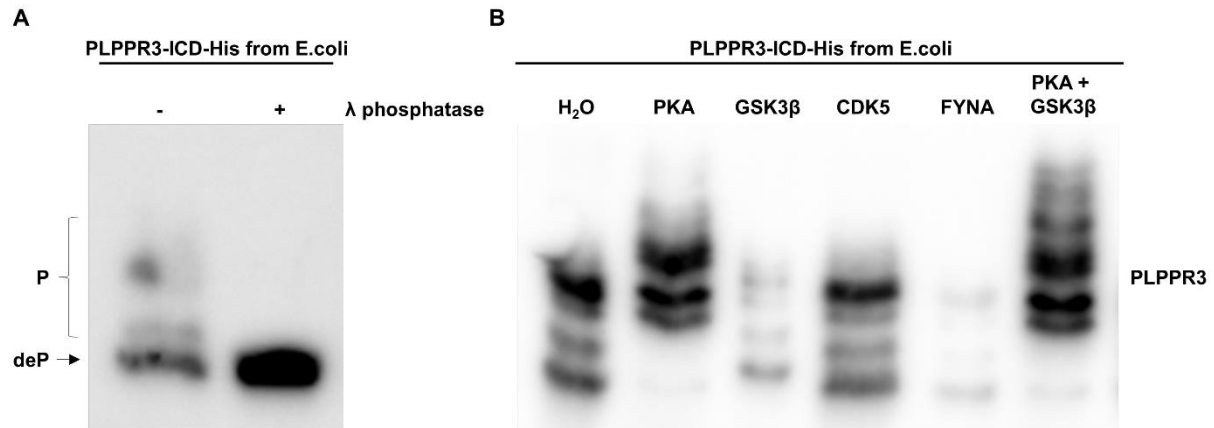
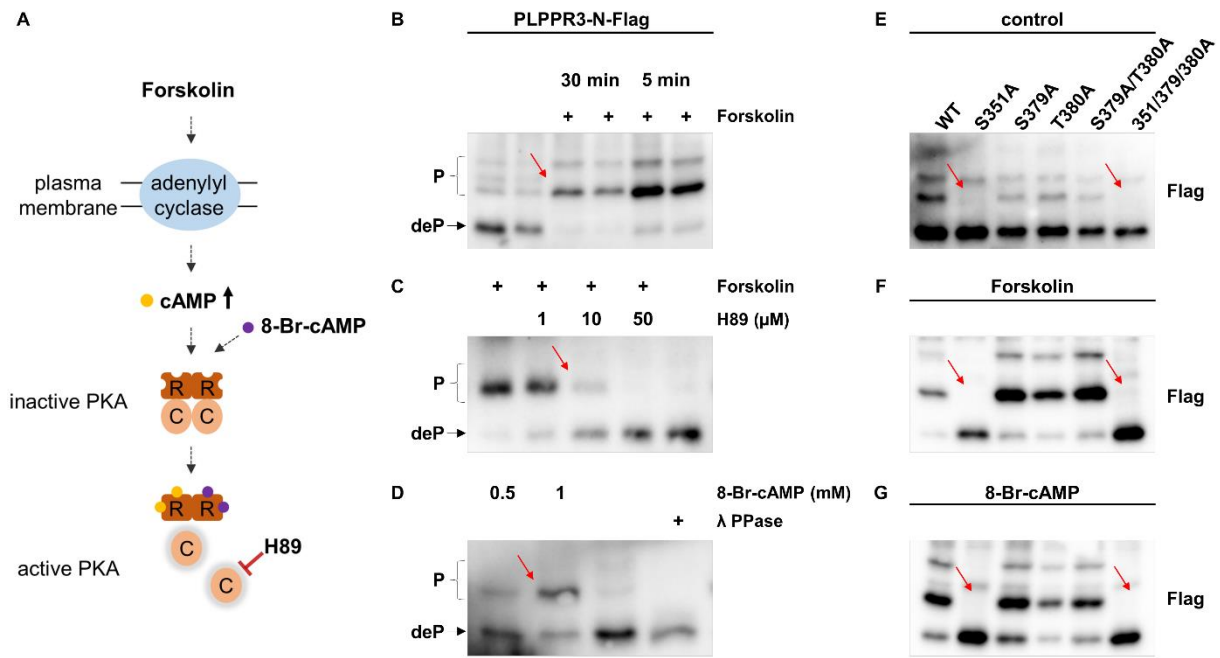


Figure 12. PKA phosphorylates PLPPR3 intracellular domain *in vitro*. (A) PLPPR3 intracellular domain purified from *E.coli* is minimally phosphorylated. 10 ng of purified protein was separated on 8% 50  $\mu$ M  $Mn^{2+}$  PhosTag gel and analyzed by western blot. Lambda phosphatase-treated sample annotates the migration height of the non-phosphorylated PLPPR3 band. (B) *In vitro* phosphorylation assay illustrates a significant shift towards phosphorylated form of the PKA treated sample, and there appears to be an additional effect of GSK3 $\beta$ . Purified PLPPR3 intracellular domain was incubated with indicated kinases in the presence of ATP for 2 hours. PKA + GSK3 $\beta$  sample was first incubated with PKA for 1 hour, then GSK3 $\beta$  was added for another 1 hour of incubation. Samples were analyzed by 8% 50  $\mu$ M  $Mn^{2+}$  PhosTag western blot.

There are multiple well-established tools to manipulate PKA activity in cells (Figure 13A). PKA is activated by the second messenger cAMP,<sup>167</sup> which is generated by adenylyl cyclases at the plasma membrane.<sup>168</sup> cAMP binds to PKA regulatory subunits, thereby releasing the catalytic subunits, which then phosphorylate PKA targets.<sup>169</sup> Forskolin, a labdane diterpene produced by the plant Blue Spur Flower (*Coleus barbatus*), activates PKA by directly stimulating adenylyl cyclases,<sup>170</sup> while a membrane permeable cAMP analog, 8-Br-cAMP, can be used to activate PKA by binding to the regulatory subunits.<sup>171</sup> PKA catalytic subunit can be blocked by a small molecule inhibitor H89, which competitively binds to the ATP site.<sup>172</sup>

To this end, I transfected N1E-115 cells with PLPPR3-N-Flag, serum-starved cells overnight to reduce overall phosphorylation levels, and stimulated the cells with 10 or 30  $\mu$ M Forskolin for 5 or 30 minutes. Cell lysates were harvested as before, and analyzed using PhosTag SDS-PAGE. As shown in Figure 13B, both Forskolin concentrations induced a prominent phosphorylation band in PLPPR3-N-Flag, and it appeared that 5 minutes of stimulation was more robust than 30 minutes, likely due to gradual return to steady-state over time.



**Figure 13. PKA phosphorylates PLPPR3 S351 in cells.** (A) Graphic illustration of mechanism of PKA modulating drugs used in this section. Forskolin activates adenylyl cyclases at the plasma membrane, increasing cellular cAMP concentration. cAMP and its analog 8-Br-cAMP bind to the regulatory subunits of PKA holoenzyme, leading to the dissociation and activation of the catalytic subunits. The small molecule inhibitor H89 competitively binds to the ATP binding site of catalytic subunit and thus inhibits its activity. R: regulatory subunit, C: catalytic subunit. (B) Forskolin stimulation induces the phosphorylation of PLPPR3-N-Flag in cells. N1E-115 cells were stimulated with 30  $\mu$ M Forskolin for 5 or 30 minutes. (C) Phosphorylation of PLPPR3-N-Flag is inhibited by increasing doses of PKA inhibitor H89. N1E-115 cells were preincubated with respective doses of H89 for 1 hour prior to stimulation with 30  $\mu$ M Forskolin for 5 minutes. (D) Stimulation with cAMP analog 8-Br-cAMP induces phosphorylation of PLPPR3-N-Flag. N1E-115 cells were stimulated with 0.5 or 1 mM of 8-Br-cAMP for 5 minutes. Comparison of phosphorylation patterns of PLPPR3-N-Flag mutants in steady-state condition (E), after 5 minute stimulation with 30  $\mu$ M Forskolin (F) and after 5 minute stimulation with 1 mM 8-Br-cAMP (G) identifies S351 as PKA phosphorylation site. In (B)-(D), (F) and (G), N1E-115 cells were serum-starved overnight. Protein lysates were separated on 8% 50  $\mu$ M  $Mn^{2+}$  PhosTag gels and analyzed by western blot. Red arrows annotate changes in phosphorylation pattern.

I next tested whether PKA inhibition can prevent phosphorylation caused by Forskolin activation. Indeed, pre-incubation with increasing concentrations of PKA inhibitor H89 led to a dose-dependent disappearance of the phosphorylation band in the PLPPR3-N-Flag (Figure 13C). Finally, I asked whether the second messenger cAMP can induce changes in the phosphorylation of PLPPR3. As seen on Figure 13D, 8-Br-cAMP induced a prominent phosphorylation band in PLPPR3-N-Flag after 5 minutes of stimulation. Notably, both Forskolin and 8-Br-cAMP induced the same distinct phospho-band directly above the established non-phospho band, indicating it may represent a specific phosphorylation event. These results support the idea that PKA activity in cells induces the phosphorylation of PLPPR3 intracellular domain.

I then asked which of these potential sites in PLPPR3-N-Flag is a *bona fide* PKA phosphorylation site. To investigate this, I mutated the two predicted serine residues – S351 and S379 – and T380, which also matches the PKA motif and was identified as a phosphorylation site in our screen (see Table 2), to alanine using site-directed mutagenesis. To account for the potential lack of single-band resolution, I also created S379 and T380 double mutant and a triple mutant. Surprisingly, PhosTag blot analysis showed that under steady-state culture conditions, the S351A mutant lacks the distinct phospho-band that could be modulated with PKA affecting drugs (Figure 13E, compare to Figures 13B, C and D). A comparable phosphorylation pattern was seen for the S351/S379/T380 triple mutant, while the other three mutants did not affect the basal PhosTag band pattern of PLPPR3-N-Flag. I also used Forskolin (Figure 13F) and 8-Br-cAMP (Figure 13G) to stimulate PKA activity in cells expressing PLPPR3 mutant variants. Neither the S351A nor the triple mutant could be phosphorylated in response to PKA activation, while S379A, T380A as well as the S379A/T380A double mutant showed the appearance of the distinct single phosphorylation band associated with PKA modulation in my assay. Taken together, these experiments unequivocally identify PLPPR3 S351 as PKA phosphorylation site and confirm a single band resolution of this site when analyzing PLPPR3-N-Flag on PhosTag SDS-PAGE.

### **3.2. Other phosphorylation events in the intracellular domain of PLPPR3**

While there are no classical PKA recognition motifs in the PLPPR3 distal C-terminus, I nevertheless decided to test whether PKA activity could lead to changes in the phosphorylation of PLPPR3-Cm-Flag. Indeed, using the same experimental setup as in figure 13B, I observed changes in the phosphorylation pattern of PLPPR3-Cm-Flag following Forskolin stimulation of N1E-115 cells (Figure 14A). On the one hand, there is an apparent increase in intensity of the lowest phosphorylation band. On the other hand, a simultaneous decrease of a higher phosphorylation band is observed. Therefore, PKA-dependent phosphorylation may also regulate PLPPR3 distal C-terminus.

The most frequently predicted kinase for PLPPR3 intracellular domain was PKC, which was predicted to target a total of 11 potential sites (Table 1). PKC is known to phosphorylate substrates that regulate filopodia formation<sup>173</sup> and axonal branching,<sup>174</sup> making it an interesting candidate kinase for phosphorylating PLPPR3. I therefore tested whether direct activation of PKC leads to phosphorylation of PLPPR3 in cells. To this end, I made use of phorbol 12-myristate 13-acetate (PMA), a known activator of PKC.<sup>175</sup> PMA stimulation induced a distinct phosphorylation band in PLPPR3-N-Flag (Figure 14B, left), and a strong shift in phosphorylation in the PLPPR3-Cm-Flag (Figure 14B, right), suggesting that there may indeed be multiple PKC phosphorylation sites in the PLPPR3 intracellular domain.

Overall these experiments indicate that, in addition to PKA, the PLPPR3 intracellular domain may be a substrate for PKC as well as GSK3 $\beta$  (see *in vitro* phosphorylation data in section 3.1).

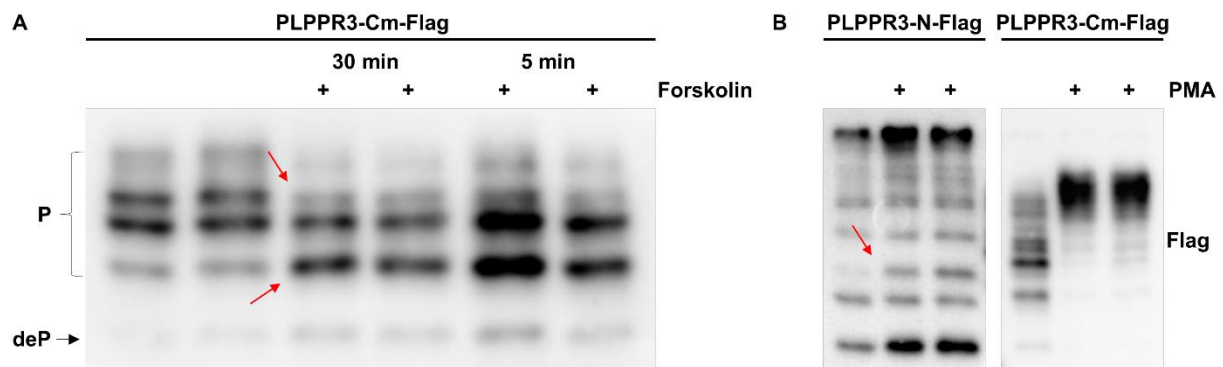


Figure 14. Other phosphorylation events in the intracellular domain of PLPPR3. (A) Forskolin stimulation induces PKA-dependent phosphorylation in the distal C-terminus of PLPPR3. N1E-115 cells were stimulated with 30  $\mu$ M Forskolin for 5 or 30 minutes. (B) PKC activation in cells leads to phosphorylation of PLPPR3-N- and C-terminus. N1E-115 cells were stimulated with 1  $\mu$ M PMA for 10 minutes. In (A) and (B), cells were starved overnight prior to stimulation, lysed, and analyzed by 8% 50  $\mu$ M Mn<sup>2+</sup> PhosTag western blot. Red arrows annotate changes in phosphorylation pattern.

### 3.3. Discussion and outlook

The experiments presented in this section establish S351 as a *bona fide* phosphorylation site of PKA in the PLPPR3 intracellular domain, and provide evidence that the intracellular domain is additionally targeted by GSK3 $\beta$  and PKC.

S351 is located within a region of the PLPPR3 intracellular domain that is highly conserved from zebrafish to human. By far the longest conserved region within the cytoplasmic C-terminus, it stretches from R339 to R377 with only a few, mostly conservative substitutions. Notably, it contains multiple other conserved residues that were identified as phosphorylation sites in my mass spectrometry screen: S343, S346, S361, S372 and T374. It is tempting to speculate that these phosphorylation sites may jointly regulate the function of this domain. Multisite phosphorylation is a relatively common mechanism that allows for fine-tuning of protein function and/or convergence of multiple signaling pathways on a single protein.<sup>176</sup> Future studies could firstly investigate the importance of this conserved region in PLPPR3 function by using deletion mutants. Phospho-dead mutants would help explore the role of phospho-regulation in this function. To this end, it would be informative to study mutants of single phospho-sites as well as combinations of sites.

Notably, the motif flanking S351 is one of the few regions of the intracellular domain that is conserved between different PLPPR family members (see Figure 2E, stretch of hydrophobic

and positively charged residues). All PLPPRs have a hydrophobic amino acid at positions 447 and 452, and a positively charged amino acid at positions 448 and 449, the only exception being PLPPR1 that has a non-conservative substitution at position 449 (amino acid numbering based on PLPPR3). This conserved motif has been proposed as one of the candidate regions for filopodia formation function in PLPPRs (see Introduction).<sup>99</sup> However, only PLPPR2 has retained a phosphorylatable serine in this motif, PLPPR1 has an already negatively charged aspartic acid, while PLPPR4 and PLPPR5 have a polar asparagine. This would argue against S351 phosphorylation being the molecular switch determining PLPPR3-induced filopodia formation. It is of interest that whichever molecular event phosphorylation of S351 triggers, the molecular switch would always be at “on” position for PLPPR1, as aspartic acid is highly similar to phosphorylated serine and serves as “phospho-mimic”. In the same vein, the molecular switch would always be “off” for PLPPR4 and PLPPR5. A unifying factor for PLPPR1 and PLPPR3 is their localization in axonal membranes of polarized neurons, as opposed to PLPPR4 and PLPPR5, which localize to dendrites.<sup>99</sup> Thus, this region could mediate axon-specific functions that are silenced in dendritic PLPPRs. Future research could investigate the role of this conserved motif in filopodia formation using deletion mutants. Whether the phosphorylation event serves as an additional layer for fine-tuning, or a different, PLPPR1, PLPPR2 and PLPPR3-specific function, could be investigated using site-directed mutagenesis. Experiments carried out in this section could be repeated with PLPPR2 to investigate whether it also serves as a substrate for PKA. Overall, compelling clues hint at the importance of this conserved region in the function of PLPPR3.

My experiments provide evidence that PLPPR3 may be phosphorylated by PKA at multiple sites. PKA activation in cells led to complex changes in the phosphorylation pattern of the distal C-terminus of PLPPR3. The increase in intensity of one phosphorylation band with the simultaneous decrease of another may indicate regulation by multiple kinases, where PLPPR3 phosphorylation by PKA suppresses phosphorylation by another kinase either directly or indirectly. In the direct model, phosphorylation by PKA could lead to changes in conformation that no longer allow access for another kinase. Alternatively, PKA-dependent phosphorylation could interfere with the binding of another kinase. In the indirect model, activation of PKA could lead to PKA-dependent inhibition of another kinase’s activity, as has been described for GSK3.<sup>126</sup> None of the other phosphorylation sites uncovered in the mass spectrometry analysis (Table 2) fit the classical PKA substrate motif, however, it is possible that our mass spectrometry analysis did not identify phosphorylation events that are more rare or transient in nature. To this end, S581 could be a potential candidate (see Table 1). Due to lack of complete single band resolution of PLPPR3-N-Flag on PhosTag SDS-PAGE, I cannot entirely rule out the possibility that S379 and T380 are also targeted by PKA. To investigate whether PKA

targets other sites in the PLPPR3 intracellular domain, a good starting point would be *in vitro* phosphorylation combined with mass spectrometry. Alternatively, PKA activation could be stimulated with Forskolin in cells, and purified PLPPR3 could then be analyzed by mass spectrometry.

GSK3 $\beta$  is another kinase that likely targets PLPPR3 intracellular domain. The typical GSK3 phosphorylation site includes a phosphorylated serine or threonine at P+4 or P+5 position C-terminal to the target serine or threonine.<sup>177,178</sup> It is tempting to speculate that S346, T560 and/or S570 could therefore be candidate sites for GSK3 phosphorylation. Manipulating GSK3 activity in cells with either activators, such as insulin, or inhibitors could verify whether GSK3 can also target PLPPR3 intracellular domain in cells. The optimized PhosTag western blot will be a useful tool in this analysis.

Finally, my experiments propose that PLPPR3 intracellular domain is also a substrate for PKC, which can target both the proximal as well as distal part of the C-terminus in a cell-based assay (Figure 14B). In the membrane-proximal intracellular domain, PKC induces changes in a single phosphorylation band, while in the distal C-terminus it triggers a major shift towards higher-order phosphorylated form, suggesting multiple phosphorylation events. This is in good agreement with prediction data (Table 1), which propose that 9 out of 11 predicted PKC sites reside in the distal C-terminus. Some predicted PKC sites that were also identified in our mass spectrometry screen include S346 and S505, which could be interesting candidates worth testing in the future.

## 4. Generation and validation of PLPPR3 pS351-specific antibody

---

Experiments in the previous section establish PLPPR3 S351 as *bona fide* PKA phosphorylation site. While PhosTag blot was a useful tool for the initial characterization of this site, a major drawback of this method was the lack of good separation of full-length recombinant or endogenous PLPPR3 protein (see Figure 8B and C). Therefore, PhosTag is only partly applicable for the study of PLPPR3 phosphorylation. In addition to this, PhosTag only allows us to study protein phosphorylation in biochemistry experiments. Thus, to further characterize PLPPR3 pS351, I set out to generate and validate a phospho-specific antibody.

In collaboration with Eurogentec, we immunized two rabbits with C+LKRApSVDVDLLA peptide under the standard 87 day program. The N-terminal cysteine allows the coupling of the peptide to the carrier protein KHL. Unfortunately, first attempt did not yield any target-specific antibodies (data not shown). In the second attempt, we tagged the peptide C-terminally and added an additional booster shot to the rabbit immunization protocol to increase the immune response. I tested the crude serum, which showed immunoreactivity with a protein of the right size in one rabbit. Eurogentec purified the serum of this animal using a two-step purification protocol where the serum is sequentially run through columns coupled with phospho-peptide and non-phospho peptide. This procedure yielded two fractions: the “phospho” fraction, with antibodies that bind specifically to the phospho-epitope, and the “pan” fraction, with antibodies that bind elsewhere in the peptide. I next set out to test the specificity of these antibodies.

### 4.1. Validation for western blot

Phospho-antibody validation is a two-step process, which requires careful confirmation of specificity towards the target protein (PLPPR3) as well as the modified epitope (pS351). I first tested the purified antibody fractions in western blot using protein lysates from N1E-115 cells expressing recombinant PLPPR3 variants. I included a non-transfected control in order to confirm specificity towards PLPPR3. S351A mutation, Forskolin stimulation and phosphatase treatment were used to confirm specificity towards phospho-S351. Parallel immunolabeling with house-made PLPPR3 antibody, which binds the distal C-terminus, confirmed the presence of equal levels of PLPPR3 intracellular domain in all protein lysates except the non-transfected control (Figure 15A, left blot). Both pan-S351 as well as phospho-S351 antibodies recognize recombinant PLPPR3 intracellular domain specifically, as illustrated by lack of reactivity with non-transfected cell lysates (Figure 15A, middle and right blots). We expected the phospho-antibody to detect phospho-signal also in nonstimulated cells, as our phospho-mass spectrometry experiment showed that PLPPR3 S351 is phosphorylated in steady-state conditions (Table 2). Surprisingly, both pan-S351 and phospho-S351 antibodies were

phospho-specific: there was a clear increase in signal in response to stimulation with PKA activator Forskolin, while neither of the antibodies recognized S351A mutant nor dephosphorylated PLPPR3 intracellular domain. The only difference between the two antibody fractions was the decreased band intensity of the phospho-S351 antibody, which could be due to lower affinity or concentration of antibodies in this fraction. Surprisingly, testing the crude anti-sera on these samples proved that the serum indeed only contained phospho-specific antibodies, as the western blot looked identical to blots with purified antibodies (Figure 15B). In conclusion, these data demonstrate the specificity of pan-S351 and phospho-S351 antibodies towards the PLPPR3 phospho-S351 epitope and validate their use in western blot application. Due to slightly more robust reactivity of the pan-S351 antibody, I decided to use this fraction in the following western blot experiments.

I next tested the specificity of this antibody towards endogenous PLPPR3 protein. To this end, I used protein lysates from primary hippocampal neurons cultured for nine days, as this is when PLPPR3 expression peaks in culture.<sup>88</sup> Neurons from *Plppr3*<sup>-/-</sup> mice were used as a control to test specificity towards PLPPR3, and Forskolin stimulation was used to test specificity towards phosphorylated S351. Immunolabeling with house-made PLPPR3 antibody confirmed the presence of equal levels of PLPPR3 in both *Wt* protein lysates, while showing no reactivity in the *Plppr3*<sup>-/-</sup> samples (Figure 15C, left blot). Tubulin labeling was used as a loading control to confirm the presence of protein in all samples. Immunolabeling with pan-S351 demonstrated that the antibody is specific for endogenous PLPPR3 as it does not label proteins in the *Plppr3*<sup>-/-</sup> samples, and a significant increase in band intensity after stimulation with Forskolin indicates specificity towards phosphorylated S351 (Figure 15C, right blot). Both the PLPPR3 and pan-S351 antibodies recognized high molecular weight PLPPR3 at the top of the running gel, possibly accounting for higher-order, oligomerized protein (Figure 15C, red arrow). The pan-S351 antibody recognized another protein around the 250 kDa mark specifically after Forskolin stimulation in both *Wt* and *Plppr3*<sup>-/-</sup> samples (Figure 15C, red asterisk). This band likely represents a protein with a very similar PKA phosphorylation motif. Given that the non-specific band is of different molecular weight than PLPPR3, it will not interfere with the analysis of PLPPR3 pS351 in western blot. In summary, these experiments illustrate that the generated antibody specifically recognizes both recombinant as well as endogenous PLPPR3 pS351 in western blot, making it a useful tool for biochemistry experiments.

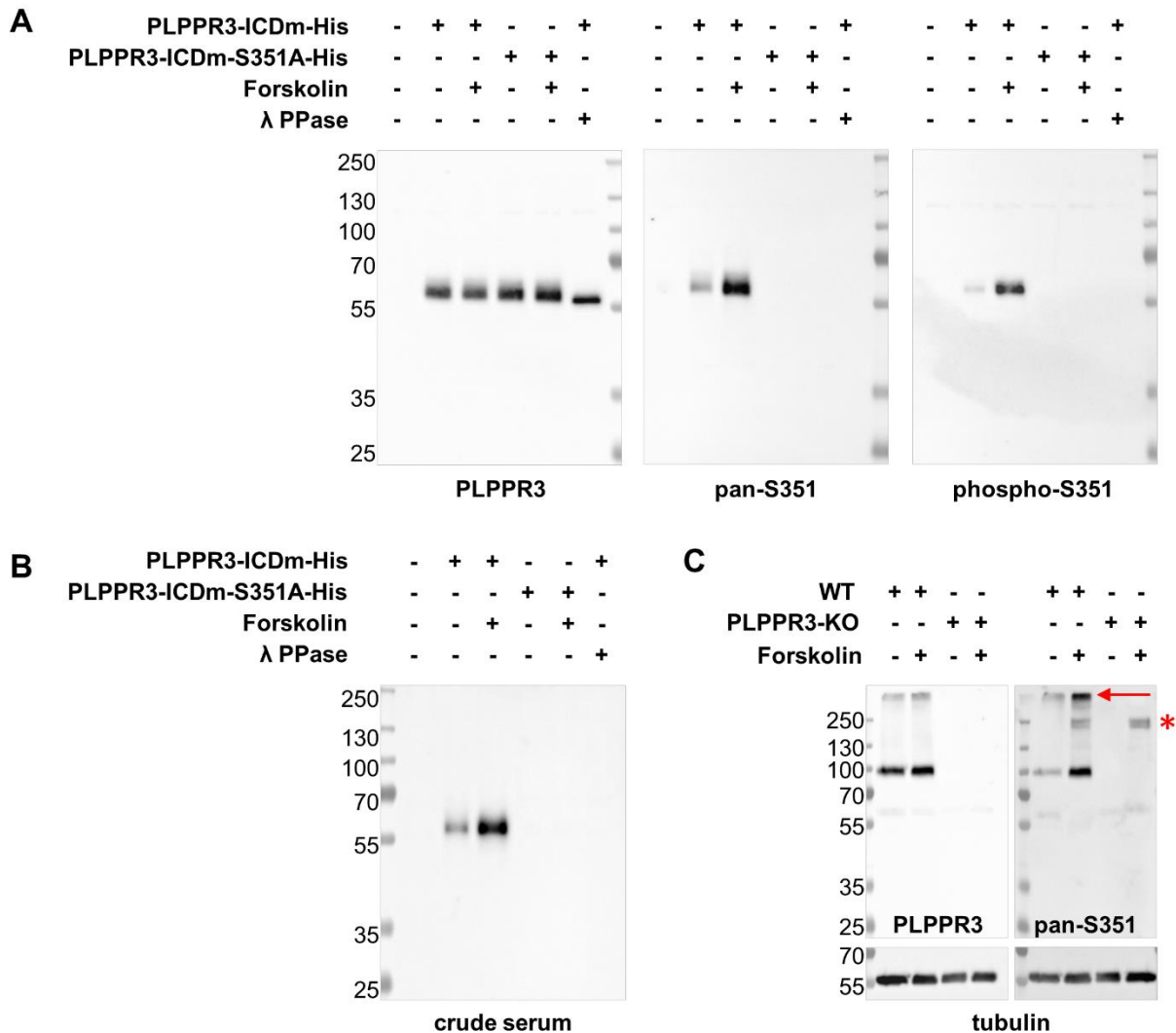


Figure 15. Validation of PLPPR3 phospho-S351 antibody in western blot. (A) Both pan-S351 and phospho-S351 antibodies are specific for recombinant PLPPR3 pS351. PLPPR3 intracellular domain variants were expressed in N1E-115 cells, stimulated with 30  $\mu$ M Forskolin for 5 minutes, and protein lysates were prepared. Lambda phosphatase-treated sample was used as non-phosphorylated control. (B) Crude serum from host rabbit contains only phospho-specific antibodies. Same samples as in (A) were used. (C) PLPPR3 pan-S351 antibody is specific for endogenous PLPPR3 pS351. Primary hippocampal neurons from Wt and *Plppr3*<sup>-/-</sup> mice were cultured for 9 days, stimulated with 30  $\mu$ M Forskolin for 10 minutes, and protein lysates were prepared. Red arrow annotates higher-molecular weight, likely oligomerized PLPPR3. Red asterisk annotates non-specific bands. Antibodies in (A) and (C) were used 1:1000, except for tubulin which was used 1:5000. Crude serum in (B) was used 1:500.

## 4.2. Validation for immunocytochemistry

I next tested whether the PLPPR3 pS351 antibody is also a useful tool for immunocytochemistry. There are significant differences in antibody performance between applications: antibodies that recognize well the denatured linearized motifs in western blot may not recognize, or have access to, epitopes in immunocytochemistry, where proteins are in semi-native conformation. Thus, to account for possible differences in performance, I tested

both the pan-S351 as well as the phospho-S351 fractions. I transfected N1E-115 cells with PLPPR3 intracellular domain variants using Lipofectamine, which regularly achieves transfection efficiency >60% in cell lines. Following transfection, cells were serum-starved overnight to decrease extracellular signaling and thus overall phosphorylation levels. Cells were fixed using 4% PFA, permeabilized and immunolabelled using standard protocol (see Materials and methods). F-actin dye Alexa-Fluor 488 phalloidin was used to counterstain all cells. As in western blot experiments, specificity towards PLPPR3 was tested using non-transfected controls, and specificity towards phosphorylated S351 was tested using S351A mutant and Forskolin stimulation. Control labeling with our in-house generated PLPPR3 antibody showed specific labeling in all PLPPR3-ICDm-transfected cells (Figure 16A).

As illustrated in Figure 16 panels B and C, neither the pan-S351 nor phospho-S351 antibodies labelled non-transfected N1E-115 cells. Pan-S351 antibody labelled serum-starved cells expressing PLPPR3-ICDm-His, while signal of phospho-S351 antibody is barely above background levels. In Forskolin stimulated cells, both antibodies show immunoreactivity. Because labeling intensity depends on the relative expression level of PLPPR3 intracellular domain in each cell, it was not possible to assess whether Forskolin led to an increase of signal in this experiment. Neither of the antibodies reacted with cells expressing PLPPR3-ICDm-S351A-His. Overall, these immunocytochemistry data are in good agreement with western blot data, which show specificity of both antibodies towards the PLPPR3 pS351, with the pan-S351 antibody showing higher efficiency. For simplicity, from here on, the pan-S351 antibody will be referred to as pS351 antibody.

In the next stage of validation, I tested the phospho-PLPPR3 antibody on endogenous PLPPR3 in neurons. To this end, I used primary hippocampal neurons at 6 days *in vitro*, which is the time point when PLPPR3 expression is nearing its peak, while it is still possible to differentiate individual neuronal processes in dense cultures. Neurons from *Plppr3*<sup>-/-</sup> mice served as a negative control, while neurons stimulated with Forskolin were used as a positive control. Coverslips were fixed with 4% PFA, permeabilized and immunolabelled for pS351 and  $\alpha$ -tubulin, which was used as counterstain to visualize all neurites. Unfortunately, pS351 antibody labelling was comparable in *Wt* and *Plppr3*<sup>-/-</sup> neurons, indicating high level of unspecific binding (Figure 17). In particular, the antibody strongly labelled cell bodies, and with comparable intensity both dendrites and axons. No labeling was observed in structures with high local levels of PLPPR3, such as filopodia or growth cones. Furthermore, Forskolin stimulation did not induce any noticeable changes in immunolabeling intensity or localization.

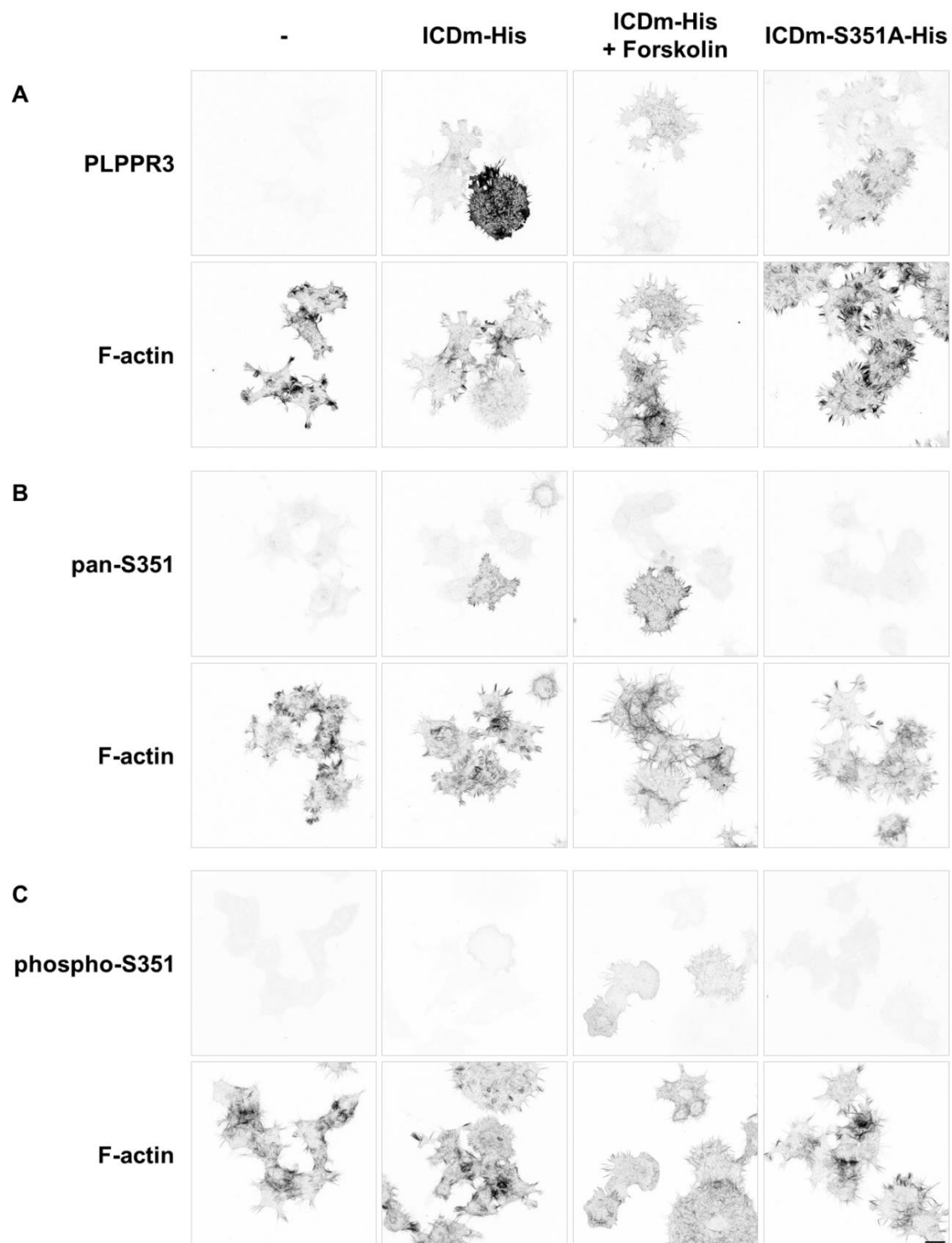


Figure 16. Validation of PLPPR3 phospho-S351 antibody in immunocytochemistry with recombinant PLPPR3. N1E-115 cells were labeled with (A) house-made PLPPR3, (B) pan-S351 or (C) phospho-S351 antibodies. Cells were transfected with respective constructs and starved overnight in serum-free medium prior to stimulation with 30  $\mu$ M Forskolin for 20 minutes. F-actin dye was used to counterstain all cells. Previously validated house-made PLPPR3 antibody was used as a positive control. Scale bar = 10  $\mu$ m.

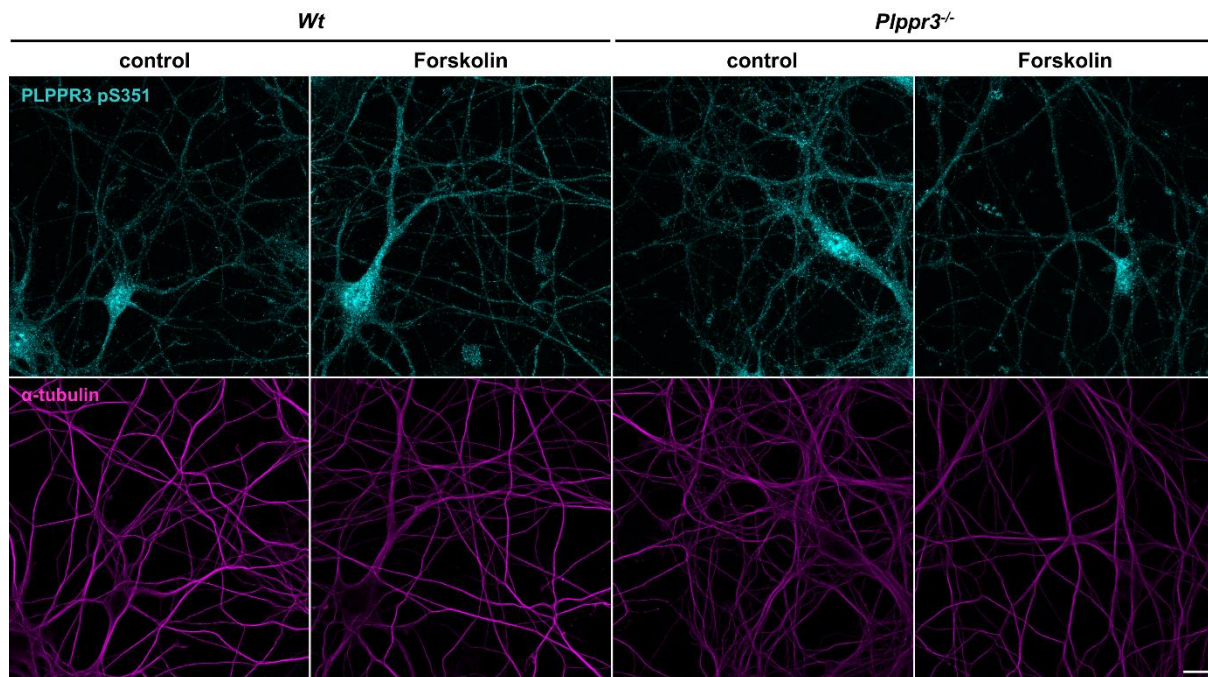


Figure 17. PLPPR3 pS351 antibody testing in Wt and *Plppr3*<sup>-/-</sup> primary hippocampal neurons fixed with 4% PFA. pS351 antibody shows a high level of non-specific labelling as evidenced by comparable signal intensity in Wt and *Plppr3*<sup>-/-</sup> cells. Neurons were stimulated with Forskolin (30  $\mu$ M, 10 minutes) at 6 DIV, fixed and immunolabelled for PLPPR3 pS351 and  $\alpha$ -tubulin. Scale bar = 10  $\mu$ m.

As the antibody showed promising results in overexpression approach, I hypothesized that the lack of specific labeling in neurons could be due to inaccessibility of the pS351 epitope in the crowded axonal environment. Although PFA is the most widely used chemical for cell and tissue fixation,<sup>179</sup> it is not suitable for all applications. PFA cross-links nearby molecules into a tight meshwork,<sup>180</sup> which in some cases may make them inaccessible to antibodies and thus interfere with immunolabeling. Antigen retrieval is a method often used in immunohistochemistry, which uses enzymes or heat to reduce PFA-induced cross-links and thus unmask the epitopes.<sup>181,182</sup> I tested whether antigen retrieval improves the immunolabeling of PLPPR3 pS351 in primary hippocampal neurons. To this end, I incubated the coverslips in citrate buffer at 92°C for five minutes prior to immunolabeling. Antigen retrieval did not improve immunolabeling, but caused damage to cell morphology in most instances (data not shown). Therefore, I concluded that poor labeling of PLPPR3 pS351 is unlikely a side effect of epitope masking due to PFA fixation.

Another reason for poor labeling of PLPPR3 pS351 in neurons could be the conformation of PLPPR3 in native conditions, which could make the antibodies not recognize the epitope, or physically restrict access of antibodies in crowded cellular environment. This may be especially relevant for antibodies generated by immunization with short peptides, such as phospho-antibodies, which are more likely to recognize linear motifs. Using organic solvents for fixation

could help overcome this issue. Organic solvents, such as methanol, work by removing lipids in the cell membrane, dehydrating the cell and thus precipitating and denaturing the proteins.<sup>183</sup> In many instances, this leads to unmasking of epitopes and better labeling.<sup>184</sup> Therefore, I tested whether methanol fixation improves the immunolabeling of PLPPR3 pS351 in neurons. Neurons were fixed with ice cold methanol on ice for five minutes and immunolabelled for pS351 and  $\alpha$ -tubulin. As seen in Figure 18, methanol fixation indeed improved labeling in structures with higher levels of PLPPR3 such as growth cones and filopodia (yellow thick arrows), and also improved  $\alpha$ -tubulin labeling. However, while specific pS351 labeling improved, non-specific labeling remained prominent in *Wt* and *Plppr3*<sup>-/-</sup> samples. Most notably, in these preparations, the pS351 antibody strongly labelled processes from non-neuronal cells, presumably astrocytes (yellow thin arrow). As with PFA fixed neurons, Forskolin stimulation did not lead to an increase in signal intensity. Importantly, methanol fixation was detrimental to cell morphology and led to degenerative swelling of neuronal processes (white arrows).<sup>185</sup>

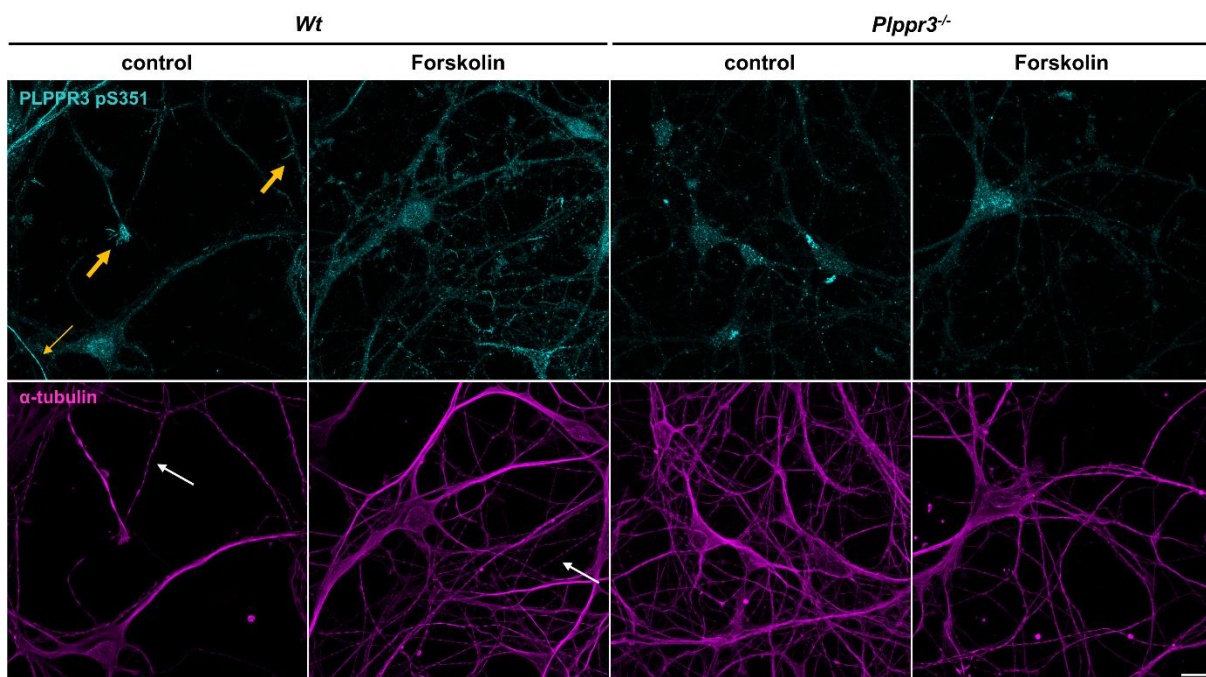


Figure 18. PLPPR3 pS351 antibody testing in *Wt* and *Plppr3*<sup>-/-</sup> primary hippocampal neurons fixed with methanol. pS351 antibody shows specific labeling in filopodia and growth cones (yellow thick arrows), while a high level of non-specific labelling is present in cell bodies and non-neuronal processes (yellow thin arrow). Methanol fixation led to notable degeneration of neuronal processes (white arrows). Neurons were stimulated with Forskolin (30  $\mu$ M, 10 minutes) at 6 DIV, fixed and immunolabelled for PLPPR3 pS351 and  $\alpha$ -tubulin. Scale bar = 10  $\mu$ m.

A sequential fixation by PFA and methanol has been recommended to combine the benefits of both methods: prior PFA fixation helps to preserve cellular morphology, while methanol treatment increases accessibility of epitopes.<sup>186</sup> I also tested this combined fixation method in my primary hippocampal neurons, however, it did not lead to improved labeling (data not

shown). In conclusion, I was not able to validate the use of PLPPR3 pS351 antibody for immunocytochemistry approaches.

### 4.3. Validation for immunohistochemistry

Finally, I attempted to validate the PLPPR3 pS351 antibody for immunohistochemistry. To this end, we prepared brain slices from postnatal day six (P6) *Wt* and *Plppr3<sup>-/-</sup>* pups. At P6, PLPPR3 levels in the brain are still elevated after peaking at P1,<sup>88</sup> while handling of brain sections is significantly easier than at P1. Brains were fixed in 4% PFA for 48 hours, followed by sequential incubation in 15% and 30% sucrose for 24 hours each. 80  $\mu$ m thick coronal slices were prepared on vibratome and sections with hippocampus and corpus callosum were used for immunolabeling. I used neuronal cell adhesion molecule L1 (NCAM-L1), which is expressed in most developing axons<sup>187</sup> as a marker for axonal tracts, and H $\ddot{o}$ chst to label nuclei.

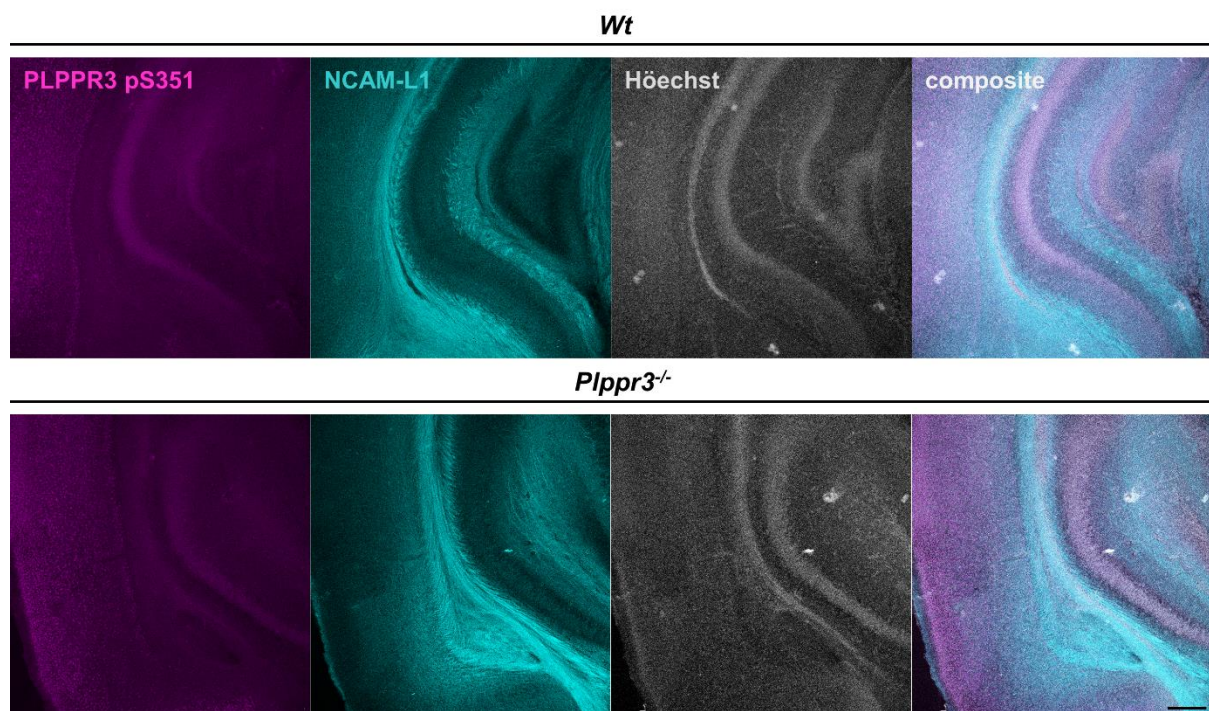


Figure 19. PLPPR3 pS351 antibody testing in *Wt* and *Plppr3<sup>-/-</sup>* postnatal day 6 brain sections. pS351 labeling is comparable in *Wt* and *Plppr3<sup>-/-</sup>*. A high level of non-specific labelling is present in cell bodies where it co-localizes with H $\ddot{o}$ chst labeling, while little overlay is detected with the axonal marker NCAM-L1. Scale bar = 200  $\mu$ m.

Unfortunately, PLPPR3 pS351 antibody is also unspecific in immunohistochemistry (Figure 19). Labeling intensity was comparable in *Wt* and *Plppr3<sup>-/-</sup>* brain sections across all analyzed brain areas. While PLPPR3 shows high co-localization with the axonal marker NCAM-L1 in axonal tracts,<sup>88</sup> little overlay was detected between pS351 and NCAM-L1. Instead, pS351 antibody showed significant overlay with nuclear staining in hippocampus and the cortex in both *Wt* and *Plppr3<sup>-/-</sup>*. I also performed antigen retrieval in brain sections in an attempt to improve labeling. To this end, sections were incubated in citrate buffer at 92°C for 10 minutes

prior to immunolabeling. Antigen retrieval did not lead to improvement of pS351 labeling, but decreased labeling quality of NCAM-L1 (data not shown). In conclusion, I could not validate the pS351 antibody for immunohistochemistry.

#### **4.4. Discussion and outlook**

Experiments presented in this section establish that the generated PLPPR3 pS351 antibody is specific in western blot applications, and immunocytochemistry when PLPPR3 is overexpressed in cell lines, and thus validate its use in these approaches. I could not validate the use of this antibody in immunolabeling in primary neurons or brain tissue due to high levels of non-specific binding. Thus, for now, this antibody has limited applicability.

The non-specific signal likely comes from an epitope with a highly similar sequence. In the generation of a phospho-specific antibody, only a short sequence flanking the phospho-residue is used, which often includes the kinase recognition motif. As kinase recognition motifs are relatively well conserved,<sup>143</sup> it is not surprising that the antibody would recognize other targets. Indeed, as seen in western blot experiment with primary neurons, an additional band appeared specifically after activating PKA signaling with Forskolin (Figure 15C), indicating binding to another PKA target.

Further optimization of immunolabeling protocol could be worth pursuing. In particular, methanol fixation protocol improved labeling of PLPPR3-rich structures in primary hippocampal neurons. To reduce non-specific binding, different blocking concentrations and reagents could be tested. In similar vein, different tissue fixation and preparation methods could be tested in combination with immunohistochemistry protocols to improve pS351 antibody specificity. Achieving specific labeling of PLPPR3 pS351, particularly in brain tissue, would be invaluable for advancing our knowledge of its function.

## 5. Functional studies

---

Experiments in chapter 3 establish that PLPPR3 is phosphorylated by PKA at S351. Sequence alignment across species show that this residue is in one of the well conserved regions of the PLPPR3 intracellular domain (Table 2), and data from proteomic discovery mass spectrometry show that pS351 is also present in brain (Table 1). Taken together, these data indicate that pS351 is a functional phosphorylation event. In the final part of my PhD, I set out to investigate the functional consequences of S351 phosphorylation. As described in introduction, the best-characterized phenotype of PLPPR3 to date is axon branch formation through induction of filopodia.<sup>88,188</sup> Therefore, I set out to investigate whether phosphorylation of S351 alters filopodia or axon branch formation.

### 5.1. Phosphorylation of PLPPR3 S351 can be triggered in primary neurons and in acute brain slices

Axonal branching is a developmentally regulated program that is initiated after axon specification. In culture, initiation of axonal branching program coincides with the steep increase of PLPPR3 expression between three to five days *in vitro*.<sup>88</sup> To investigate whether PLPPR3 pS351 levels are also dynamically regulated, I analyzed protein lysates from cultured primary hippocampal neurons at different developmental time points. Total PLPPR3 protein levels followed the dynamic pattern described previously, with expression levels upregulated between three and five days *in vitro* and peaking at nine days *in vitro* (Figure 20A). Overall, PLPPR3 pS351 level followed the same pattern as total PLPPR3, increasing between five to nine days *in vitro* and decreasing thereafter. However, the increase in pS351 levels was not as pronounced as in total PLPPR3 levels, and in relation to total PLPPR3 levels, phosphorylation of S351 may even be suppressed between five to nine days *in vitro*. Therefore, I decided to use Forskolin to see if I can trigger S351 phosphorylation in neurons (Figure 20B). Curiously, while PKA activation triggers increase in pS351 levels at all tested time points, the largest increase was observed at nine days *in vitro*. Therefore, as pS351 levels are increased similarly to PLPPR3 levels at a time neurons undergo axon growth and branching, it could indicate a function of pS351 in filopodia or branch formation.

Taking a step further, I was interested in testing whether I can induce PKA-dependent PLPPR3 phosphorylation in tissue. Acute brain slice is one of the most widespread models in experimental neuroscience.<sup>189</sup> In slice preparations, unlike in primary neuronal culture, the structural and functional integrity of intrinsic synaptic connections is maintained.<sup>190</sup> On the other hand, it offers significantly more experimental control than working with living animals. For example, it facilitates manipulations with drugs that would otherwise not cross the blood

brain barrier.<sup>189</sup> Thus, acute brain slice model is the intermediate step between 2D primary cultures and *in vivo* animal models.

I collaborated with Dr. Timothy Zolnik (Charité Universitätsmedizin Berlin) to obtain acutely prepared adolescent mouse brain slices. Coronal sections including the hippocampus and striatum were stimulated with 30  $\mu$ M Forskolin for 15 minutes in artificial cerebrospinal fluid with oxygen/carbon dioxide supply. Tissue was lysed to extract proteins and analyzed by western blot. I used AMPA receptor 1 phospho-S845 (GluA1 pS845) as a positive control of PKA activation.<sup>191</sup> As seen on figure 20C, Forskolin stimulation led to phosphorylation of GluA1 S845. Likewise, Forskolin stimulation led to a strong increase in PLPPR3 pS351 levels. Tubulin and PLPPR3 labeling confirmed the equal input of total protein. In conclusion, this experiment confirms that S351 phosphorylation can be modified in “*in vivo-like*” setting and further reinforces the idea that it is a functionally relevant regulatory site.

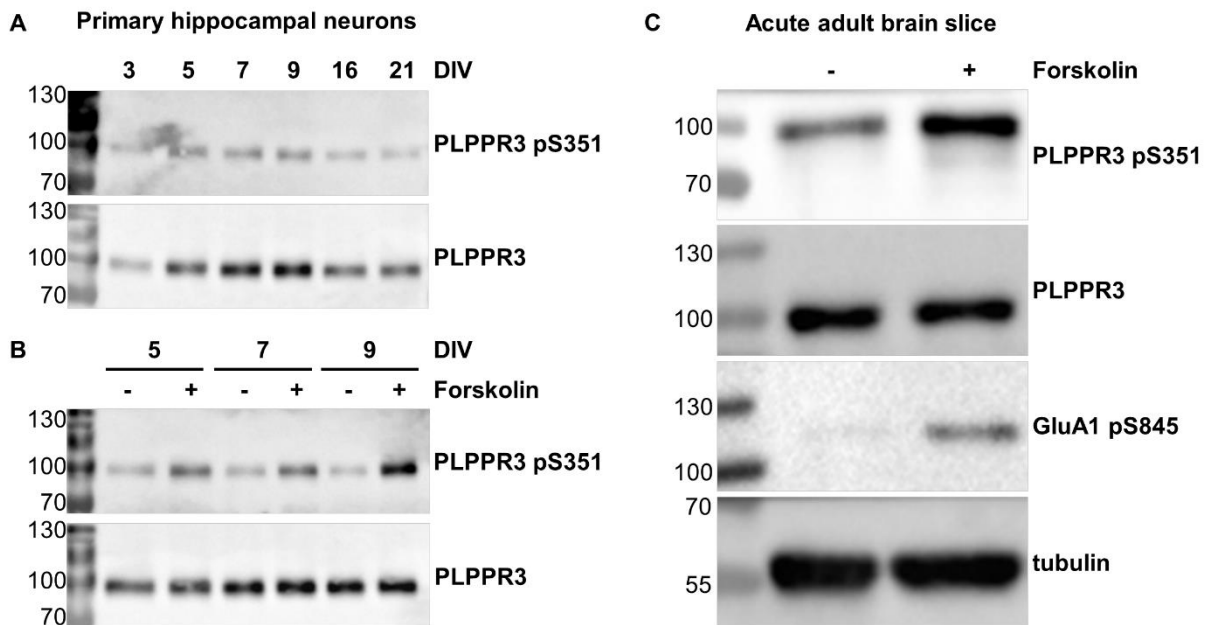


Figure 20. Phosphorylation of PLPPR3 S351 can be triggered in primary neurons as well as in acute brain slices. (A) PLPPR3 pS351 expression dynamics mimic total PLPPR3 expression levels during different developmental stages. (B) Phosphorylation of PLPPR3 S351 is most potently triggered at nine days *in vitro* (DIV). Neurons were stimulated with 30  $\mu$ M Forskolin for 5 minutes prior to lysis. In (A) and (B) primary hippocampal neurons were lysed at indicated time points and protein levels were analyzed by western blot. (C) Activation of PKA by Forskolin leads to increased phosphorylation of PLPPR3 S351 in acute brain slices. Brain slices were stimulated with 30  $\mu$ M Forskolin for 15 minutes and protein extracts were analyzed by western blot.

## 5.2. Phosphorylation of S351 does not regulate filopodia or axonal branch formation

As the overall pattern of pS351 levels mimicked that of PLPPR3 levels in different developmental stages, I hypothesized that phosphorylation of S351 may regulate filopodia

formation and axon branching. To this end, I generated full-length PLPPR3 S351 phospho-mimic (PLPPR3-S351D-Flag) and phospho-dead (PLPPR3-S351A-Flag) mutants and used them in cell morphological assays. Previous studies in our lab have shown that compared to the wild-type, *Plppr3*<sup>-/-</sup> neurons have fewer filopodia at early days – 1.5 to 3 DIV – of axon development.<sup>88,188</sup> Methodologically, it is difficult to measure the effect of reconstituted PLPPR3 phospho-mutants at such early stages in primary neurons, as it requires transfection of low density cultures that have generally low viability. Therefore, I opted to measure pS351-dependent filopodia formation in a cell line. Previous experiments in the lab have shown that expression of PLPPR3-Flag in N1E-115 cells significantly increases filopodia density compared to non-transfected controls, albeit with small effect size.<sup>192</sup> Building on that, I analyzed whether S351 phospho-mutants lead to altered filopodia density compared to the wild-type protein in these cells. As full-length PLPPR constructs tend to show defects in trafficking to the plasma membrane, with unclear consequences to their filopodia-inducing activity,<sup>99</sup> I only included cells with plasma membrane localized PLPPR3 in my analysis. I co-expressed membrane-bound GFP, which served as an independent marker of membrane protrusions. As cells make various membrane protrusions that are often mistaken for filopodia,<sup>99</sup> I additionally labelled F-actin as an independent filopodia marker. Indeed, as seen on Figure 21, PLPPR3 variants localized to filopodia as evidenced by their co-localization with membrane GFP and F-actin (Figure 21A). I quantified filopodia density in these cells using a semi-automated analysis developed by my colleague Joachim Fuchs.<sup>192</sup> Filopodia density did not differ between wild-type and phospho-mutant expressing cells (Figure 21B). However, N1E-115 cells are characterized by a high number of basal level filopodia, making it difficult to distill the effect of phospho-mutants on filopodia density. Therefore, I decided to test the effect of phospho-mutants on axon morphology in primary hippocampal neurons.

PLPPR3-induced filopodia are precursors for axonal branches, as fewer filopodia at early days of axon development directly translate into fewer branches at later stages.<sup>88</sup> I tested whether expression of phospho-mutants alters axonal branch density in primary hippocampal neurons. To this end, I infected *Plppr3*<sup>-/-</sup> neurons with wild-type PLPPR3-Flag, PLPPR3-S351A-Flag or PLPPR3-S351D-Flag lentiviruses directly after plating. I transfected the cells with cytosolic GFP, which allowed me to analyze the morphology of individual axons in dense cultures, and served as an independent marker of neuronal processes (Figure 21C). In this experimental setup, PLPPR3 re-expression has been shown to rescue the branching phenotype, with an additional effect on total axon length.<sup>88</sup>

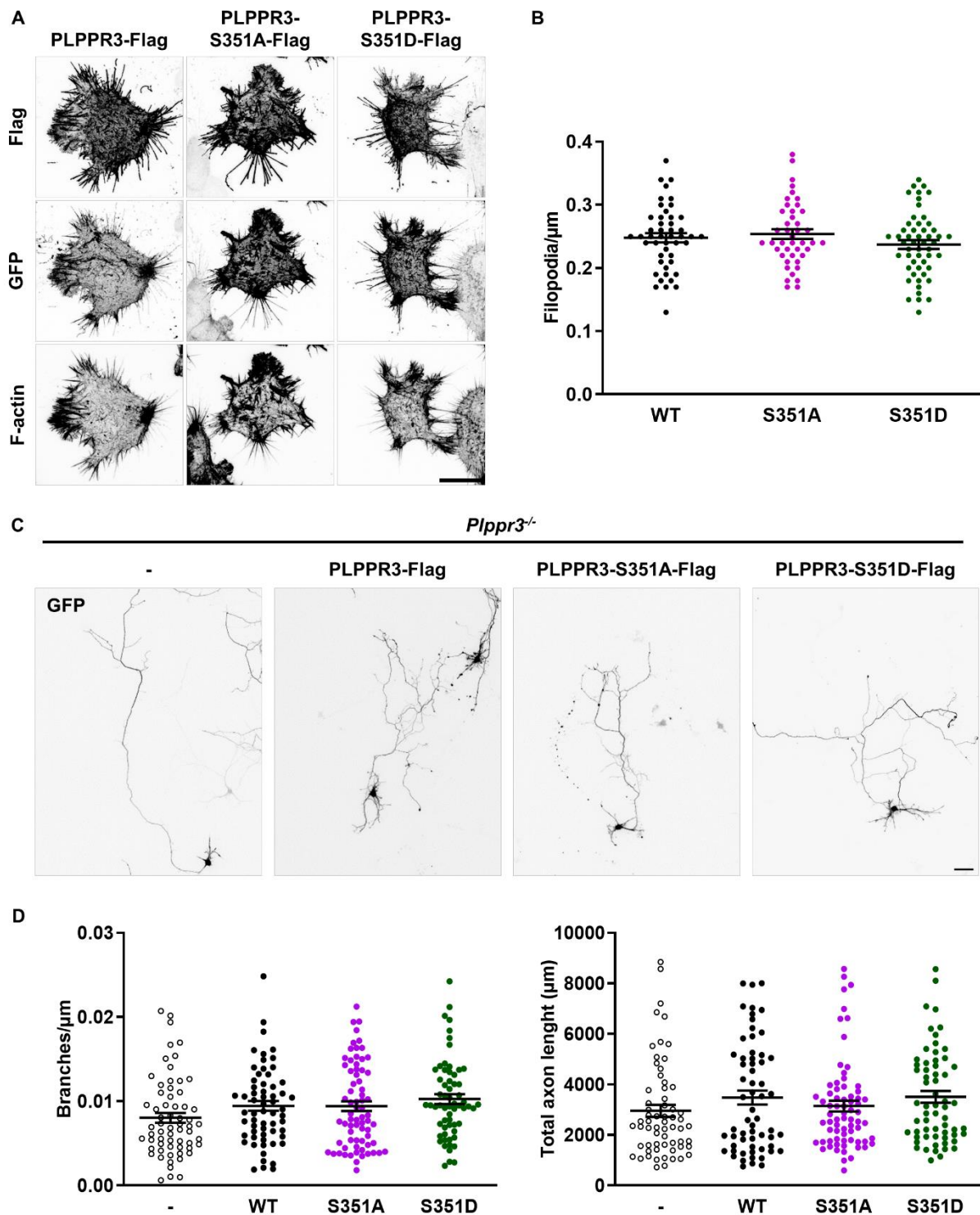


Figure 21. PLPPR3 S351 phosphorylation does not alter filopodia formation or axon branching. (A) Filopodia formation was analyzed in N1E-115 cells expressing wild-type or phospho-mutant PLPPR3 variants. Membrane-bound GFP served as an independent marker of membrane protrusions, and F-actin labeling was used to differentiate filopodia from other membrane-protrusions. Scale bar = 20  $\mu\text{m}$ . (B) Quantification of (A).  $n = 43\text{-}52$ ,  $N = 3$ . (C) Axon branching was analyzed in hippocampal *Plppr3<sup>-/-</sup>* neurons expressing wild-type or phospho-mutant PLPPR3 variants. Cytosolic GFP served as an independent marker of neuronal processes. Scale bar 50  $\mu\text{m}$ . (D) Quantification of (C).  $n = 61\text{-}71$ ,  $N = 2$ . In (B) and (D), no statistically significant differences were detected with one-way ANOVA.

Indeed, also in my hands, reconstitution of wild-type PLPPR3 showed a trend towards increased branch density and total axon length in *Plppr3<sup>-/-</sup>* neurons (Figure 21D). However, analysis of two biological replicates did not show an effect of phospho-mutants on branch density compared to the wild-type. Minor trends in total axon length were observed, with the phospho-dead being more similar to the knock-out, and phospho-mimic being more similar to the reconstituted wild-type. Sample size calculation with G\*Power based on previous measurements in the lab<sup>192</sup> estimated that to detect the effect size observed between *Wt* and *Plppr3<sup>-/-</sup>* neurons, at least eight biological replicates would be required. Given that the effect of phosphorylation on branch density in the first experiments was minimal, it is reasonable to assume an even larger number of replicates would be needed to detect any differences. For this reason, this experiment was discontinued. Taken together these data do not suggest a function of S351 phosphorylation on filopodia formation or axonal branching.

### 5.3. PLPPR3 pS351 mediates its binding to BASP1

As PLPPR3 pS351 does not appear to regulate filopodia formation and axonal branching, the best-described phenotype of PLPPR3 to date, I turned to other approaches to learn more about this phosphorylation site. Phosphorylation often regulates binding of interaction partners (see Figure 4 in Introduction), therefore I established an unbiased screen to search for binding partners of pS351 using mass spectrometry. I made use of affinity columns conjugated with pS351 (phospho; LKRApSVDVDLLA) and S351 (non-phospho; LKRASVDVDLLA) peptides that I had previously used to purify the pS351 antibody in the first antibody generation attempt (see chapter 4). I incubated the columns with freshly prepared adult mouse brain lysate and eluted bound proteins with low pH buffer (Figure 22A). I concentrated the proteins by methanol precipitation and analyzed them by mass spectrometry in collaboration with Dr. Kathrin Textoris-Taube (Core Facility High Throughput Mass Spectrometry, Charité) and Dr. Marieluise Kirchner (Proteomics Core Facility, Berlin Institute of Health).

I first analyzed the eluted samples by SDS-PAGE and Coomassie staining to see whether there were distinct protein bands present. The eluate from phospho-peptide column showed a single band at 55 kDa, and a higher-order aggregation of proteins that had not entered the running gel (Figure 22B). The aggregation is likely a byproduct of protein concentration step. In the pilot experiment, I cut out the distinct bands for mass spectrometry analysis as indicated by boxes in Figure 22B. However, in order to see which proteins are enriched on the phospho-peptide column, and to capture potential candidates from all molecular sizes, we decided to analyze the whole gel with non-phospho eluate as a control. To this end, proteins were run on SDS-PAGE until they had entered the running gel and just started separating, and the whole area was cut out and analyzed (Figure 22C, boxes indicate where the gel was cut).

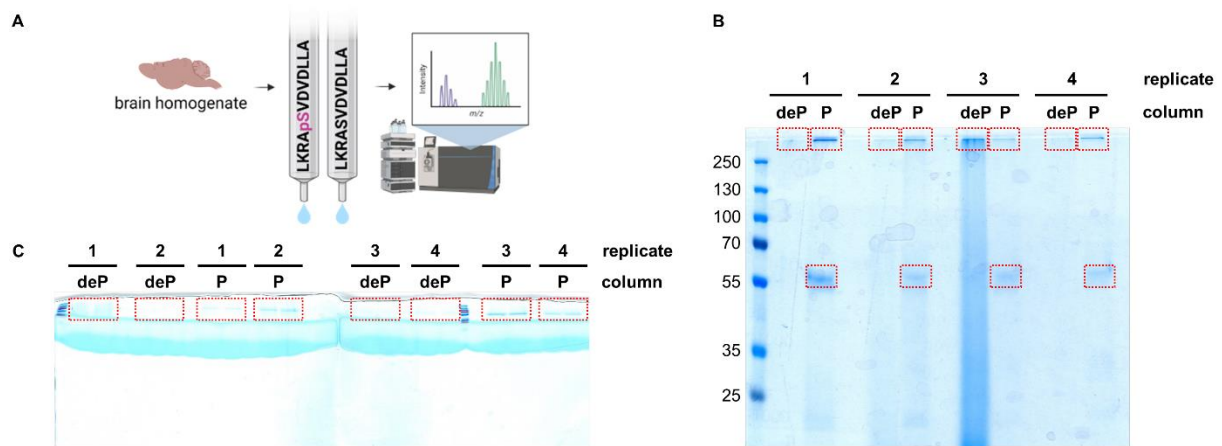


Figure 22. Affinity chromatography combined with mass spectrometry to identify interaction partners of PLPPR3 pS351. (A) Experimental workflow. Phospho- and non-phosphopeptide columns were incubated with fresh adult brain lysate, eluted and analyzed by mass spectrometry. Created with BioRender.com. (B) Pilot experiment showed a distinct protein band at 50 kDa and protein aggregations on top of the running gel. Annotated bands were cut out and analyzed. (C) Bands analyzed in the final experiment. Proteins were allowed to enter the running gel, after which electrophoresis was stopped, bands were cut out and analyzed. deP – dephosphorylated, P – phosphorylated.

Mass spectrometry analysis showed a high enrichment of rabbit immunoglobulins in the phospho-column eluate (Table 3). These immunoglobulins likely account for the 55 kDa protein band seen in Coomassie stainings on Figures 22B and C, and are contaminants from the antibody purification procedure described in the beginning of chapter 4. However, analysis also uncovered three mouse proteins: BASP1, ATP5B and HIST1H1E. BASP1, or Brain acid soluble protein 1, is localized in axon terminals and associated with axon growth and regeneration.<sup>193</sup> ATP5B is a subunit of the ATP synthase found on the inner mitochondrial membrane,<sup>194</sup> while HIST1H1E is a nuclear protein with a function in chromatin structure.<sup>195</sup> As there are no known mitochondrial or nuclear functions of PLPPR3, only BASP1 was considered as a potential interaction partner. Curiously, BASP1 showed significant enrichment in the phospho-column compared to the non-phospho column, suggesting a favored binding to pS351.

Table 3. List of potential interaction partners from mass spectrometry analysis of PLPPR3 pS351 affinity chromatography. Intensity and enrichment values are on log2 scale. P = phosphopeptide, deP = non-phospho peptide.

| Gene names              | Nr of peptides | Nr of unique peptides | Intensity deP column | Intensity P column | Enrichment P vs deP | Mol. weight (kDa) | Species |
|-------------------------|----------------|-----------------------|----------------------|--------------------|---------------------|-------------------|---------|
| Ig $\gamma$ chain C     | 32             | 29                    | 0                    | 36                 | exclusive           | 35                | rabbit  |
| Ig $\kappa$ -b4 chain C | 6              | 6                     | 0                    | 29                 | exclusive           | 11                | rabbit  |
| Ig $\mu$ chain C        | 20             | 20                    | 0                    | 29                 | exclusive           | 50                | rabbit  |
| Basp1                   | 25             | 25                    | 10                   | 29                 | 19                  | 22                | mouse   |
| Atp5b                   | 35             | 26                    | 24                   | 30                 | 6                   | 56                | mouse   |
| Hist1h1e                | 17             | 3                     | 29                   | 27                 | -2                  | 22                | mouse   |

Next, I directly tested the interaction of PLPPR3 intracellular domain and BASP1 using co-immunoprecipitation. I used HEK293T cells to co-express tagged BASP1 (BASP1-tGFP) and the membrane-bound intracellular domain (PLPPR3-ICDm-His), prepared cell lysates and precipitated BASP1 using the tGFP antibody. I used Forskolin stimulation and S351A mutant to test the phospho-dependence of this possible interaction. Analysis by western blot showed that I was able to pull down PLPPR3 intracellular domain with immunoprecipitated BASP1 under steady state conditions (Figure 23A). In line with the increased binding to the phospho-column (Table 3), there was increased binding of PLPPR3-BASP1 after PKA activation with Forskolin, as evidenced by increased amount of co-immunoprecipitated PLPPR3 (Figure 23B). In contrast, PLPPR3-ICDm-S351A mutant showed decreased binding to BASP1. The co-immunoprecipitation was specific to binding of BASP1 and PLPPR3, as in the absence of tGFP antibody (IgG control) or BASP1-tGFP protein, PLPPR3 was not detected. These data confirm BASP1 as a novel interaction partner of PLPPR3 intracellular domain and suggest that this interaction is mediated by phosphorylation of S351.

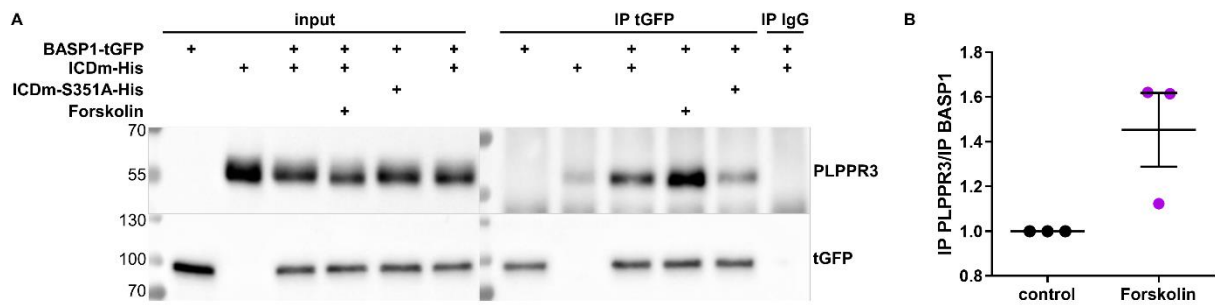


Figure 23. PLPPR3 intracellular domain interacts with BASP1 in a pS351-dependent manner. (A) Co-immunoprecipitation of BASP1 and PLPPR3 intracellular domain. HEK293T cells expressing respective constructs were stimulated with 30  $\mu$ M Forskolin for 10 minutes, BASP1 was immunoprecipitated and the samples were analyzed by western blot. (B) Quantification of (A). Control samples were normalized to 1. N=3.

#### 5.4. PLPPR3 and BASP1 co-localize in clusters along axons

BASP1 was extensively studied in the early 1990-2000s, and it was demonstrated to regulate axon growth and regeneration.<sup>193</sup> BASP1 has been reported to localize to the inner leaflet of plasma membrane, where it can induce actin-based structures such as filopodia by modulating PIP<sub>2</sub> availability.<sup>196</sup> Thus, I initially set out to investigate the localization of BASP1 in N1E-115 cells. I expressed BASP1-Flag in N1E cells and co-labelled the cells for Flag and the actin cytoskeleton. For the latter, I made use of the phalloidin-Atto 488, which selectively binds F-actin and thus allows to visualize filopodia. As seen on figure 24A, BASP1-Flag localizes to the cell periphery and its protrusions, showing high co-localization with F-actin. Curiously, in some instances, BASP1 accumulates at the tips of filopodia, which occasionally also include accumulated F-actin (white arrow).

I investigated the localization of BASP1 also in primary hippocampal neurons. Unfortunately, I was unable to validate any BASP1 antibodies for endogenous labeling (see Appendix) and thus relied on overexpression approach. I used calcium phosphate transfection method to introduce BASP1-Flag into *Wt* neurons and grew them to seven days *in vitro*. Immunolabeling with Flag antibody detected clustered BASP1 along axons, which closely resembled presynaptic boutons. In dense primary cultures, such as the one analyzed here, presynaptic compartments can be detected as early as 3-4 days *in vitro* when neurons start to make contacts.<sup>197</sup> Thus, I decided to investigate whether BASP1 co-localizes with presynaptic markers.

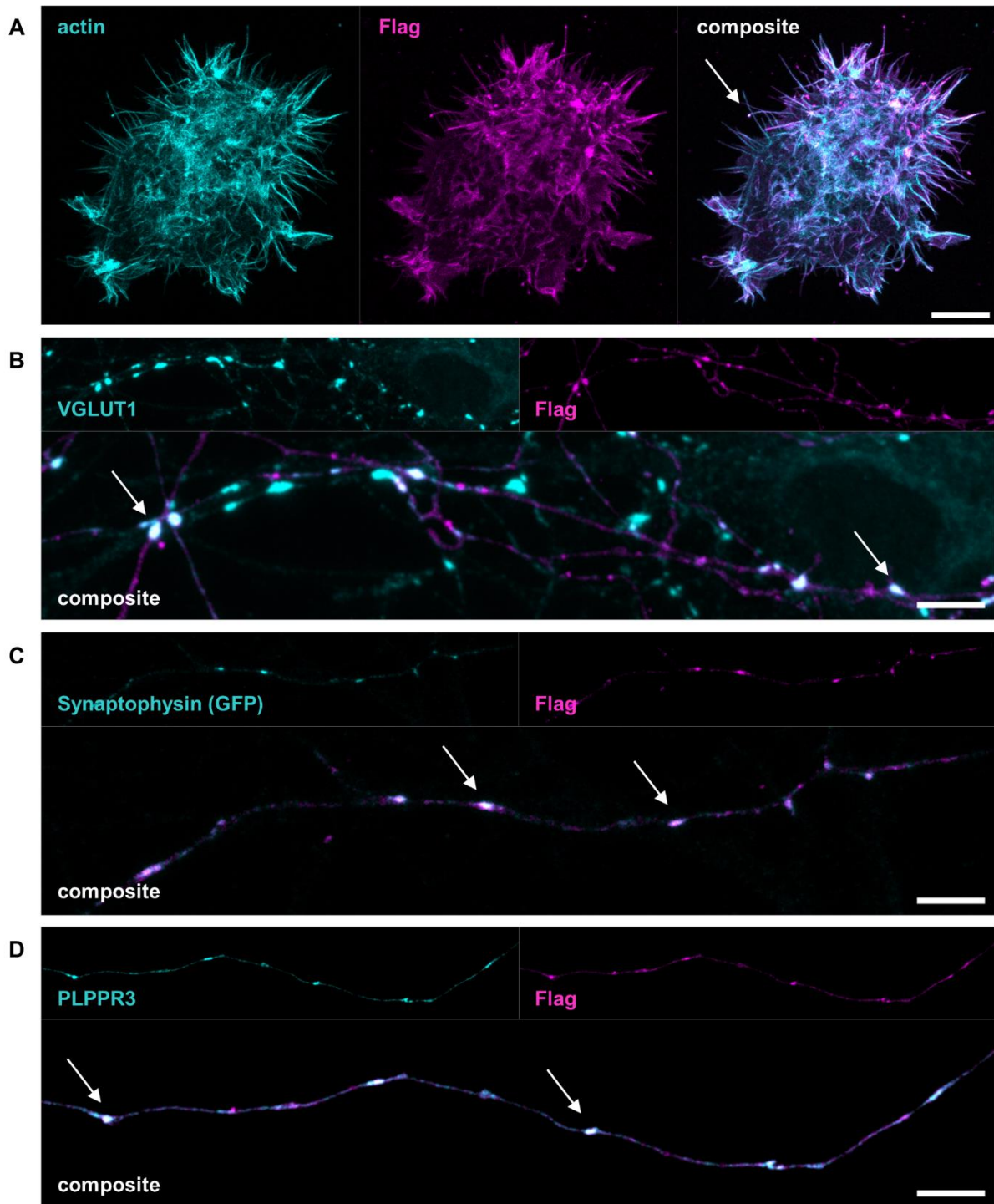


Figure 24. BASP1 and PLPPR3 intracellular domain co-localize in clusters along axons in primary hippocampal neurons. (A) BASP1 localizes to the cell periphery and membrane protrusions in N1E-115 cells, showing high co-localization with F-actin. In some instances, BASP1 clusters at the tip of filopodia together with F-actin (white arrow). N1E cells were transfected with BASP1-Flag and co-labelled with phalloidin-Atto 488. Scale bar = 10  $\mu$ m. (B) BASP1-Flag forms clusters along the axons of primary hippocampal neurons which show co-localization with presynaptic marker VGLUT1. Wt primary hippocampal neurons were transfected with BASP1-Flag, fixed at 7 DIV, and immunolabelled for Flag and endogenous VGLUT1. (C) BASP1-Flag co-localizes with co-expressed presynaptic marker synaptophysin-1. Wt primary hippocampal neurons were transfected with BASP1-Flag and synaptophysin-GFP, fixed at 7 DIV, and immunolabelled for Flag and GFP. (D) BASP1 and PLPPR3 intracellular domain co-localize in clusters along axons. Wt primary hippocampal neurons were transfected with BASP1-Flag

and PLPPR3-ICDm-His, fixed at 7 DIV and immunolabelled for Flag and PLPPR3. In (B)-(D), some of the co-localized clusters are indicated with white arrows. Scale bar = 5  $\mu$ m.

Glutamate is the primary excitatory neurotransmitter in the brain, and vesicular glutamate transporters (VGLUTs), which concentrate glutamate into synaptic vesicles, the key anatomic and functional presynaptic markers.<sup>198</sup> I labelled BASP1-Flag expressing *Wt* neurons for VGLUT1, the most abundant VGLUT isotype.<sup>199</sup> As seen in Figure 24B, VGLUT1 showed distinct labeling of presynaptic compartments, and many of these co-localized with BASP1 clusters (white arrows). However, analyzing co-localization in this experimental approach was complicated by the fact that the endogenous VGLUT1-positive clusters in dense neuronal culture far outnumbered the overexpressed BASP1 clusters. Thus, I opted to co-express BASP1-Flag with a presynaptic marker to better assess co-localization.

Synaptophysin is the second most abundant protein on synaptic vesicles in boutons,<sup>200</sup> and is therefore often used as a marker for presynapses. I co-expressed BASP1-Flag with synaptophysin-GFP in *Wt* primary hippocampal neurons and investigated their co-localization at seven days *in vitro*. Synaptophysin-GFP localized in distinct puncta along axons (Figure 24C) while its expression was almost entirely missing in the somatodendritic compartment (data not shown). The majority of BASP1 puncta co-localized with synaptophysin clusters (white arrows), suggesting that the observed BASP1 puncta could indeed be presynaptic boutons. Finally, I examined the co-localization of BASP1 with PLPPR3. I co-expressed BASP1-Flag with PLPPR3-ICDm-His, the construct used in co-immunoprecipitation experiments, in *Plppr3*<sup>-/-</sup> primary hippocampal neurons and analyzed their co-localization at seven days *in vitro*. Curiously, PLPPR3 intracellular domain also localized in distinct clusters along axons that showed high overlap with BASP1 clusters (Figure 24D, white arrows). In summary, these data suggest that BASP1 and PLPPR3 may co-localize at presynaptic boutons.

### **5.5. PLPPR3 and PLPPR3 pS351 are enriched in synaptosomes**

The localization of PLPPR3 in presumed presynaptic compartments prompted me to investigate it with additional independent experimental methods. Biochemical isolation of synaptosomes and analysis of its contents by western blot or mass spectrometry is a common method of investigating synaptic proteins. Crude synaptosomes can be generated by multiple centrifugation steps leading to the isolation of synaptic compartments and cytosolic proteins. Synaptosomes (fraction P2) contain the entire presynaptic terminal with mitochondria and synaptic vesicles, as well as the postsynaptic membrane and the postsynaptic density, while the cytosolic fraction (S2) contains soluble proteins.<sup>201</sup> Comparison of the relative amount of specific proteins in the two fractions allows to see which of them are enriched in synaptic

compartments. I used western blot to analyze crude synaptosomes from adult mice prepared by my colleague Dimitra Ranti. As seen in Figure 25, both PLPPR3 as well as PLPPR3 pS351 were exclusively present in synaptosomal fractions. Enrichment of presynaptic synaptophysin-1 and postsynaptic PSD-95 in these fractions confirm the successful isolation of crude synaptosomes. Unfortunately, detection of endogenous BASP1 by western blot was not possible due to lack of validated antibodies (see Appendix), but BASP1 was among the top 20 most enriched proteins in synaptosomal fraction based on mass spectrometry analysis (data not shown). In conclusion, these data add further evidence to the presence of PLPPR3 and PLPPR3 pS351 in presynaptic compartments.

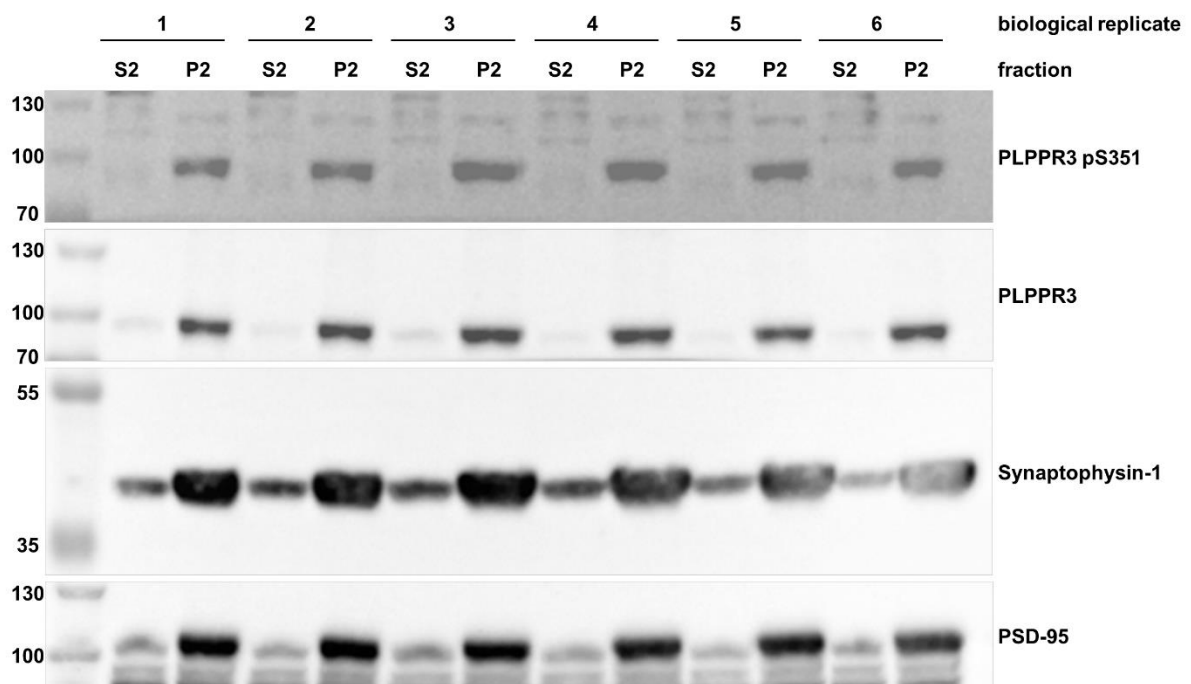


Figure 25. PLPPR3 and PLPPR3 pS351 are enriched in crude synaptosomes. Crude synaptosomes were isolated from adult mouse brains using subcellular fractionation by centrifugation and analyzed by western blot. Successful synaptosome isolation was confirmed by detection of known synaptic proteins, the presynaptic synaptophysin-1 and the postsynaptic PSD-95. S2 = cytosolic fraction, P2 = crude synaptosomes.

## 5.6. Discussion and outlook

Experiments in this chapter establish that although PLPPR3 pS351 levels follow the same pattern as total PLPPR3, the primary function of this phosphorylation event does not appear to be regulation of filopodia formation or axonal branching. Instead, I demonstrate that BASP1 is a novel, phospho-mediated interaction partner of PLPPR3, and that BASP1-PLPPR3 co-localize in presynaptic compartments along axons.

It is of interest that S351 phosphorylation can most potently be triggered at nine days *in vitro*, precisely the time when PLPPR3 expression peaks in cell culture. This could indicate

increased availability of the kinase PKA at this timepoint, or increased effectiveness of signaling due to maturation of PKA signaling complexes in the axon. PKA subcellular localization is controlled by A kinase anchoring proteins (AKAPs), and the role of MAP2 as the dominant organizer of PKA in dendrites has been well established.<sup>202–205</sup> In contrast, less is known about PKA signalosomes in axons despite the prominent role of cAMP-PKA signaling in axon morphogenesis.<sup>73,163</sup> Future experiments could focus on identifying whether PKA-PLPPR3 signaling is mediated by AKAPs. To this end, AKAP inhibitor peptides<sup>206</sup> could be tested.

The cell-based assays presented in this chapter did not reveal an effect of pS351 on filopodia or axon branch formation. N1E-115 have been useful for studying PLPPR3 as they show good trafficking of most PLPPR3 constructs to the plasma membrane (our observations), however, their high number of filopodia undermines the sensitivity of filopodia formation assays. Future work could focus on establishing assays in cells that allow for efficient screening of filopodia formation. To this end, B16 melanoma cell line that is often used for studying actin cytoskeleton could be a great candidate.

I identified BASP1 as a novel interaction partner of PLPPR3 intracellular domain. BASP1 binding to PLPPR3 appears to be mediated by phosphorylated S351, as illustrated by its increased binding to the pS351-column compared to the S351-column (Table 3), and increased co-immunoprecipitation after Forskolin stimulation (Figure 23). My experiments do not conclude whether phosphorylation of S351 determines BASP1 binding, although they indicate that binding to PLPPR3 S351A is barely distinguishable from background binding. Future experiments could focus on establishing which residues or regions are essential for BASP1 binding, as disturbing this interaction enables us to study its function. A further intriguing question is whether other PLPPRs bind BASP1. As shown in Figure 2, the site of S351 is well conserved in PLPPR2, indicating this site could be targeted by PKA, and potentially bind BASP1. In PLPPR1 the motif is partially conserved, but there is a negatively charged aspartic acid instead of phosphorylatable serine. Aspartic acid is often used to mimic phospho-serine, thus, it could be possible that also PLPPR1 interacts with BASP1.

Immunocytochemistry in primary hippocampal neurons illustrates a distinct localization of BASP1 and PLPPR3 intracellular domain in clusters along axons. BASP1 clusters co-localize with presynaptic markers VGLUT1 and synaptophysin-1 (Figure 24B, C), while PLPPR3 and PLPPR3 pS351 show enrichment in isolated crude synaptosomes (Figure 25). Previous experiments in our lab have shown that PLPPR3 localizes in semi-regular nanoclusters along the axonal plasma membrane at nine days *in vitro*,<sup>88</sup> however, localization to larger microdomains has not been observed before. It is thus tempting to hypothesize that

overexpression of BASP1 organizes PLPPR3 to these clusters. However, the opposite hypothesis – that it is the membrane-embedded protein with a long intracellular domain that positions the cytosolic protein – is even more appealing. Future experiments could test this relationship in analyzing BASP1 clusters in *Wt* and *Plppr3*<sup>-/-</sup> neurons, and PLPPR3 clusters in *Wt* and *Basp1*<sup>-/-</sup> neurons.

This far, PLPPR3 has been described as a developmentally regulated protein with functions in axonal branching and guidance.<sup>88,188,207</sup> Although PLPPR3 expression is reduced in later stages of development,<sup>88</sup> my experiments show that PLPPR3 as well as PLPPR3 pS351 are present in the adult brain, as demonstrated by western blot experiments with acute brain slices (Figure 20) and crude synaptosomes (Figure 25). Localization of PLPPR3 in axonal compartments resembling presynapses (Figure 24) suggests a novel function of PLPPR3 in synapse formation or maintenance. Future experiments could investigate whether PLPPR3 is essential for synaptogenesis by comparing synaptic connectivity in *Wt* and *Plppr3*<sup>-/-</sup> neurons in later stage cultures. To this end, functional synapses could be determined with pre- and postsynaptic markers. The function of pS351 could be assessed with reconstitution of PLPPR3-S351A in *Plppr3*<sup>-/-</sup> neurons, or manipulations of PKA activity using activators or inhibitors.

A major shortcoming of these experiments is lack of tools to study endogenous BASP1 (see Appendix). Only one of the antibodies reliably recognizes BASP1-Flag in immunocytochemistry, while none of them detect the overexpressed BASP1 as the most prominent band in western blot. Future work needs to focus on validating BASP1 antibodies using knockdown, or by utilizing the existing BASP1 knockout mice (Caroni lab).

## 6. Appendix

### 6.1. Validation of BASP1 antibodies

BASP1, also known as NAP22 or CAP23, was first described in the early 1990s as a brain-enriched protein with an unusual amino acid composition.<sup>208,209</sup> Although just 22 kDa in calculated molecular weight, it migrates at 55 kDa mark in 10% SDS-PAGE due to its acidic amino acid composition.<sup>208</sup> Since its discovery, numerous antibodies against BASP1 have been made by laboratories as well as commercial vendors. In order to study endogenous BASP1-PLPPR3 interaction, I tested several antibodies in their ability to reliably detect BASP1. To this end, I purchased BASP1 antibodies that showed a protein band at around 55 kDa molecular weight, or that had been validated in publications. I additionally tested two custom-made antibodies that I was able to obtain. An overview of tested BASP1 antibodies is given in Table 4. For simplicity, the antibodies will be referred to by their order number on Table 4.

Table 4. List of tested BASP1 antibodies.

| Nr | Source, catalog nr         | Immunogen                                 |
|----|----------------------------|---|
| 1  | Invitrogen, #703692        | human BASP1 aa 7-24, 138-155              |
| 2  | Synaptic Systems, #246003  | rat BASP1 aa 1-220                        |
| 3  | R&D Systems, # AF6479      | human BASP1 aa 2-45                       |
| 4  | Caroni lab <sup>208</sup>  | chick BASP1                               |
| 5  | Roberts lab <sup>210</sup> | GST-BASP1 (species of sequence not clear) |
| 6  | Aviva, # ARP59932_P050     | human BASP1 aa 134-183                    |

To validate BASP1 antibodies, I used the strategy of parallel detection with an independent antibody binding the affinity tag, which is one of the five recommended antibody validation methods.<sup>211</sup> I first tested these antibodies in immunocytochemistry using N1E-115 cells transfected with BASP1-Flag. The cells were labelled with Flag and BASP1 antibodies, and antibody specificity was assessed by overlap of immunofluorescence. As seen in Figure 26, BASP1-Flag expression was detected with Flag antibody at the cell membrane, and dorsal and peripheral membrane protrusions. Antibodies 1, 2, 4 and 6 failed to detect BASP1-Flag, and instead showed prominent labeling in the cytosol. Antibody 6 showed distinct perinuclear labeling. Antibodies 3 and 5 were able to detect overexpressed BASP1-Flag, although antibody 3 showed very weak and poor quality of labelling, probably due to self-aggregation.

Of the tested antibodies, only antibody 5 showed convincing, good quality detection of BASP1-Flag.

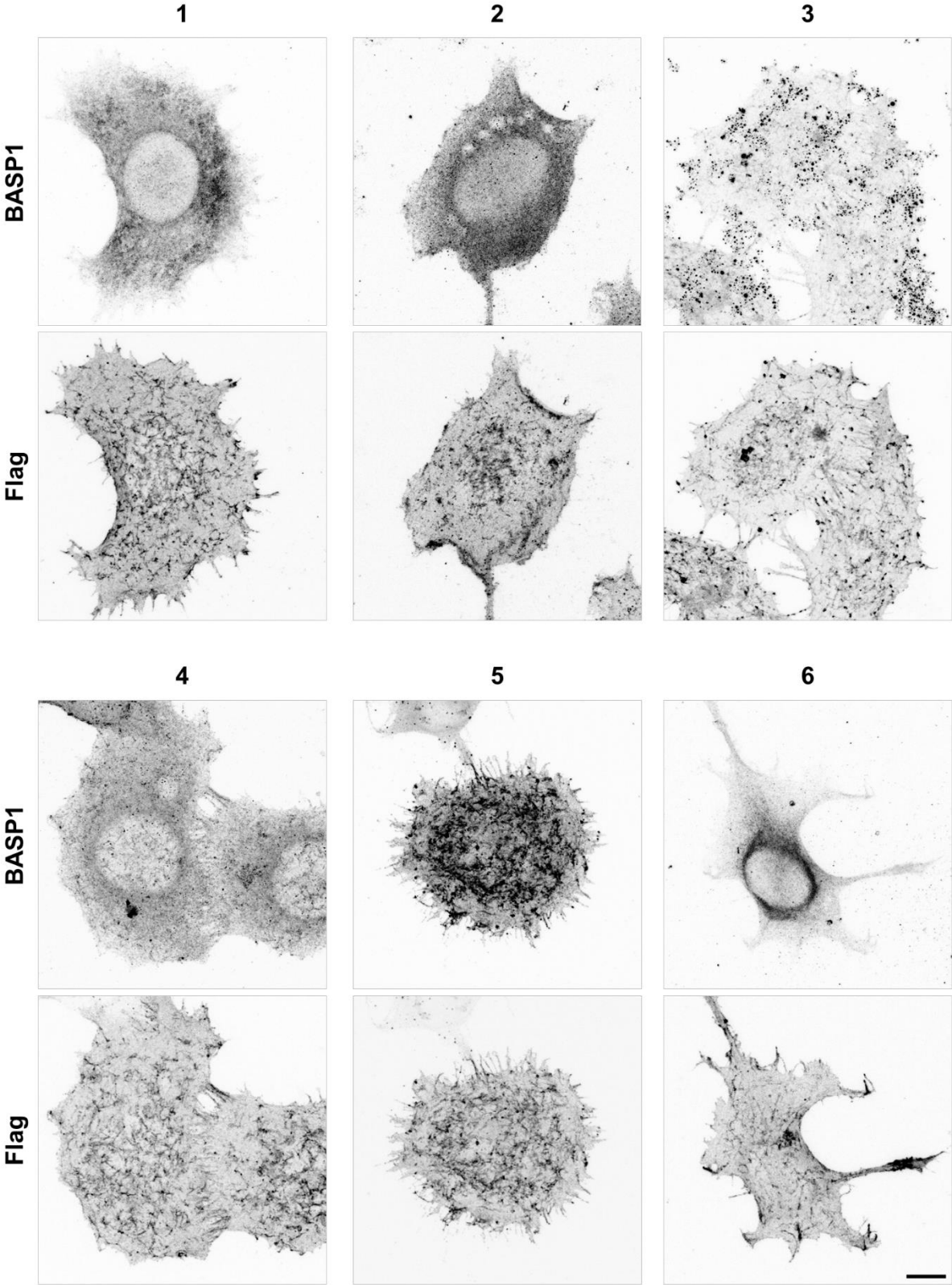
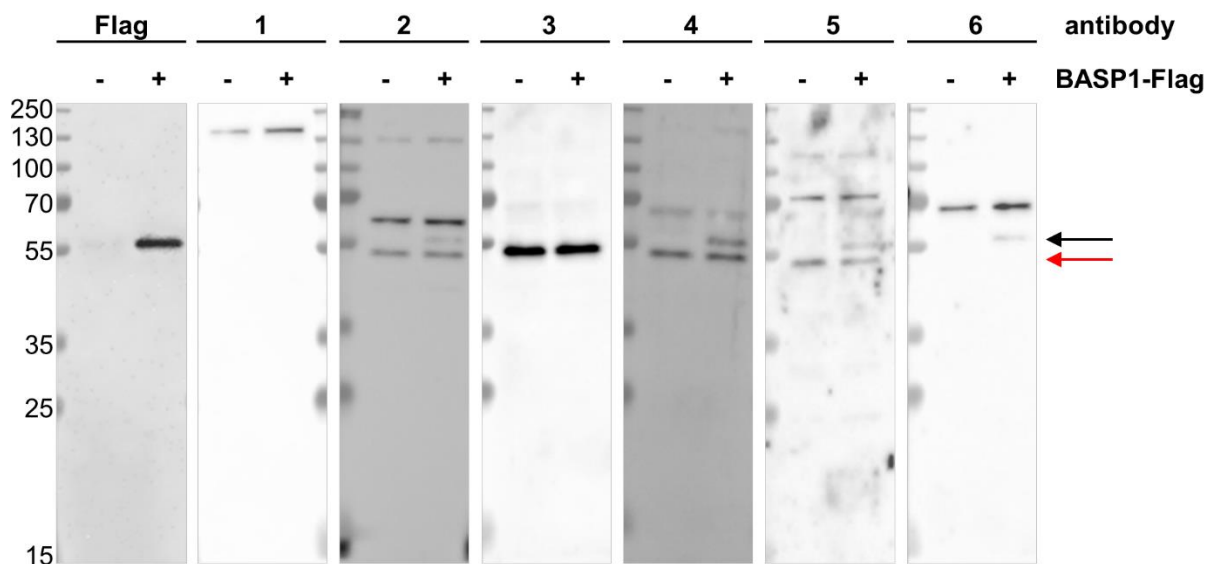


Figure 26. Validation of BASP1 antibodies in immunocytochemistry. BASP1-Flag was expressed in N1E-115 cells,

and labelled with Flag and BASP1 antibodies. Only antibodies 3 and 5 were able to detect the plasma membrane-localized BASP1-Flag, while quality of labeling was significantly better with antibody 5. Scale bar = 10  $\mu$ m.

I next tested these antibodies in western blot assay using protein lysates from BASP1-Flag expressing N1E-115 cells. I used protein lysates from non-transfected cells as a negative control. Blots were immunolabelled with Flag or BASP1 antibodies using the concentrations recommended by manufacturer or original publication, if available.



*Figure 27. Validation of BASP1 antibodies in western blot. Antibodies 2, 4, 5 and 6 recognize recombinant BASP1 with low affinity (black arrow), while antibodies 2-5 recognize a protein that may be endogenous BASP1 (red arrow). BASP1-Flag was expressed in N1E-115 cells and protein lysates were analyzed by western blot. Parallel control labeling was performed with Flag antibody, and protein lysates from non-transfected cells were used as a negative control.*

As seen in Figure 27, Flag antibody specifically recognized BASP1-Flag in protein lysates from transfected cells, while no signal was detected in the negative control sample. Tagged BASP1 was detected at an anticipated molecular weight of just above the 55 kDa mark (black arrow). BASP1 antibodies 2, 4, 5 and 6 also detected the corresponding BASP1-Flag band, albeit with much lower affinity. Antibodies 2-5 detected a protein band just below the 55 kDa mark, which could correspond to endogenous BASP1 (red arrow). BASP1 has been reported in N1E-115 cells before,<sup>212</sup> although lack of molecular weight markers on their western blots make it difficult to compare results. Furthermore, the authors nor the vendor of the antibody provide no validation data on the used BASP1 antibody, further obscuring the findings. Antibodies 2-6 additionally react with a protein just below the 70 kDa mark. No BASP1 forms have been reported that migrate higher than the canonical isoform, although multiple shorter BASP1 forms have been reported.<sup>213</sup> Antibodies 1, 2, 4 and 5 furthermore react with a protein at around 130 kDa molecular weight. I attempted to establish a knockdown of BASP1-Flag by co-expressing BASP1 shRNAs in order to validate antibodies. However, none of the six tested

shRNA sequences led to reduction of BASP1-Flag nor the suspected endogenous BASP1 bands in western blot (data not shown).

In conclusion, I was unfortunately unable to validate any BASP1 antibodies for endogenous labeling in cells or in western blot. Antibody 5 can be used to detect overexpressed BASP1 in immunocytochemistry and western blot. Antibodies 2, 4 and 6 are also suitable for western blot approaches. It is possible that poor labeling is due to differences in amino acid sequence between species. Most of the antibodies selected for testing are made with human protein sequence and some differences – although primarily conservative substitutions – do exist. In the future, it could be worth testing antibodies based on mouse BASP1 sequence.

## 7. General discussion

---

In summary, the work presented here identifies PLPPR3 S351 as a *bona fide* phosphorylation site of PKA. PKA has been linked to numerous phosphorylation events that regulate neuronal morphogenesis, such as filopodia formation.<sup>132</sup> While filopodia formation is also the best-studied function of PLPPR3,<sup>88</sup> phosphorylation of S351 does not appear to regulate induction of filopodia or axonal branches. Instead, S351 phosphorylation by PKA leads to binding of BASP1, a protein that has previously been implicated to play key roles during neuronal morphogenesis and regeneration.<sup>193,214,215</sup> PLPPR3 and PLPPR3 pS351 are enriched in synaptosomes, and BASP1 and PLPPR3 intracellular domain co-localize in presynaptic compartments. Thus, my work describes a novel protein complex in the presynaptic compartment with hitherto unknown function, and a PKA signaling event that regulates their binding. Furthermore, my work shows that the intracellular domain of PLPPR3 harbors numerous other phosphorylation sites, implicating the membrane protein as a signaling integrator at neuronal synapses.

### 7.1. PLPPR3 is a highly phosphorylated protein

My work identifies PLPPR3 as a highly phosphorylated protein with 26 high-confidence phosphorylation sites in its ~400 amino acid long intracellular domain. The phosphorylation sites are not distributed uniformly – instead, two apparent hotspots emerge. One of the phosphorylation-rich regions resides in the membrane-proximal part, stretching from amino acids 343 through 400. This phosphorylation hotspot includes nine phosphorylation events with an average distance of five amino acids from each other, which are located in a highly conserved region (see Table 2 and discussion in chapter 2). The second hotspot lies in the distal C-terminus between residues 560 and 575. Within this short stretch, there are six phosphorylation sites with an average distance of only two residues from each other. While high density of phosphorylation sites is in itself an interesting feature due to the added net negative charge, what makes the case of PLPPR3 intracellular domain particularly compelling is the unique stretch of 20 glutamic acids that is located in-between the two phosphorylation hotspots (the polyE box, see Figure 2 and chapter 2). Even without the phosphorylations, the isoelectric point of PLPPR3 intracellular domain is 5.3 and the net charge at pH 7.4 -15 (calculated with <https://www.protpi.ch/Calculator/ProteinTool>). Why, then, would a protein require so many phosphorylations?

There are few proteins for which such a high number of phosphorylation sites have been identified. Notable examples in the literature include the potassium channel Kv2.1 and the *Drosophila* transient receptor potential (TRP) channel.<sup>216–218</sup> Ion channels allow the passage of ions across the cell membrane and thereby play a critical role in controlling neuronal

excitability.<sup>219</sup> In resting mammalian neurons, the Kv2.1 channel harbors 15 phosphorylation sites in its C-terminal, and a single phosphorylation site in its N-terminal domain. Seven of these sites were shown to be dephosphorylated by the Ca<sup>2+</sup>-dependent phosphatase calcineurin. The large number of phosphorylation sites along with the different combinations of dephosphorylation patterns allow graded regulation of channel gating and neuronal firing properties.<sup>216</sup> The *Drosophila* TRP ion channel, which is part of the visual transduction cascade in *Drosophila* photoreceptors, was found to have 28 unique phosphorylation sites.<sup>217,218</sup> Many of these sites were shown to be regulated by the activity of the ion channel.<sup>218</sup> Thus, it emerges that one of the functions of multisite phosphorylation is enabling graded, fine-tuned responses.

In addition to fine-tuning, multisite phosphorylation could mediate topological rearrangements, binding of interaction partners and integration of signaling cascades. The inner leaflet of the plasma membrane is negatively charged,<sup>220</sup> and highly phosphorylated regions would be repelled from the plasma membrane. Thus, multisite phosphorylation could function to ensure the positioning of the intracellular domain in the cytosol. Additionally, this would make the PLPPR3 intracellular domain available for cytosolic interactions, and regulation of interactions is one of the essential functions of phosphorylation (see Figure 4). Indeed, the idea that the long intracellular domain functions as a scaffold to attract multivalent interactions via multisite phosphorylation is an attractive one. Computational analysis has shown that binding hotspots in proteins have a tendency to be phosphorylated and that phosphorylation sites at the interfaces are more likely to be evolutionarily conserved (see also Table 2).<sup>221</sup> For example, the presynaptic active zone scaffold proteins bassoon and piccolo have been shown to be highly phosphorylated, having 48 and 31 phosphorylation sites, respectively.<sup>222</sup> Thus, the phosphorylation hotspots found in PLPPR3 could be mediators of interactions. Finally, the presence of numerous phosphorylation sites sets PLPPR3 at the interface of multiple signaling cascades, with my data implicating involvement of PKC, PKA and GSK3-dependent signaling. Thus, PLPPR3 could function as a signaling integrator that combines information sourced from multiple pathways. The proposed functions of multisite phosphorylation of PLPPR3 are shown in Figure 28.

## Possible functions of multisite phosphorylation of PLPPR3

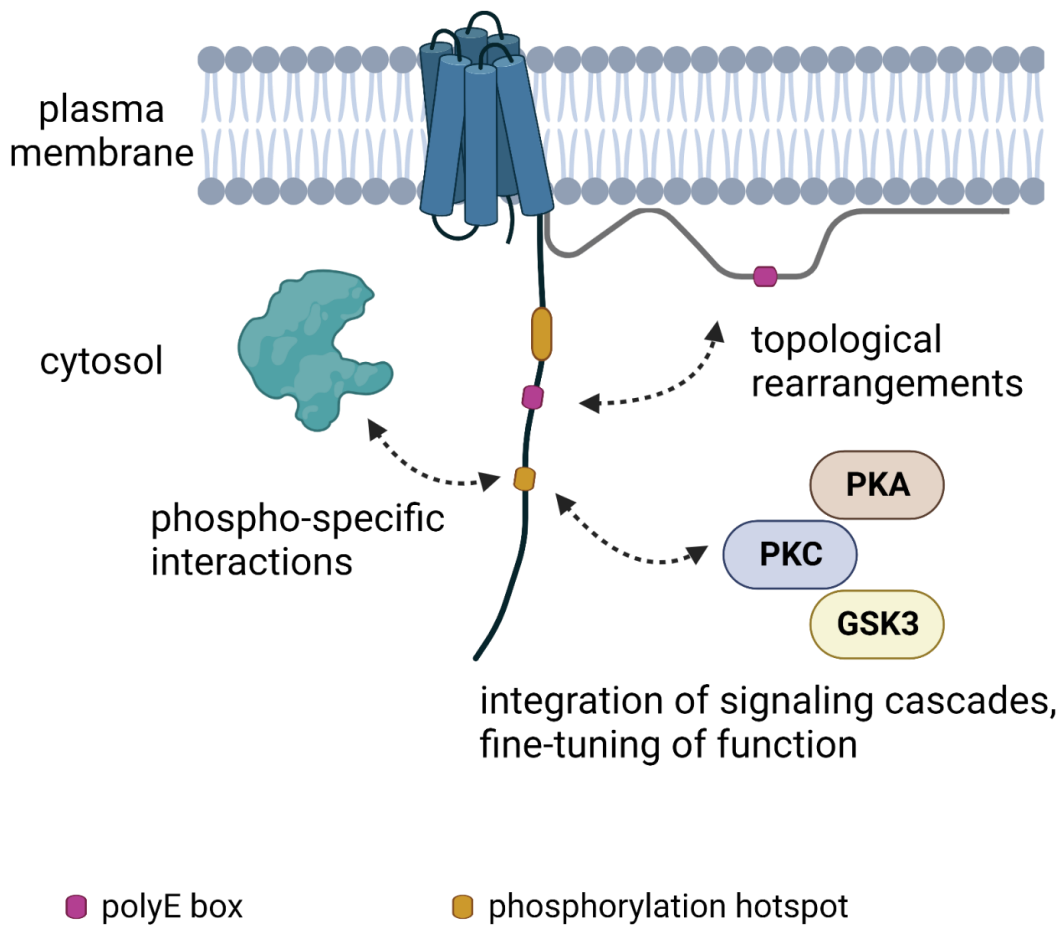


Figure 28. Possible functions of multisite phosphorylation of PLPPR3. PLPPR3 intracellular domain contains two phosphorylation hotspots, and further negative charge is added by the polyE box. These phosphorylation hotspots could function to ensure the localization of the intracellular domain in the cytosol by repelling it from the inner membrane. Localization to the cytosol would make the intracellular domain available for multivalent phosphorylation-dependent interactions. Multisite phosphorylation by different kinases allows for integration of signaling cascades. Finally, multisite phosphorylation enables fine-tuning of function by graded responses. Created with BioRender.com.

### 7.2. Possible roles for BASP1-PLPPR3 protein complex at the synapse

BASP1, belongs to a group of growth-associated proteins that also include GAP-43 (growth associated protein 43) and MARCKS (myristoylated alanine-rich protein kinase C substrate). Although these proteins do not belong to the same family, they share a number of characteristics.<sup>223,224</sup> They interact with the inner plasma membrane via acylation: BASP1 and MARCKS are co-translationally myristoylated, while GAP-43 is post-translationally palmitoylated.<sup>225</sup> The proteins have an unusual amino acid composition that is deficient in hydrophobic, and enriched in charged residues, making them highly disordered.<sup>226</sup> BASP1, GAP-43 and MARCKS have a positively charged effector domain that binds membrane

phospholipids and calmodulin, and is phosphorylated by PKC.<sup>130,209,224,225,227–229</sup> These proteins are highly expressed in the nervous system, particularly during early development, where they are associated with axon development and synaptogenesis.<sup>193,214,230,231</sup>

BASP1 has been primarily studied in the context of morphogenesis and regeneration. In cell lines, BASP1 accumulates actin at the cell periphery, and induces actin-based structures such as filopodia via modulation of PIP<sub>2</sub>.<sup>223</sup> In sensory neurons, loss of BASP1 leads to deficits in axon development that phenocopies axons grown in the presence of F-actin destabilizing drug, while overexpression of BASP1 in hippocampal neurons stimulates neurite outgrowth.<sup>214,215</sup> BASP1 expression is upregulated in regeneration, and it promotes sprouting in the neuromuscular junction.<sup>214,232</sup> Interestingly, it has been shown that BASP1 and GAP43 can in some cases functionally substitute each other.<sup>214,215</sup> However, already early *in vivo* studies identified the localization of BASP1 in neuronal processes, dendritic spines and axon terminals, where high BASP1 immunoreactivity was found in presynaptic densities and synaptic vesicles.<sup>233,234</sup> Despite these suggestions of synaptic function, none of the studies this far have characterized or tested BASP1 in synapses. The data presented in this thesis identifies a novel interaction of BASP1 and PLPPR3 intracellular domain in presynaptic structures and further characterizes the localization of BASP1 to glutamatergic synaptic boutons.

What could be the function of BASP1-PLPPR3 complexes in the presynapse? The high expression level of both proteins in early development could suggest a possible role in synapse formation. A commonality between BASP1 and PLPPR3 is their ability to induce rearrangements of the actin cytoskeleton.<sup>88,214,223</sup> Local rearrangements of F-actin in the axon, particularly its accumulation, is important in the early stages of synaptogenesis, as it provides a scaffold for the other presynaptic components, such as synaptic vesicles.<sup>235,236</sup> Thus, one of the possible working models involves signal-induced binding of BASP1 to the intracellular domain of PLPPR3 at distinct axonal locations, and triggering accumulation of F-actin. This model is consistent with described function of PLPPR3 in axonal filopodia formation, as filopodia formation and axonal branching are intricately connected to synaptogenesis.<sup>82,237</sup>

What could be the molecular mechanism leading to actin accumulation? GAP-43 and MARCKS, the proteins belonging to the same functional group with BASP1, have both been shown to interact with F-actin, and are likely capable of inducing actin polymerization.<sup>130,227,238–240</sup> However, to date, neither BASP1 nor PLPPR3 have been shown to directly bind actin. Both proteins have been shown to modulate membrane phospholipids and thus it is likely that they regulate the actin cytoskeleton via availability or stabilization of phosphoinositides PI(4,5)P<sub>2</sub> or PI(3,4,5)P<sub>3</sub>. PLPPR3-BASP1 are likely part of a larger molecular complex that includes actin

binding proteins. Radixin is one of the few reported interaction partners of PLPPR3.<sup>207</sup> It belongs to a group of three related proteins – ezrin, radixin and moesin, together known as ERM proteins – that organize membrane domains through their ability to link transmembrane proteins and the actin cytoskeleton.<sup>241</sup> ERM proteins are present in synaptic compartments, and they may play a role in the activation of pre-synaptic boutons via a mechanism that involves actin polymerization.<sup>242</sup> Thus, via regulation of membrane lipids, the PLPPR3-BASP1 complex may recruit other actin regulators to induce synapse formation.

In recent years, liquid-liquid phase separation (LLPS) has been increasingly recognized as a mechanism that organizes molecular machinery in the cell.<sup>243</sup> LLPS is a biological phenomenon whereby components of similar properties, such as proteins or RNA, condensate into a distinct phase enabled by weak multivalent interactions. At the synapse, LLPS has been shown to organize the presynaptic active zone<sup>244–246</sup> and assembly of the post-synaptic density.<sup>245,247–250</sup> Intriguingly, it has been shown that phase separation can create reaction compartments for actin polymerization,<sup>251,252</sup> even without actin-binding proteins.<sup>253</sup> BASP1 has been proposed to undergo phase separation,<sup>193</sup> while work in our lab has established that PLPPR3 forms liquid condensates that co-partition with actin and may induce its polymerization (our unpublished data). Our preliminary data indicates that BASP1 may also co-partition into PLPPR3 phases (not shown here). Thus, liquid-liquid phase separation offers an alternative model of early presynapse assembly via PLPPR3 phase-dependent actin accumulation. Possible molecular mechanisms of PLPPR3-BASP1 complex in synapse formation are depicted in Figure 29.

## Possible molecular mechanisms of PLPPR3-BASP1 complex in synapse formation

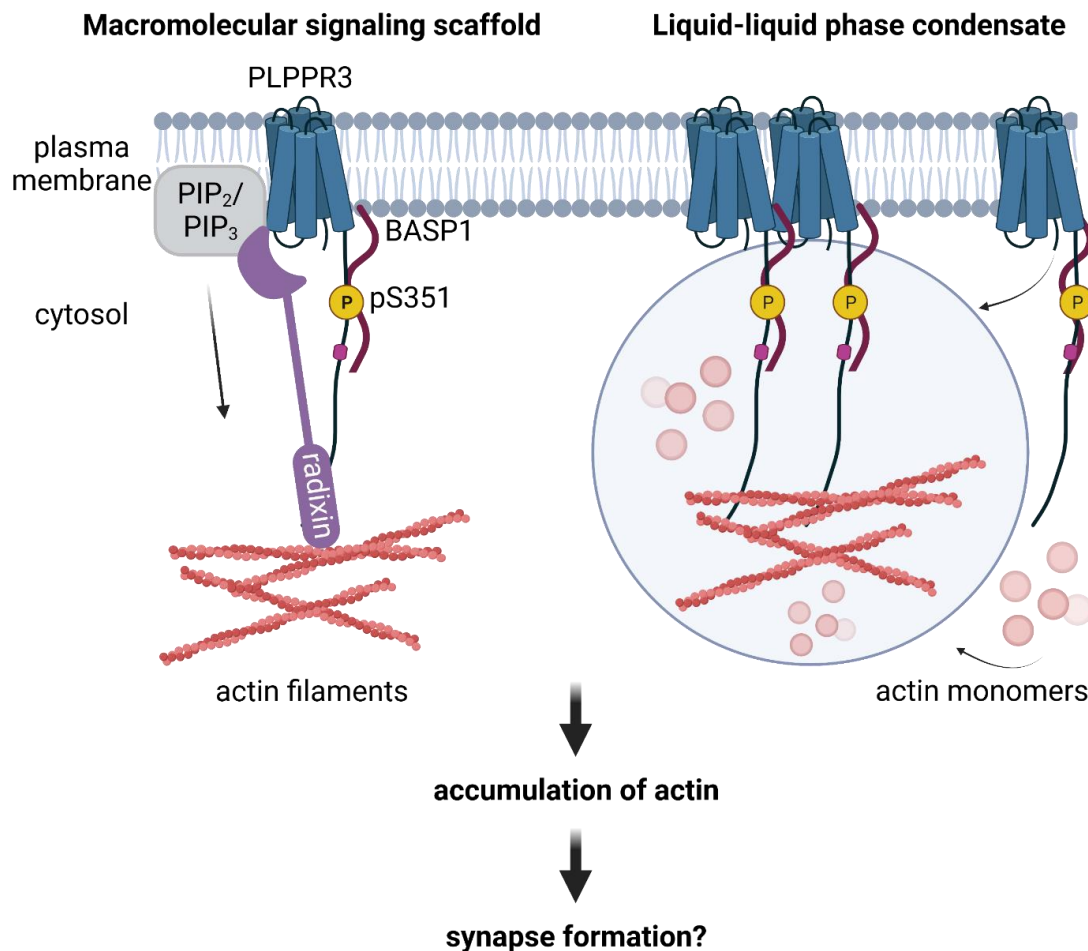


Figure 29. Possible molecular mechanisms of PLPPR3-BASP1 complex in synapse formation. Accumulation of actin filaments is one of the early stages of synapse formation which provides a scaffold for the synaptic machinery. The PLPPR3-BASP1 complex may form a signaling scaffold that regulates availability of phosphoinositides and downstream signaling cascades that induce actin polymerization. Radixin, another interaction partner of PLPPR3, could provide a link between the plasma membrane and the actin in this model. Alternatively, PLPPR3-BASP1 could undergo liquid-liquid phase separation. The PLPPR3-BASP1 condensate can recruit actin monomers and due to the high local concentration of actin, induce its polymerization. In both models, this leads to local accumulation of actin and synapse formation. Created with BioRender.com.

What could be the extracellular signal that leads to PKA-dependent PLPPR3 S351 phosphorylation? PKA activation requires the second messenger cAMP, which is produced by adenylyl cyclases (see Figure 13A). Adenylyl cyclases are regulated by G-protein-coupled receptors (GPCRs), of which G<sub>s</sub>-coupled receptors activate and G<sub>i/o</sub>-coupled receptors inhibit cAMP production.<sup>270</sup> Many neuromodulators, such as adenosine, serotonin, endocannabinoids, vasoactive intestinal peptide (VIP) and dopamine have been shown to regulate PKA-dependent signaling in the brain, inducing its activation or inhibition depending on the subtype of the receptor involved. In classical view, adenosine receptor A<sub>2A</sub>, serotonin

receptors 5-HT<sub>4-7</sub>, vasoactive intestinal peptide receptors VPAC<sub>1</sub> and VPAC<sub>2</sub>, and dopamine receptors D<sub>1</sub> and D<sub>5</sub> lead to PKA activation, while adenosine receptor A<sub>1</sub>, serotonin receptor 5-HT<sub>1</sub>, cannabinoid receptors CB<sub>1</sub> and CB<sub>2</sub> as well as dopamine receptors D<sub>2-4</sub> lead to PKA inhibition.<sup>271-277</sup> This classification is undoubtedly too simplistic, as many of these receptors form heterocomplexes between different subtypes as well as with different GPCRs.<sup>278-280</sup> Importantly, at least CB<sub>1</sub> and A<sub>2A</sub> receptor activation has been directly linked to synaptogenesis.<sup>256,257</sup> Going forward, it would be worth testing ligands for these receptors in their ability to trigger or inhibit PLPPR3 S351 phosphorylation and synapse formation. To this end, the acute brain slice stimulation assay established in this work will be a useful starting point to screen candidates, along with the many commercially available subtype-specific receptor agonists. However, it is worth noting that there are still hundreds of orphan GPCRs with hitherto unknown ligands.<sup>281</sup> The possible signaling cascade regulating PLPPR3 S351 phosphorylation and BASP1 binding is depicted in Figure 30.

### Possible signal transduction in the regulation of the PLPPR3-BASP1 complex

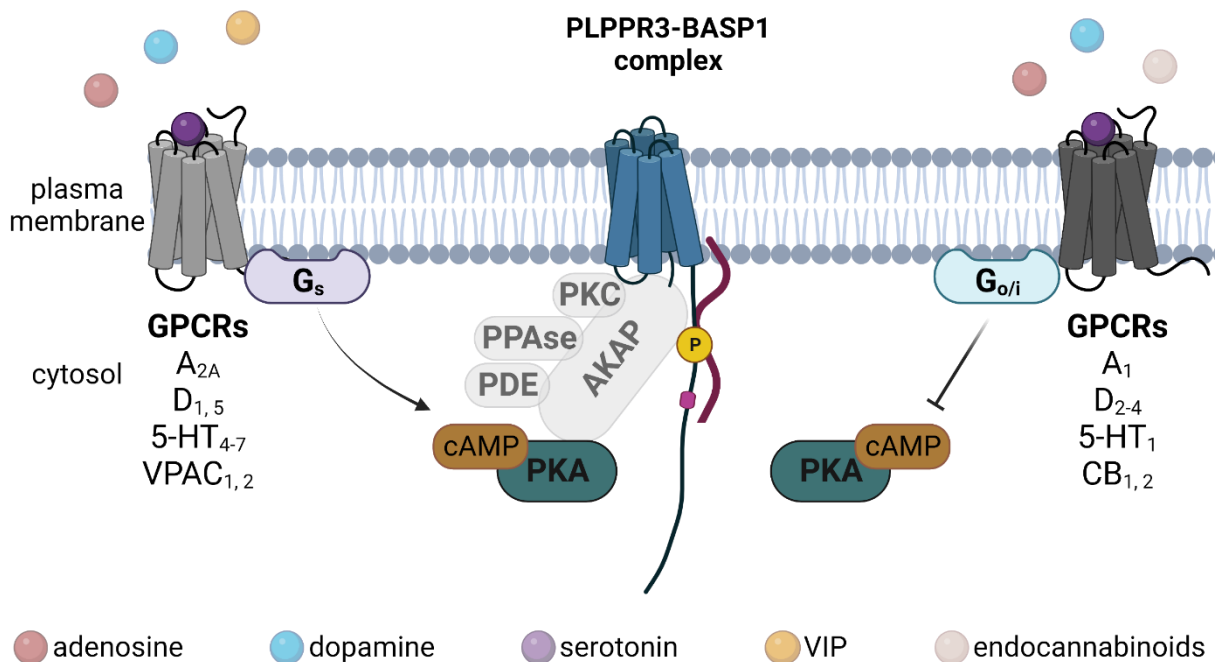


Figure 30. Possible signaling cascade regulating the phosphorylation of PLPPR3 S351 and binding of BASP1. PKA is activated by G<sub>s</sub>-coupled GPCRs that increase intracellular cAMP, and inhibited by G<sub>o/i</sub>-coupled GPCRs that decrease cAMP. Ligands that are known to regulate PKA include adenosine, dopamine, serotonin, endocannabinoids and vasoactive intestinal peptide (VIP). PKA activation leads to phosphorylation of PLPPR3 S351 and increases its binding to BASP1. PKA signaling to PLPPR3 could involve anchoring by a hitherto unknown AKAP (A kinase anchoring protein), which can additionally anchor phosphodiesterases (PDE), phosphatases (PPase), or other kinases such as PKC in the vicinity of PLPPR3-BASP1 complex, creating a signaling compartment. Created with BioRender.com.

### 7.3. Do PLPPR3 and BASP1 play a role in synaptic transmission?

While GPCR-activated phosphorylation of PLPPR3 implies regulation of PLPPR3 by GPCR-mediated extracellular signals, an interesting alternative – or parallel – question is whether PLPPR3 itself could modulate GPCR signaling and thus synaptic transmission. Two members of the PLPPR family, the postsynaptically located PLPPR4 and PLPPR5, have previously been implicated in glutamatergic synaptic transmission. Loss of PLPPR4 leads to increased excitatory transmission and epilepsy *in vivo*,<sup>282</sup> while loss PLPPR5 leads to susceptibility of epilepsy *in vivo*.<sup>283</sup> Currently, there have been no electrophysiological characterizations of PLPPR3 KO, however, there is some indication that PLPPR3-dependent modulation of synaptic transmission may be worth exploring. In a recent GPCR interactome screen using the yeast-two hybrid approach, PLPPR3 was found to interact with the dopamine receptor D<sub>2</sub>.<sup>284</sup> It would be interesting to test whether PLPPR3 alters dopamine signaling. To this end, electrophysiological responses to activation of D<sub>2</sub> receptors in *Wt* and *Plppr3*<sup>-/-</sup> acute brain slices could be measured.

Several hints in the literature also connect BASP1 to synaptic transmission. It was shown to possess ion channel activity in lipid bilayers,<sup>285</sup> although electrophysiological recordings in cells or brain tissue have never been reported. In a mass spectrometry screen, BASP1 was identified as an interaction partner of the kainate receptor GluK<sub>1</sub>.<sup>286</sup> GluK<sub>1</sub> is an ionotropic glutamate receptor with pre- and postsynaptic roles in synaptic transmission.<sup>287</sup> GluK<sub>1</sub> receptor is also linked to PKA signaling, as it can activate adenylyl cyclases non-canonically by influx of Ca<sup>2+</sup>.<sup>288</sup> Furthermore, an intriguing set of interaction partners – the synaptic vesicle-associated synaptojanin-1 and dynamin-1<sup>289,290</sup> – could suggest a role for BASP1 in synaptic vesicle recycling.<sup>291,292</sup> Synaptic vesicle recycling is the exo- and endocytosis of membrane that coats the synaptic vesicles, directly affecting synaptic transmission. In summary, there are indications that both PLPPR3 and BASP1 may be involved also in synaptic transmission. Future studies could explore their individual as well as cooperative contributions.

### 7.4. Conclusion

In this PhD project, I establish PLPPR3 as a highly phosphorylated signal integrator at neuronal synapses. My work identified 26 high-confidence phosphorylation sites in the intracellular domain of PLPPR3, and some of the kinases that target PLPPR3 include PKA, PKC and GSK3 $\beta$ . I showed that PKA phosphorylates PLPPR3 at S351 *in vitro*, in cells as well as in acute brain slice preparations. My experiments concluded that S351 phosphorylation does not regulate filopodia formation, which is a well-known function of PLPPR3 and the PLPPR family. Instead, phosphorylation of S351 regulates PLPPR3 binding to BASP1, an axonal protein implicated in morphogenesis and regeneration. I characterized PLPPR3 and pS351 exclusive

localization in synaptosomes, and the co-localization of BASP1 with presynaptic markers. The PLPPR3-BASP1 protein complex appears to be a novel presynaptic component with yet unknown function.

In addition, I generated and validated a phospho-specific antibody for PLPPR3 pS351, and tested multiple BASP1 antibodies in their ability to reliably detect BASP1. In summary, my work provides new tools and multiple intriguing avenues for future research.

## 8. Materials and methods

### 8.1. Antibodies

Table 5. Antibodies used in this thesis. Please note that antibodies in our lab are aliquoted and thus the majority of lot numbers were not traceable.

| Antibody                                     | Source                                    | Catalog nr | RRID        | Dilution | Application |
|--|---|------------|-------------|----------|-------------|
| <b>PLPPR3</b>                                | custom made <sup>88</sup><br>(Eurogentec) | NA         | NA          | 1:1000   | WB          |
|  |   |            |             | 1:250    | ICC         |
| <b>PLPPR3<br/>pan-S351</b>                   | custom made<br>(Eurogentec)               | NA         | NA          | 1:1000   | WB          |
|  |   |            |             | 1:500    | ICC, IHC    |
| <b>PLPPR3<br/>phospho-<br/>S351</b>          | custom made<br>(Eurogentec)               | NA         | NA          | 1:1000   | WB          |
|  |   |            |             | 1:500    | ICC         |
| <b>Akt pT450</b>                             | Cell Signaling<br>Technologies            | 9267       | AB_823676   | 1:1000   | WB          |
| <b>GAPDH<br/>(clone 6C5)</b>                 | EMD Millipore                             | CB1001     | -           | 1:3000   | WB          |
| <b>α-tubulin</b>                             | Sigma-Aldrich                             | T6199      | AB_477583   | 1:5000   | WB          |
|  |   |            |             | 1:500    | ICC         |
| <b>β3-tubulin</b>                            | Sigma-Aldrich                             | T2200      | AB_262133   | 1:500    | ICC         |
| <b>GFP</b>                                   | Genetex                                   | GTX13970   | AB_371416   | 1:1000   | ICC         |
| <b>NCAM-L1<br/>(clone 324)</b>               | Millipore                                 | MAB5272    | AB_2133200  | 1:500    | IHC         |
| <b>GluA1<br/>pS845<br/>(clone<br/>D10G5)</b> | Cell Signaling<br>Technologies            | 8084       | AB_10860773 | 1:1000   | WB          |
| <b>VGLUT1</b>                                | Synaptic Systems                          | 135303     | AB_887875   | 1:1000   | ICC         |

|                                       |                              |               |             |        |         |
|---------------------------------------|------------------------------|---------------|-------------|--------|---------|
| <b>Tau1 (clone PC1C6)</b>             | Millipore                    | MAB3420       | AB_94855    | 1:500  | ICC     |
| <b>Flag</b>                           | Sigma-Aldrich                | F1804         | AB_262044   | 1:1000 | WB, ICC |
| <b>Synaptophysin-1 (clone SVP-38)</b> | Sigma-Aldrich                | S5768         | AB_477523   | 1:1000 | WB      |
| <b>PSD-95</b>                         | Antibodies Incorporated      | 75-028        | AB_2292909  | 1:1000 | WB      |
| <b>turbo GFP (clone2H8)</b>           | Origene                      | TA150041      | AB_2622256  | 1:1000 | WB, ICC |
|                                       |                              |               |             | 1:50   | IP      |
| <b>BASP1</b>                          | Invitrogen                   | 703692        | AB_2815337  | 1:500  | WB, ICC |
| <b>BASP1</b>                          | Synaptic Systems             | 246003        | AB_10807100 | 1:1000 | WB, ICC |
| <b>BASP1</b>                          | R&D Systems                  | AF6479        | AB_10718853 | 1:200  | WB, ICC |
| <b>BASP1</b>                          | Caroni lab <sup>208</sup>    | NA            | NA          | 1:500  | WB, ICC |
| <b>BASP1</b>                          | Roberts lab <sup>210</sup>   | NA            | NA          | 1:1000 | WB, ICC |
| <b>BASP1</b>                          | Aviva                        | ARP59932_P050 | -           | 1:500  | WB, ICC |
| <b>Phalloidin-Atto 488</b>            | Sigma-Aldrich                | 49409         | -           | 1:500  | ICC     |
| <b>Alexa Fluor 568 phalloidin</b>     | Invitrogen                   | A12380        | -           | 1:500  | ICC     |
| <b>Alexa Fluor 647 phalloidin</b>     | Invitrogen                   | A22287        | -           | 1:500  | ICC     |
| <b>Höchst</b>                         | Immunochemistry technologies | ICT-639       | AB_2651135  | 1:5000 | IHC     |
| <b>α-rabbit IgG-HRP</b>               | Vector Laboratories          | PI-1000       | AB_2916034  | 1:5000 | WB      |

|                           |                        |             |             |        |          |
|---------------------------|------------------------|-------------|-------------|--------|----------|
| <b>α-mouse IgG-HRP</b>    | Vector Laboratories    | PI-2000     | AB_2336177  | 1:5000 | WB       |
| <b>α-sheep IgG-HRP</b>    | Jackson ImmunoResearch | 713-035-003 | AB_2340709  | 1:5000 | WB       |
| <b>α-chicken-Alexa488</b> | Jackson ImmunoResearch | 703-545-155 | AB_2340375  | 1:500  | ICC      |
| <b>α-mouse-DyLight488</b> | Novus Biologicals      | NBP1-75125  | AB_11009963 | 1:500  | ICC, IHC |
| <b>α-mouse-DyLight550</b> | Novus Biologicals      | NBP1-75616  | AB_11027384 | 1:500  | ICC, IHC |
| <b>α-rabbit-Alexa488</b>  | Jackson ImmunoResearch | 711-545-152 | AB_2313584  | 1:500  | ICC, IHC |
| <b>α-rabbit-Cy3</b>       | Jackson ImmunoResearch | 711-165-152 | AB_2307443  | 1:500  | ICC, IHC |
| <b>α-sheep-Alexa488</b>   | Jackson ImmunoResearch | 713-545-147 | AB_2340745  | 1:500  | ICC, IHC |
| <b>α-rat-DyLight650</b>   | Novus Biologicals      | NBP1-75663  | AB_11041265 | 1:500  | ICC, IHC |
| <b>mouse IgG</b>          | Jackson ImmunoResearch | 015-000-003 | AB_2337188  | 1:50   | IP       |

## 8.2. Animal procedures

Animals were housed and handled following the local animal experiment ethical guidelines and protocols. Animals were housed in the facilities of Charité Center for Experimental Medicine (FEM) under standard conditions with 12 hour light/dark cycle and food and water available *ad libitum*. All animal experiments were registered in the Landesamt für Gesundheit und Soziales Berlin (LaGeSo) under license T0347/11. All used animal strains were in the C57 Bl/6NCrl background. Wild-type and *Pten<sup>fl/fl</sup>* primary neuronal cultures were used as controls for the *Plppr3<sup>-/-</sup>*.<sup>88,293</sup> No experiments were analyzed by sex.

### **8.3. Cell line culturing and transfection**

HEK293T (#LV900A-1, BioCAT/SBI, RRID: CVCL\_UL49) and N1E-115 (#CRL-2263, ATCC, RRID: CVCL\_0451) cells were cultured in DMEM high glucose (#11965092, Life Technologies) supplemented with 10% fetal bovine serum (#F7524, Sigma) and 1% penicillin/streptomycin (#15140122, Gibco) under steady conditions at 37°C with 5% CO<sub>2</sub>. Cells were passaged twice a week at a ratio 1:4.

For experiments with HEK293T cells, glass coverslips or plastic cell culture dishes were coated with 15 µg/ml poly-DL-ornithine (#P8638, Sigma), while N1E-115 cells were grown without substrate. 6-well culture dishes (#92006, TPP) were used for western blot and immunoprecipitation experiments and cells were plated at a density of 300 000 cells/well. 12-well culture plates (#92012, TPP) were used for immunolabeling experiments and cells were plated at a density of 20 000 (HEK293T) or 30 000 (N1E-115) per well. Cells were grown overnight before transfection.

Cell lines were transfected with Lipofectamine 2000 (#11668019, Invitrogen) and Opti-MEM reduced serum medium (#31985062, Gibco). 1 µg of total DNA and 2 µl of Lipofectamine was used per well. 300 µl of Opti-MEM/well was used for 12-well plates, for 6-well plates 400 µl/well was used. To prepare transfection mix, half of the Opti-MEM volume was first mixed with DNA, and the other half with Lipofectamine, mixed, and incubated at room temperature for 5 minutes. The DNA and Lipofectamine were then pooled and incubated at 37°C for 10 minutes. Transfection mix was added to cells dropwise, and cells were incubated for 5 hours. Finally, cells were changed into fresh complete medium and grown overnight. For experiments that required starvation, cells were changed into FBS-free medium.

### **8.4. Primary neuronal culture and transfection**

Cortices and hippocampi of male and female embryos from E16.5 pregnant mice were dissected into individual Eppendorf tubes with cold HBSS (2 hippocampi/tube, one hemisphere of cortex/tube), rinsed with fresh HBSS, and digested with 20 U/ml papain (#LS003126, Worthington Biochemical) (500 µl per one hippocampi Eppendorf, 1 ml for cortex) for 30 minutes on thermomixer at 37°C with gentle shaking (350 rpm). Digestion was stopped by replacing the supernatant with prewarmed inactivation solution [DMEM with 10% FCS, 1% Pen/Strep, 2.5 mg/ml Albumin/BSA (#A2153, Sigma) and 2.5 mg/ml trypsin inhibitor (#T9253, Sigma)] and incubating at 37°C for 5 minutes. Next, supernatant was replaced with 200 µl plating medium (Neurobasal, 10% heat inactivated FCS, 2% B27, 1% GlutaMax and 1% Pen/Strep) and tissue was disrupted by gentle trituration. Neurons from different preparation tubes were pooled and counted. Neurons were plated in plating medium and changed to

complete medium (Neurobasal, 2% B27, 0.5% Glutamax and 1% Pen/strep) after 2 hours. For immunolabeling experiments, neurons were plated on 15 µg/ml poly-DL-ornithine + 20 µg/ml laminin (#L2020, Sigma-Aldrich) coated coverslips at a density of 120 000 neurons/18 mm (12-well) coverslip or 80 000 neurons/13 mm (24-well; #92024, TPP) coverslip. For western blot experiments, 0.5 million neurons were plated directly on poly-DL-ornithine coated plastic culture dish.

Primary neurons were transfected using the calcium phosphate method.<sup>294</sup> Transfections were carried out on 12-well culture plates, each well containing 120 000 neurons. CaCl<sub>2</sub> (2.5 µl/well) was diluted in H<sub>2</sub>O (22.5 µl/well) and briefly mixed, then DNA was added to the mix (4 µg/well for single, 2+2 µg/well for double transfections). 2xBSS buffer (25 µl/well; 50 mM BES, 280 mM NaCl, 1.5 mM Na<sub>2</sub>HPO<sub>4</sub>, pH 7.26) was added dropwise to the DNA-calcium mix and gently mixed by tapping. Finally, prewarmed Neurobasal medium with 2% B27 and 0.25% GlutaMax was added and the mix was incubated for 15 minutes at 37°C. Culture medium was collected and exchanged with transfection medium and neurons were transfected for 20 minutes in the incubator. Wells were washed three times with 500 µl HBSS buffer (135 mM NaCl, 4 mM KCl, 1 mM Na<sub>2</sub>HPO<sub>4</sub>, 2 mM CaCl<sub>2</sub>, 1 mM MgCl<sub>2</sub>, 20 mM HEPES, 20 mM d-Glucose, pH 7.3). After final wash, warm conditioned medium was added back to wells.

### **8.5. Acute brain slice preparation**

300 µm thick coronal sections containing hippocampus and striatum were prepared from adolescent *Wt* mice in solution (110 mM choline chloride, 2.5 mM KCl, 1.25 mM NaH<sub>2</sub>PO<sub>4</sub>, 26 mM NaHCO<sub>3</sub>, 11.6 mM sodium ascorbate, 3.1 mM sodium pyruvate, 7 mM MgCl<sub>2</sub>, 0.5 mM CaCl<sub>2</sub> and 10 mM d-glucose, pH 7.4) at close to 0°C, followed by incubation in the same solution at 32°C for 5 minutes. The slices were then transferred to artificial cerebrospinal fluid (ACSF; 125 mM NaCl, 2.5 mM KCl, 1.25 mM NaH<sub>2</sub>PO<sub>4</sub>, 25 mM NaHCO<sub>3</sub>, 2 mM CaCl<sub>2</sub>, 1 mM MgCl<sub>2</sub>, and 25 mM dextrose) and incubated at room temperature for at least 30 minutes before stimulation with Forskolin (30 µM 15 minutes) was carried out. Forskolin was added directly into the ACSF and briefly allowed to diffuse by gas flow before slices were transferred into the stimulation chamber. Stimulation was carried out at room temperature. Following stimulation, brain slices were collected into an Eppendorf with a brush, snap frozen in liquid nitrogen and stored in -80°C until further use. All solutions were saturated with 95% O<sub>2</sub>/5% CO<sub>2</sub>.

### **8.6. Cloning**

All plasmids generated during the course of this thesis are in pCAX backbone (CAG promoter, ampicillin-resistant), have the same restriction sites for insertion (NheI N-terminally, NotI C-terminally, and an additional BamHI site between the gene and Flag tag), and carry a C-

terminal tag (Flag tag separated with a flexible GSGGGSG-linker, His tag with a VDGRP-linker). General cloning workflow included PCR (KOD Hot Start DNA polymerase, #71086-3, Merck Millipore) followed by digest with restriction enzymes (FastDigest, Thermo Scientific), gel electrophoresis on 1-2% agarose gel, gel purification (NucleoSpin Gel and PCR Clean-up kit, #740609.25, Macherey-Nagel), ligation (T4 DNA ligase, #M0202L, NEB) and transformation into competent *E.coli* (DH5 $\alpha$ ). Bacteria were plated on agar with selection antibiotic and grown overnight at 37°C. Individual colonies were grown in 5 ml LB medium with selection antibiotic overnight, and plasmid DNA was purified using the NucleoSpin Plasmid Mini kit (#740588.50, Macherey-Nagel) according to the manufacturer's protocol. Control digests with restriction enzymes cutting within the insert were performed whenever possible. Clones were sent for sequencing at LGC. Correct clones were transformed into *E.coli*, the transformation mix was added directly into 200 ml LB medium with selection antibiotic and grown overnight, after which the plasmid was purified with NucleoBond Xtra Maxi Plus kit (#740416.50, Macherey-Nagel) according to the manufacturer's protocol. DNA concentration was measured using ND-1000 Spectrophotometer (Thermo Fisher Scientific).

Subcloning was performed using standard PCR protocol (first denaturation at 95°C for 2.5 minutes, then 33 cycles of denaturation at 95°C for 30 seconds, annealing at 63°C for 20 seconds, elongation at 70°C for 50 seconds. A final elongation for 3 minutes at 70°C was carried out at the end). To amplify GC-rich BASP1 DNA, 4  $\mu$ l of DMSO was added into 50  $\mu$ l PCR reaction to decrease thermostability, and annealing was done at 50°C. Subcloning to insert a membrane-tag to PLPPR3 intracellular domain was achieved using oligonucleotide annealing. pMT4-PLPPR3-ICD-His vector (Fatih Ipek) was digested with EcoRI and PstI to excise a short N-terminal sequence, purified via gel extraction and dephosphorylated with Antarctic phosphatase (#M0289L, NEB) according to manufacturer's protocol. Oligonucleotides (10  $\mu$ M, see Table 6) were annealed in T4 ligase buffer by heating to 95°C for 5 minutes and gradual cooling to room temperature over 30 minutes. Annealed oligonucleotides were phosphorylated with T4 PNK (#M0201L, NEB) according to manufacturer's protocol, ligated into vector and transformed into competent bacteria.

Point mutations to generate phospho-mutants were introduced via a two-step PCR with overlapping primers. First, standard PCR was used to generate DNA fragments from the N-terminus to the point mutation and from the point mutation to the C-terminus. The fragments were purified via gel extraction. In the second step, splice-overhang extension PCR was used to merge the two fragments into one insert. In this PCR reaction, the first 10 cycles were run without primers to achieve annealing between the two overlapping fragments. After adding N- and C-terminal primers, the reaction was run another 30 cycles to amplify the full-length insert. To generate the PLPPR3-N-S351A/S379A/T380A triple mutant, PLPPR3-N-S379A/T380A

mutant was used as a template to introduce the additional S351A mutation. Subcloning of PLPPR3-S351A/D-Flag into lentiviral vectors was achieved by PCR with forward and reverse primers covering the entire insert (see Table 5 for primers). Lentiviruses were produced by the Viral Core Facility (Charité).

Table 6. Plasmids and viruses generated during this PhD project.

| Plasmid                        | Cloning primers   | Description                                 |
|--------------------------------|---|---|
| pCAX_PLPPR3-ICDm-His           | <b>fw:</b> aattcgCTAGCgccaccAtgggctgcgtgcagtgcaaaga<br>taaagaagcgcaggcaccacctgca<br><b>rev:</b> ggtggtgcctgcgcttctttatctttgcactgcacgcagcccaTg<br>gtggcGCTAGcg   | Δ1-283, with membrane-targeting sequence    |
| pCAX_PLPPR3-ICDm-S351A-His     | <u>Mutagenesis primers:</u><br><b>fw:</b> CTGAAGCGAGCCgcCGTGGATGTGGAC<br><b>rev:</b> GTCCACATCCACGgcGGCTCGCTTCAG<br><u>Extension primers:</u><br><b>fw:</b> same as for PLPPR3-ICDm-His<br><b>rev:</b> gtgatggggccggccgctgcacgtcctgttacctcctggcc                  | Same as above, S351A (phospho-dead)         |
| pCAX_PLPPR3-ICDc-His           | <b>fw:</b> aattcgCTAGCgccaccAtggCGtgctgcagtgcaaag<br>ataaagaagcgcaggcaccacctgca<br><b>rev:</b> ggtggtgcctgcgcttctttatctttgcactgcacgcaCGccaT<br>ggtggcGCTAGcg  | Δ1-283, mutated membrane-targeting sequence |
| pCAX_PLPPR3-N-S351A-Flag       | <u>Mutagenesis primers:</u><br><b>fw:</b> CTGAAGCGAGCCgcCGTGGATGTGGAC<br><b>rev:</b> GTCCACATCCACGgcGGCTCGCTTCAG<br><u>Extension primers (same for all of the following):</u><br><b>fw:</b> GCTAGCgtcaccATGCTTGCTATG<br><b>rev:</b> gtcgcgccgctTACTTGTCATCGTCATCC | N-terminal half of PLPPR3, S351A            |
| pCAX_PLPPR3-N-S379A-Flag       | <u>Mutagenesis primers:</u><br><b>fw:</b> CTGCCCCGGGTCgcCACGCCCTCGCTG<br><b>rev:</b> CAGCGAGGGCGTGgcGACCCGGGGCAG  | N-terminal half of PLPPR3, S379A            |
| pCAX_PLPPR3-N-T380A-Flag       | <u>Mutagenesis primers:</u><br><b>fw:</b> CCCCgggtcagcgcgcccctcgctg<br><b>rev:</b> CAGCGAGGGCGcGCTGACCCGGGG   | N-terminal half of PLPPR3, T380A            |
| pCAX_PLPPR3-N-S379A/T380A-Flag | <u>Mutagenesis primers:</u><br><b>fw:</b> CTGCCCCGGGTCgcCgCGCCCTCGCTG<br><b>rev:</b> CAGCGAGGGCGcGgcGACCCGGGGCAG  | N-terminal half of PLPPR3, S379A, T380A     |

|                                      |  |  |
|--------------------------------------|--|--|
| pCAX_PLPPR3-N-S351A/S379A/T380A-Flag | Same primers as for S351A and S379A/T380A mutants  | N-terminal half of PLPPR3, S351A, S379A, T380A   |
| pCAX_PLPPR3-S351A-Flag               | Same primers as for PLPPR3-N-S351A-Flag  | Full length S351A  |
| pCAX_PLPPR3-S351D-Flag               | Same primers as for PLPPR3-N-S351D-Flag  | Full length S351D (phospho-mimic)  |
| pCAX_BASP1-Flag                      | <b>fw:</b> tagagCTAGCgccaccATGGGAGGCAAGCTGAGC<br><b>rev:</b> ccaccggatccCTCTTTGACGGCCACGCTTTGCTCGGAG | Flag-tagged BASP1  |
| f(CAG)_PLPPR3-S351A-Flag             | <b>fw:</b> GCTAGCgtcaccATGCTTGCTATG<br><b>rev:</b> AAGGCGCGCCTTACTTGTCATCGTCATCC                     | full-length S351A in lentiviral vector; virus produced by Viral Core Facility, Charité |
| f(CAG)_PLPPR3-S351D-Flag             | Same as above  | full-length S351D in lentiviral vector; virus produced by Viral Core Facility, Charité |

Table 7. Other plasmids and viruses used in this project.

| Plasmid             | Source or reference                                     | Description  |
|---------------------|---|--|
| pPAL_PLPPR3-ICD-His | Fatih Ipek  | PLPPR3 intracellular domain (aa 284-716) in bacterial vector |
| pCAX_PLPPR3-N-Flag  | Dr. Joachim Fuchs/ Dr. George Leondaritis <sup>88</sup> | aa 1-407, deletion of distal C-terminus                      |
| pCAX_PLPPR3-C-Flag  |   | aa 408-716, deletion of N-terminal half, membrane-bound      |
| pCAX_PLPPR3-Cm-Flag |   | same as above, cytosolic                                     |
| pCMV6_BASP1-tGFP    | #MG217147, Origene                                      | mouse turboGFP-tagged BASP1                                  |
| pCAX_PLPPR3-Flag    | <sup>88</sup>   | Flag-tagged full length PLPPR3                               |
| f(syn)_U6_GFP       | AG Rosenmund, Charité                                   | cytosolic GFP under synapsin promoter                        |

|                                  |   |  |
|----------------------------------|---|--|
| pN1_GFP-F                        | <sup>295</sup>                              | membrane-localized GFP                           |
| f(CAG)_PLPPR3-Flag               | <sup>88</sup>                               | full length PLPPR3 in lentiviral vector          |
| f(syn)-NLS.RFP-P2A-MSCW (BL-181) | Viral Core Facility, Charité                | lentivirus encoding nuclear RFP                  |
| f(syn)-Syp-GFP-w                 | Viral Core Facility, Charité <sup>296</sup> | GFP-tagged synaptophysin under synapsin promoter |

### 8.7. Treatments: Forskolin, 8-Br-cAMP, H89, PMA, DMSO

Forskolin (#11018, Cayman Chemical) was used at a final concentration of 10-30  $\mu$ M for 5-30 minutes, depending on experiment (see figure descriptions). 8-Br-cAMP (#B7880, Sigma-Aldrich) was used at 0.5-1 mM concentration for 5 minutes. H89 (#2910, Tocris) was used at 1-50  $\mu$ M concentration for 1 hour. PMA (#10008014, Cayman Chemical) was used at 1  $\mu$ M concentration for 10 minutes. For experiments requiring DMSO control treatments, at least one control treatment was carried out per experiment to ensure the solvent has no effect. For treatment of cells, all drugs were added directly into medium and mixed by gentle trituration. For acute brain slice treatment, Forskolin was added into 100 ml ACSF and the mixture was allowed to homogenize by air flow for a few minutes before brain slices were added.

### 8.8. Cell and tissue lysis, total protein concentration measurement

Cells, neurons and brain tissue were lysed in Ripa buffer (50 mM Tris-HCl, 150 mM sodium chloride, 1% NP-40, 0.5% sodium deoxycholate and 0.1% sodium dodecyl sulfate, pH 8.0) supplemented with lab-made phosphatase (1 mM  $\text{Na}_2\text{MO}_4$ , 1 mM NaF, 20 mM  $\beta$ -glycerophosphate, 1 mM  $\text{Na}_3\text{VO}_4$  and 500 nM Cantharidin (#3322.1 Roth)) and commercial protease inhibitors (protease inhibitor cocktail III, #539134, Calbiochem). Phosphatase inhibitors were omitted when Lambda phosphatase treatment was required.

For cell lysis, culture medium was aspirated and cells were briefly rinsed with ice cold PBS (prepared from tablets, #A9191, Applichem). PBS was aspirated and lysis buffer (200  $\mu$ l for neurons, 300  $\mu$ l for cell lines) was added, cells were scraped off the surface and collected into an Eppendorf tube. Cells were lysed at 4°C for 20 minutes with overhead rotation, and cell debris was pelleted with centrifugation at 14 000 rpm for 20 minutes at 4°C. Supernatant containing proteins was collected into a fresh tube, and samples were either used directly or kept in -20°C until use.

For brain lysates used for Figure 22, whole adult mouse brain (ca 0.45 g) was mechanically disrupted in 4.5 ml Ripa with phosphatase and protease inhibitors using Dounce homogenizer. For the experiment with acute brain slices (Figure 20C) a total of three slices were used per experimental condition, each constituting half of a coronal section. The slices were homogenized in 1 ml Ripa with phosphatase and protease inhibitors using micro tissue homogenizer and trituration with pipet. In both cases, tissue homogenates were lysed at 4°C for 20 minutes with overhead rotation, and cell debris was pelleted with centrifugation at 14 000 rpm for 20 minutes at 4°C. Supernatant containing proteins was collected into a fresh tube, and samples were either used directly or kept in -20°C until use.

All samples used for western blot experiments, except the co-immunoprecipitation samples, were measured for total protein concentration using the Pierce BCA Protein Assay Kit (#23225, Thermo Scientific) following the manufacturer's protocol.

### **8.9. Lambda phosphatase treatment**

For western blot experiments with cell lysates, 48 µl of protein lysate was mixed with 6 µl of 10x NEBuffer for Protein MetalloPhosphatases (PMP), 6 µl of 10 mM MnCl and 6 µl (=2400 units) of Lambda phosphatase (#P0753, NEB). For phospho-mass spectrometry experiments, 400 µl of purified PLPPR3 ICD proteins were mixed with 50 µl of 10x NEBuffer for Protein MetalloPhosphatases (PMP), 50 µl of 10 mM MnCl and 10 µl of Lambda phosphatase. For PLPPR3 ICD purified from *E.coli*, 40 µl of protein (roughly 100 ng) was mixed with 5 µl of 10x NEBuffer for Protein MetalloPhosphatases (PMP), 5 µl of 10 mM MnCl and 2 µl of Lambda phosphatase. Dephosphorylation was carried out at 30°C for 30 minutes and stopped by addition of Roti Load buffer (#K929.1, Roth). Treatment control included H<sub>2</sub>O instead of Lambda phosphatase and was also kept at 30°C for 30 minutes. Phosphorylated control was diluted with H<sub>2</sub>O to the same final volume of other samples and kept on ice for 30 minutes.

### **8.10. *In vitro* phosphorylation assay**

Prior to phosphorylation assay, protease inhibitors were added to the purified PLPPR3 ICD (1:100 AEBSF; #1421, Applichem). 4.1 µl of purified PLPPR3 ICD from *E.coli* (final concentration 0.075 mg/ml) was mixed with 0.2 µl purified kinase, 0.8 µl phosphorylation buffer (final concentration of 25 mM HEPES, 100 mM NaCl, 5 mM MgCl, 2 mM EGTA, 25 mM DTT), 1 µl ATP (final concentration 1 mM) and 14 µl H<sub>2</sub>O. Final concentrations of purified kinases were: PKA (20 000 Units; #P6000S, Biolabs), GSK3β (5.1 µg/ml; #40007, BPS Bioscience), CDK5 (1 µg/ml; #C0745, Sigma-Aldrich), FYNA (5.1 µg/ml; #F6557, Sigma-Aldrich). Phosphorylation was carried out at 30°C for 2 hours. In the case of dual phosphorylation,

GSK3 $\beta$  was added 1 hour into phosphorylation with PKA. The reaction was stopped by addition of Roti Load buffer. Samples were analyzed by PhosTag western blot.

### **8.11. Co-immunoprecipitation**

For co-immunoprecipitation, protein lysates (prepared as described above) from 2 wells of 300 000 HEK293T cells each were pooled. 30  $\mu$ l of protein lysate was taken for input control, mixed with Roti Load and boiled for 5 minutes at 95°C. 12  $\mu$ l of tGFP or IgG antibody was added to the rest of the protein lysate and incubated at 4°C overnight with overhead rotation. Dynabeads Protein A (#10002D, Invitrogen) were washed with Ripa three times, and 20  $\mu$ l of slurry was added to each sample. The sample was incubated for 1 hour at 4°C with overhead rotation, and washed 4 x 15 minutes with Ripa at 4°C with overhead rotation. Finally, the beads were eluted with 30  $\mu$ l 1x Roti Load by boiling at 95°C for 3 minutes, and repeated once more to maximize yield. Samples were analyzed by western blot.

### **8.12. SDS-PAGE, PhosTag SDS-PAGE and western blotting**

All western blot samples were prepared by adding Roti Load to the final concentration of 1x and boiling at 95°C for 5 minutes. 20  $\mu$ g of total protein from HEK293T or N1E-115 cells, or 40  $\mu$ g of total protein from neuronal lysates were separated on 8-12% acrylamide gels at 80V for 15 minutes followed by 120V until the dye front ran out. Proteins were transferred onto 20  $\mu$ m pore size nitrocellulose membranes (#1620097, Biorad) for 2.5 hours at 400 mA on ice. Membrane was rinsed in dH<sub>2</sub>O, labeled with Ponceau S (#A2935, Applichem) solution according to manufacturer's protocol and de-stained in dH<sub>2</sub>O. Membrane was blocked in 5% skim milk (#T145.2, Carl Roth) in TBS-T (5 mM Tris-HCl, 15 mM NaCl, 0.005% Tween20, pH 7.4) for 1 hour at room temperature and incubated with primary antibodies (see Table 5) in blocking solution at 4°C overnight. Membrane was washed 3 x 10 minutes in TBS-T and incubated with secondary antibodies (see Table 5) in blocking solution at room temperature for 1 hour, followed by 3 x 10 minutes washes in TBS-T. Blots were developed with ECL Western Blotting Substrate (#W1001, Promega) or ECL Select Western Blotting Detection Reagent (#RPN2235, Cytiva) according to manufacturer's protocol. Images of western blots were acquired with Fusion SL camera (VilberLourmat, Germany) and manufacturer's software using automatic exposure mode. Chemiluminescent signal image and molecular weight marker image were automatically overlaid by the software. For all SDS-PAGE experiments presented in this work, molecular weight marker ranging from 10 to 250 kDa was used (#26620, Thermo Scientific).

PhosTag acrylamide (#AAL-107, FUJIFILM) gels were prepared according to manufacturer's protocol. 6% gels were used for PLPPR3 full-length variants, and 8% gels for shorter variants.

Gel electrophoresis was run under a constant current (30 mA/gel) until the dye front ran out. Gels were washed 3 x 10 minutes in transfer buffer containing 10 mmol/L EDTA, and 1 x 10 minutes in transfer buffer without EDTA prior to transfer. Proteins were transferred onto a PVDF membrane with 0.2  $\mu\text{m}$  pore size (#88520, Thermo Scientific) for 2.5 hours at 400 mA on ice. The rest of the steps were carried out as described above.

### **8.13. Quantification of western blot band intensities**

Quantification of protein band intensities was carried out in Fiji using the Analyze->Gels command. Composed protein band and molecular weight marker images were used for quantification. Rectangular selection, big enough to include the biggest band, was used to select each protein band. Each lane was plotted using the Plot lanes command, and if necessary, a straight line was drawn to close off the area under the curve. Intensity was measured for each band. Co-immunoprecipitation band (PLPPR3) was normalized to immunoprecipitation band (tGFP) by dividing the intensity PLPPR3/tGFP. The value of each non-stimulated replicate was normalized to 1, and the value of Forskolin-stimulated sample was expressed as Forskolin/control. Wilcoxon statistical analysis was used to compare control and treatment.

### **8.14. Purification of PLPPR3 ICD constructs**

$12 \times 10^6$  HEK293T cells were seeded in 150  $\text{cm}^2$  Corning flasks (#CLS431465, Merck) and cultured for 1 day. Cells were transfected with PLPPR3-ICDm-His or PLPPR3-ICDc-His constructs using 75  $\mu\text{g}$  of total DNA and 225  $\mu\text{l}$  PEI in 5 ml serum free hybridoma medium (#11279023, Gibco), and grown for 1 day. Cells were washed with ice cold PBS once and scraped off the flask in fresh 10 ml ice cold PBS on ice. Following centrifugation at 4000 rpm for 1 min at 4°C, PBS was aspirated and the cell pellet was either frozen or used directly for purification. Four independent replicates were purified and analyzed in parallel.

For purification, frozen pellets were thawed on ice, lysis buffer was added [20 mM Hepes, 150 mM NaCl, 20 mM Imidazole, phosphatase inhibitor cocktail (1:25), Cantharidin (1:50), protease inhibitor tablets (1 tbl/10 ml, #4693159001, Roche), AEBSF (1:100, #A1421, Applichem), pH 7.4] and the pellets were sonicated 3 x 60 seconds with 6 cycles and 60% power. Lysate was cleared by centrifugation at 21 000 g at 4°C for 30 minutes. For the purification of cytosolic PLPPR3-ICDc-His, the supernatant was collected and incubated with Ni Sepharose™ 6 Fast Flow (GE) beads (300  $\mu\text{l}$ /sample) overnight at 4°C on a rotator. For the purification of membrane-bound PLPPR3-ICDm-His, protein was extracted from the pellet with 0.5% Fos-choline 14 (#F312, Anatrace) at 4°C for 40 minutes and centrifuged at 21 000 g for 1 hour at 4°C. Supernatant was collected and incubated with Ni Sepharose™ 6 Fast Flow (GE) beads

overnight at 4°C on a rotator. Sample was cleared on Pierce centrifugal columns (#89896, Thermo Scientific) by gravity flow and washed three times with 20 ml wash buffer (Wash 1: 20 mM Hepes, 150 mM NaCl, 50 mM Imidazole, pH 8.5; Wash 2: 20 mM Hepes, 500 mM NaCl, 50 mM Imidazole, pH 8.5; Wash 3: 20 mM Hepes, 150 mM NaCl, pH 8.5). Finally, beads were solubilized in 800 µl of buffer (20 mM Hepes, 150 mM NaCl, pH 8.5). Half of the sample (400 µl) was subjected to phosphatase treatment to confirm true phosphorylation sites (see section on Lambda phosphatase treatment). After phosphatase treatment, the protein was washed on beads three times with 5 ml buffer (20 mM Hepes, 150 mM NaCl, pH 8.5) to get rid of the phosphatase. The buffer was discarded and dry beads with protein were handed to the mass spectrometry facility. Phosphorylation status of samples was confirmed by PhosTag SDS-PAGE prior to mass spectrometry analysis.

### **8.15. Affinity chromatography to identify binding partners**

Sulfolink columns (#44999, Thermo Scientific) were coupled with peptides constituting the S351 phosphorylation site (phospho: LKRApSVDVDLLA; non-phospho: LKRASVDVDLLA) according to manufacturer's protocol. Affinity purification was carried out following the manufacturer's protocol using gravity flow instead of centrifugation. Affinity columns were equilibrated to room temperature for 15 minutes before use, and equilibrated three times with 2 ml of PBS. Columns were incubated with 400 µl of freshly prepared brain lysate (see section on Cell and tissue lysis) in 1600 µl PBS for 1.5 hours at room temperature with overhead rotation. Columns were washed with 2 ml PBS four times, and eluted with 2 ml of elution buffer (0.2 M glycine-HCl, pH 2.5) in ~500 µl fractions into a fresh tube containing 100 µl neutralization buffer (1 M Tris-HCl, pH 8.5). The protein concentration in each fraction was measured by Nanodrop, and fractions with highest protein content were pooled to concentrate protein by ethanol precipitation. For precipitation, 9 volumes of ice cold 100% ethanol was added to 1 volume of protein solution. To aid precipitation, 2 µl of Glycoblue (#AM9515, Invitrogen) was added to the mix, and the protein was precipitated overnight at 4°C. The following day, the precipitation solution was centrifuged at 14 000 rpm for 1 hour at 4°C, the aqueous solution discarded, and the protein pellet resolubilized in 100 µl Roti Load buffer and boiled at 95°C for 5 minutes. The protein samples were run on SDS-PAGE and bands cut out of gel as described in the Results section.

### **8.16. Mass spectrometry analysis**

**Phospho-mass spectrometry:** Prior to mass spectrometry analysis, beads were resuspended in 20 µl urea buffer (2M urea, 50 mM ammonium bicarbonate, pH 8.0), reduced in 12 mM dithiothreitol at 25°C for 30 minutes, followed by alkylation with 40 mM chloroacetamide at 25 °C for 20 minutes. Samples were digested with 0.5 µg Trypsin/LysC,

Trypsin/GluC or GluC overnight at 30°C. The peptide-containing supernatant was collected and digestion was stopped with 1% formic acid. Peptides were desalted and cleaned up using Stage Tip protocol (PMID: 12585499). Samples were eluted with 80% acetonitrile/0.1% formic acid, dried using speedvac, resuspended in 3% acetonitrile/0.1% formic acid and analysed by LC-MS/MS. Peptides were separated on a reversed-phase column, a 20 cm fritless silica microcolumn with an inner diameter of 75 µm, packed with ReproSil-Pur C18-AQ 3 µm resin (Dr. Maisch GmbH) using a 90 min gradient with a 250 nl/min flow rate of increasing Buffer B concentration (from 2% to 60%) on a High-Performance Liquid Chromatography (HPLC) system (Thermo Fisher Scientific), ionized with electrospray ionization (ESI) source (Thermo Fisher Scientific) and analyzed on a Thermo Q Exactive Plus instrument. The instrument was run in data dependent mode selecting the top 10 most intense ions in the MS full scans (ranging from 350 to 2000 m/z), using 70 K resolution with a  $3 \times 10^6$  ion count target and 50 ms injection time. Tandem MS was performed at a resolution of 17.5 K. The MS2 ion count target was set to  $5 \times 10^4$  with a maximum injection time of 250 ms. Only precursors with charge state 2–6 were selected for MS2. The dynamic exclusion duration was set to 30 s with a 10 ppm tolerance around the selected precursor and its isotopes. Raw data were analyzed using MaxQuant software package (v1.6.3.4, PMID: 27809316) using a human UniProt database (HUMAN.2019-07) and PLPPR3 sequence database, containing forward and reverse sequences. The search included variable modifications of serine, threonine and tyrosine. Minimal peptide length was set to seven amino acids and a maximum of 3 missed cleavages was allowed. The FDR was set to 1% for peptide and protein identifications. Phosphosite intensity values were normalized for PLPPR3 protein abundance. Results were filtered for reverse database hits and potential contaminants. Phosphosites found in 3/4 replicates with localization probability >0.75 and good spectra were considered high-confidence.

**Identification of interaction partners:** The samples were run on SDS-PAGE gel, cut out of the gel, and digested with Trypsin prior to mass spectrometry analysis. Protein samples were concentrated on a trap column (PepMap C18, 5 mm x 300 µm x 5 µm, 100Å, Thermo Fisher Scientific) with 2:98 (v/v) acetonitrile/water containing 0.1% (v/v) trifluoroacetic acid at a flow rate of 20 µl/min for a total of 4 minutes. The samples were analyzed by nanoscale LC-MS/MS using a Q Exactive Plus mass spectrometer coupled with an Ultimate 3000 RSLCnano (Thermo Fisher Scientific). The system contained a 75 µm i.d. x 250 mm nano LC column (Acclaim PepMap C18, 2 µm; 100 Å; Thermo Fisher Scientific). The mobile phase A consisted of 0.1% (v/v) formic acid in H<sub>2</sub>O, while mobile phase B consisted of 80:20 (v/v) acetonitrile/H<sub>2</sub>O containing 0.1% (v/v) formic acid. The samples were eluted using a gradient of mobile phase B (3-53%) in 16 minutes, followed by washing with 98% of phase B and equilibration with starting condition using a flow rate of 300 nl/min. Full MS spectra (350–1,650 m/z) were

acquired at a resolution of 70 000 (FWHM), followed by data-dependent MS/MS fragmentation (300-2,000 m/z) of the top 10 precursor ions (dissociation method HCD, resolution 17 500, 1+ charge state excluded, isolation window of 1.6 m/z, NCE of 27%, dd 10s, MS 1e6, MSMS AGC 5e5). Maximum ion injection time was set to 50 ms for MS, and 120 ms for MS/MS scans. Background ions at m/z 391.2843 and 445.1200 act as lock masses. Quantification of proteins was performed with MaxQuant software version 1.6.0.1 using default Andromeda LFQ parameter.<sup>297</sup> The search included the following modifications: methionine oxidation and N-terminal acetylation (variable), carbamidomethyl cysteine (fixed). The false discovery rate was set to 0.01 for peptide and protein identifications. MS2 identifications were transferred between runs using the “Match between runs” option, in which the maximal retention time window was set to 0.7 min. Protein intensities were normalized using the in-built label-free quantification algorithm. Data analysis was performed using Perseus software (v1.6.0.2).<sup>298</sup> Technical and biological replicates for each condition were defined as groups, label-free quantification intensity values were filtered for minimum value of 2 per group and transformed to log2 scale. Missing values were imputed with random numbers from normal distribution, and mean and standard deviation were chosen to best simulate low abundance values below the noise level (width = 0.3; shift = 1.8). Spectra were matched to murine (<https://www.uniprot.org/>; 17 073 reviewed entries), contaminant, and decoy database. Differences in protein levels between samples with enriched unphosphorylated and phosphorylated epitopes were calculated using two-sample Student’s t-test. Significantly enriched proteins for each condition were determined by a significance cut off p-value  $\leq 0.05$  and log2 ratio  $\geq 2$ .

### **8.17. Immunofluorescent labelling**

For the majority of experiments, cells were fixed with pre-warmed 4% PFA (#1040051000, Merck) PBS for 15 minutes, and rinsed with PBS. Cells were permeabilized and nonspecific binding blocked with PBS containing 0.5% TritonX100 (#T8655, US Biological) and 5% goat serum (#16210-072, Gibco) for 1 hour at room temperature. Coverslips were incubated with primary antibodies (total volume 100  $\mu$ l/coverslip; see Table 5) overnight at 4°C, and washed 2 x 10 minutes with PBS 0.1% Tween-20 followed by 2 x 10 minute washes with PBS. Secondary antibodies (total volume 100  $\mu$ l/coverslip; see Table 5) were applied for one hour at room temperature, followed by 2 x 10 minute washes with PBS 0.1% Tween-20 and 2 x 10 minute washes with PBS. All antibodies were diluted in PBS containing 0.1% Tween-20 (#655205, Calbiochem) and 5% goat serum. Coverslips were mounted with Prolong Glass Antifade Mountant (#P36984, Invitrogen) and kept at 4°C.

For the experiment in Figure 18, cells were fixed on ice with ice cold methanol (#CP43.4, Carl Roth) for 5 minutes and rinsed with PBS. Nonspecific binding was blocked with PBS containing

5% goat serum for 1 hour at room temperature. The rest of the immunolabeling was carried out as described above.

For immunohistochemistry, brains from postnatal day 6 pups were harvested and fixed in 4% PFA PBS for 48 hours, followed by sequential incubation in 15% and 30% sucrose (#9097.1, Carl Roth) for 24 hours each. 80 µm thick coronal sections were prepared on vibratome, and sections with corpus callosum, hippocampus and striatum were chosen for immunolabeling. Immunolabeling was carried out on free floating sections. Nonspecific binding was blocked with PBS containing 0.1% TritonX100 and 10% goat serum for 1 hour. Brain slices were incubated with primary antibodies (see Table 5) in PBS containing 0.1% TritonX100 and 2% goat serum for 72 hours. The slices were washed 4 x 10 minutes with PBS 0.1% Tween-20, followed by incubation with secondary antibodies (see Table 5) in PBS 0.1% Tween-20 for 24 hours. Finally, brain slices were washed 2 x 10 minutes with PBS 0.1% Tween-20 and 2 x 10 minutes with PBS. The sections were mounted with Prolong Glass Antifade Mountant and kept at 4°C.

### **8.18. Filopodia density measurements**

N1E-115 cells were transfected with farnesylated GFP (independent membrane marker) and PLPPR3-Flag, PLPPR3-S351A-Flag or PLPPR3-S351D-Flag, and labelled for F-actin (independent filopodia marker). Images of individual, non-overlapping cells were acquired with 63x objective (see also the section on Microscopy). Filopodia density measurements were performed using an ImageJ macro developed by my colleague Dr. Joachim Fuchs.<sup>192</sup> The macro automatically detects the borders of a cell and outlines it, providing a measurement of circumference. Filopodia are detected as intensity peaks along this outline. The analysis was carried out in the membrane marker channel. The semi-automated analysis was validated by parallel manual analysis of a pilot experiment. The ImageJ macro of this analysis is available at ([https://github.com/jo-fuchs/Filopodia\\_Membrane\\_recruitment](https://github.com/jo-fuchs/Filopodia_Membrane_recruitment)).

### **8.19. Axonal branch density measurements**

To analyze axon branch densities, *Plppr3*<sup>-/-</sup> primary hippocampal neurons were infected with nuclear RFP (control), PLPPR3-Flag, PLPPR3-S351A-Flag or PLPPR3-S351D-Flag lentiviruses 2 hours after plating, and transfected with cytosolic GFP at 2 days *in vitro* using the calcium phosphate method (see also section Primary neuronal culture and transfection). Neurons were fixed at 5 days *in vitro* with 4% PFA for 15 minutes and immunolabelled for GFP, PLPPR3 and tau. Images of healthy, non-overlapping neurons were acquired with a widefield microscope. Images of large neurons were automatically stitched using the large image scan function of Nikon. Expression of PLPPR3 was confirmed by visual inspection, but only GFP

and tau channels were acquired. Resulting images were 12-bit. Image acquisition and analysis were performed blinded to the experimental groups.

Neuronal morphology was measured in the GFP channel (independent marker of all processes). Images were converted to 8-bit containing only the GFP channel. Axons and dendrites were tracked using the NeuronJ plugin,<sup>299</sup> and all processes were assigned to groups based on branching order. The primary axon was defined as the longest consecutively traceable process. Primary branches were defined as those branching off the primary axon, secondary branches as those branching off the primary branches, and so forth. Resulting measurement files were summarized in RStudio 1.04.1717 using a package developed by my colleague Dr. Joachim Fuchs (Branching\_analysis.R available from [https://github.com/jo-fuchs/Branching\\_fixed](https://github.com/jo-fuchs/Branching_fixed)).

## **8.20. Preparation of crude synaptosomes**

Crude synaptosomes were prepared from the brains of 5 week old female and male mice. Brains were dissected to exclude the cerebellum and the olfactory bulb. The brain was weighed and homogenized in 1 ml/100 mg homogenization buffer (final concentration 5 mM Tris, 1 mM EDTA, 0.32 M sucrose, pH 7.4) supplemented with protease and phosphatase inhibitors (see section on Cell and tissue lysis). The lysate was cleared of nuclei and cell debris by centrifugation at 1000 g for 10 minutes. Supernatant (S1) was collected and centrifuged at 15 000 g for 30 minutes, after which the supernatant (S2) was collected. The remaining pellet (P2) containing the synaptosomes (with myelin, membranes and mitochondria) was resuspended in homogenization buffer without sucrose (Tris-EDTA, pH 7.4, see above) and centrifuged at 15 000 g for 30 minutes. Supernatant was discarded and the pellet (P2) was snap frozen. All work was carried out at 4°C or on ice.

Prior to western blot analysis, S2 and P2 fractions were thawed on ice, and the P2 were resuspended in 150 µl homogenization buffer (roughly equal to the volume of S2 fractions). The samples were incubated on ice with 15 µl of 10% TritonX-100 for 10 minutes to break open synaptosomal membranes. Total protein concentration was measured with BCA assay (see Cell and tissue lysis) and 25 µg of total protein was loaded on the gel.

## **8.21. Microscopy**

Axonal branching experiment of GFP epifluorescence was imaged on Nikon Ti widefield inverted microscope using the 20x objective at room temperature. The imaging was performed blinded to the experimental groups to avoid bias. PLPPR3 expression was confirmed by visual inspection, but only GFP (488) and tau (647) channels were acquired sequentially. All of the rest of microscopy images were acquired on inverted confocal Leica SP8 microscope. For cells

and neurons I used the 63x objective, for brain sections the 20x objective was used. Channels were acquired sequentially and acquisition filters were adjusted to avoid crosstalk of fluorophores. Z-stacks with a step size of 0.6  $\mu\text{m}$  (cell lines) or 0.3  $\mu\text{m}$  (neurons) covering the entire cell were acquired, for brain sections only one plane was imaged.

## 8.22. Prediction of phosphorylation sites and conservation analysis

Prediction of phosphorylation sites was carried out in NetPhos3.1 server (<https://services.healthtech.dtu.dk/services/NetPhos-3.1/>). The server predicts for 17 kinases (ATM, CKI, CKII, CaM-II, DNAPK, EGFR, GSK3, INSR, PKA, PKB, PKC, PKG, RSK, SRC, CDC2, CDK5 and p38MAPK). The primary amino acid sequence of PLPPR3 intracellular domain (aa 284-716) was submitted, and phosphorylation of serine, threonine and tyrosine residues was selected for prediction. Only scores  $>.75$  were displayed. To analyze conservation of phosphorylation sites across species, Constraint-Based Multiple Alignment Tool (COBALT, <https://www.ncbi.nlm.nih.gov/tools/cobalt/cobalt.cgi?CMD=Web>) was used. FASTA sequences of mouse (*Mus musculus*; Q7TPB0-1), human (*Homo sapiens*; Q6T4P5), zebrafish (*Danio rerio*; B0V0Y5), tropical clawed frog (*Xenopus tropicalis*; B1H174), rhesus monkey (*Macaca mulatta*; F7GER3) and chicken (*Gallus gallus*; A0A1D5PYJ6) from Uniprot database (<https://www.uniprot.org/>) were used. The sequences were aligned with default settings.

## 8.23. Statistics and data visualization

All western blot experiments, with the exception of Figure 20, were performed a minimum of three times with different passages of cells. Filopodia density experiment in N1E-115 cells was replicated 3 times with different passages of cells. Axon branching experiment was replicated 2 times with primary neuron preparations from different animals. The affinity chromatography experiment was replicated 4 times with brain lysates from 4 different mice. The synaptosomes were prepared from 6 different animals. Statistical analysis and data visualization was performed with Graphpad Prism 8.4.3 (686). Filopodia and axon branch densities were compared with one-way ANOVA, changes in co-immunoprecipitation were compared with Wilcoxon test.

## 9. References

---

1. Silbereis, J. C., Pochareddy, S., Zhu, Y., Li, M. & Sestan, N. The Cellular and Molecular Landscapes of the Developing Human Central Nervous System. *Neuron* **89**, 248–268 (2016).
2. Passingham, R. E. *What is special about the human brain?* (Oxford University Press, 2008).
3. Donato, A., Kagias, K., Zhang, Y. & Hilliard, M. A. Neuronal sub-compartmentalization: a strategy to optimize neuronal function. *Biol Rev Camb Philos Soc* **94**, 1023–1037 (2019).
4. Rakic, P. Neurons in Rhesus Monkey Visual Cortex: Systematic Relation between Time of Origin and Eventual Disposition. *Science* **183**, 425–427 (1974).
5. Takahashi, T., Goto, T., Miyama, S., Nowakowski, R. S. & Caviness, V. S. Sequence of Neuron Origin and Neocortical Laminar Fate: Relation to Cell Cycle of Origin in the Developing Murine Cerebral Wall. *J. Neurosci.* **19**, 10357–10371 (1999).
6. Villalba, A., Götz, M. & Borrell, V. The regulation of cortical neurogenesis. in *Current Topics in Developmental Biology* vol. 142 1–66 (Elsevier, 2021).
7. Kay, J. N. Radial migration: Retinal neurons hold on for the ride. *J Cell Biol* **215**, 147–149 (2016).
8. Auladell, C., Martinez, A., Alcantara, S., Supèr, H. & Soriano, E. Migrating neurons in the developing cerebral cortex of the mouse send callosal axons. *Neuroscience* **64**, 1091–1103 (1995).
9. Noctor, S. C., Martínez-Cerdeño, V., Ivic, L. & Kriegstein, A. R. Cortical neurons arise in symmetric and asymmetric division zones and migrate through specific phases. *Nat Neurosci* **7**, 136–144 (2004).
10. Callaway, E. & Katz, L. Emergence and refinement of clustered horizontal connections in cat striate cortex. *J. Neurosci.* **10**, 1134–1153 (1990).
11. Callaway, E. & Katz, L. Development of axonal arbors of layer 4 spiny neurons in cat striate cortex. *J. Neurosci.* **12**, 570–582 (1992).

12. Callaway, E. M. & Lieber, J. L. Development of axonal arbors of layer 6 pyramidal neurons in ferret primary visual cortex. *J. Comp. Neurol.* **376**, 295–305 (1996).
13. Borrell, V. & Callaway, E. M. Reorganization of Exuberant Axonal Arbors Contributes to the Development of Laminar Specificity in Ferret Visual Cortex. *J. Neurosci.* **22**, 6682–6695 (2002).
14. Callaway, E. M. & Borrell, V. Developmental Sculpting of Dendritic Morphology of Layer 4 Neurons in Visual Cortex: Influence of Retinal Input. *J. Neurosci.* **31**, 7456–7470 (2011).
15. Dotti, C., Sullivan, C. & Banker, G. The establishment of polarity by hippocampal neurons in culture. *J. Neurosci.* **8**, 1454–1468 (1988).
16. Polleux, F. & Snider, W. Initiating and Growing an Axon. *Cold Spring Harbor Perspectives in Biology* **2**, a001925–a001925 (2010).
17. Acebes, A. & Ferrús, A. Cellular and molecular features of axon collaterals and dendrites. *Trends in Neurosciences* **23**, 557–565 (2000).
18. Mihailoff, G. A. & Haines, D. E. The Cell Biology of Neurons and Glia. in *Fundamental Neuroscience for Basic and Clinical Applications* 15-33.e1 (Elsevier, 2018). doi:10.1016/B978-0-323-39632-5.00002-5.
19. Gibson, D. A. & Ma, L. Developmental regulation of axon branching in the vertebrate nervous system. *Development* **138**, 183–195 (2011).
20. Davis, B. M., Frank, E., Johnson, F. A. & Scott, S. A. Development of central projections of lumbosacral sensory neurons in the chick. *J. Comp. Neurol.* **279**, 556–566 (1989).
21. Gallo, G. The cytoskeletal and signaling mechanisms of axon collateral branching. *Devel Neurobio* **71**, 201–220 (2011).
22. Ye, X., Qiu, Y., Gao, Y., Wan, D. & Zhu, H. A Subtle Network Mediating Axon Guidance: Intrinsic Dynamic Structure of Growth Cone, Attractive and Repulsive Molecular Cues, and the Intermediate Role of Signaling Pathways. *Neural Plast* **2019**, 1719829 (2019).
23. Tessier-Lavigne, M., Placzek, M., Lumsden, A. G. S., Dodd, J. & Jessell, T. M. Chemotropic guidance of developing axons in the mammalian central nervous system. *Nature* **336**, 775–778 (1988).

24. Shen, K. & Cowan, C. W. Guidance molecules in synapse formation and plasticity. *Cold Spring Harb Perspect Biol* **2**, a001842 (2010).
25. Bush, J. O. Cellular and molecular mechanisms of EPH/EPHRIN signaling in evolution and development. in *Current Topics in Developmental Biology* vol. 149 153–201 (Elsevier, 2022).
26. Hu, S. & Zhu, L. Semaphorins and Their Receptors: From Axonal Guidance to Atherosclerosis. *Front Physiol* **9**, 1236 (2018).
27. Limoni, G. & Niquille, M. Semaphorins and Plexins in central nervous system patterning: the key to it all? *Current Opinion in Neurobiology* **66**, 224–232 (2021).
28. Blockus, H. & Chédotal, A. Slit-Robo signaling. *Development* **143**, 3037–3044 (2016).
29. Boyer, N. P. & Gupton, S. L. Revisiting Netrin-1: One Who Guides (Axons). *Front Cell Neurosci* **12**, 221 (2018).
30. Zang, Y., Chaudhari, K. & Bashaw, G. J. New insights into the molecular mechanisms of axon guidance receptor regulation and signaling. *Curr Top Dev Biol* **142**, 147–196 (2021).
31. Douceau, S., Deutsch Guerrero, T. & Ferent, J. Establishing Hedgehog Gradients during Neural Development. *Cells* **12**, 225 (2023).
32. He, C.-W., Liao, C.-P. & Pan, C.-L. Wnt signalling in the development of axon, dendrites and synapses. *Open Biol* **8**, 180116 (2018).
33. Yam, P. T. & Charron, F. Signaling mechanisms of non-conventional axon guidance cues: the Shh, BMP and Wnt morphogens. *Current Opinion in Neurobiology* **23**, 965–973 (2013).
34. Onesto, M. M., Short, C. A., Rempel, S. K., Catlett, T. S. & Gomez, T. M. Growth Factors as Axon Guidance Molecules: Lessons From in vitro Studies. *Front Neurosci* **15**, 678454 (2021).
35. Short, C. A., Onesto, M. M., Rempel, S. K., Catlett, T. S. & Gomez, T. M. Familiar growth factors have diverse roles in neural network assembly. *Curr Opin Neurobiol* **66**, 233–239 (2021).
36. Gillespie, L. N. Regulation of axonal growth and guidance by the neurotrophin family of neurotrophic factors. *Clin Exp Pharmacol Physiol* **30**, 724–733 (2003).

37. Kalil, K., Szebenyi, G. & Dent, E. W. Common mechanisms underlying growth cone guidance and axon branching. *J Neurobiol* **44**, 145–158 (2000).
38. Dent, E. W., Barnes, A. M., Tang, F. & Kalil, K. Netrin-1 and semaphorin 3A promote or inhibit cortical axon branching, respectively, by reorganization of the cytoskeleton. *J Neurosci* **24**, 3002–3012 (2004).
39. Kollins, K. M. & Davenport, R. W. Branching Morphogenesis in Vertebrate Neurons. in *Branching Morphogenesis* 8–65 (Springer US, 2005). doi:10.1007/0-387-30873-3\_2.
40. Cohen-Cory, S. BDNF modulates, but does not mediate, activity-dependent branching and remodeling of optic axon arbors in vivo. *J Neurosci* **19**, 9996–10003 (1999).
41. Lom, B. & Cohen-Cory, S. Brain-derived neurotrophic factor differentially regulates retinal ganglion cell dendritic and axonal arborization in vivo. *J Neurosci* **19**, 9928–9938 (1999).
42. Gallo, G. & Letourneau, P. C. Localized sources of neurotrophins initiate axon collateral sprouting. *J Neurosci* **18**, 5403–5414 (1998).
43. Yamamoto, N. & López-Bendito, G. Shaping brain connections through spontaneous neural activity: Shaping brain connections through spontaneous neural activity. *European Journal of Neuroscience* **35**, 1595–1604 (2012).
44. Vaughn, J. E., Barber, R. P. & Sims, T. J. Dendritic development and preferential growth into synaptogenic fields: A quantitative study of Golgi-impregnated spinal motor neurons. *Synapse* **2**, 69–78 (1988).
45. Matsumoto, N., Hoshiko, M., Sugo, N., Fukazawa, Y. & Yamamoto, N. Synapse-dependent and independent mechanisms of thalamocortical axon branching are regulated by neuronal activity: Axon Branching and Synapse Formation. *Devel Neurobio* **76**, 323–336 (2016).
46. Shimada, T., Yoshida, T. & Yamagata, K. Neuritin Mediates Activity-Dependent Axonal Branch Formation in Part via FGF Signaling. *J Neurosci* **36**, 4534–4548 (2016).
47. Constance, W. D. *et al.* Neurexin and Neuroligin-based adhesion complexes drive axonal arborisation growth independent of synaptic activity. *Elife* **7**, e31659 (2018).

48. Patzke, C., Acuna, C., Giam, L. R., Wernig, M. & Südhof, T. C. Conditional deletion of L1CAM in human neurons impairs both axonal and dendritic arborization and action potential generation. *J Exp Med* **213**, 499–515 (2016).
49. Osterhout, J. A., Stafford, B. K., Nguyen, P. L., Yoshihara, Y. & Huberman, A. D. Contactin-4 mediates axon-target specificity and functional development of the accessory optic system. *Neuron* **86**, 985–999 (2015).
50. Pischedda, F. & Piccoli, G. The IgLON Family Member Negr1 Promotes Neuronal Arborization Acting as Soluble Factor via FGFR2. *Front Mol Neurosci* **8**, 89 (2015).
51. Bijata, M., Wlodarczyk, J. & Figiel, I. Dystroglycan controls dendritic morphogenesis of hippocampal neurons in vitro. *Front Cell Neurosci* **9**, 199 (2015).
52. Soba, P. *et al.* The Ret receptor regulates sensory neuron dendrite growth and integrin mediated adhesion. *Elife* **4**, e05491 (2015).
53. Molumby, M. J., Keeler, A. B. & Weiner, J. A. Homophilic Protocadherin Cell-Cell Interactions Promote Dendrite Complexity. *Cell Rep* **15**, 1037–1050 (2016).
54. Kostadinov, D. & Sanes, J. R. Protocadherin-dependent dendritic self-avoidance regulates neural connectivity and circuit function. *Elife* **4**, e08964 (2015).
55. Mountoufaris, G. *et al.* Multicluster Pcdh diversity is required for mouse olfactory neural circuit assembly. *Science* **356**, 411–414 (2017).
56. Kulkarni, V. A. & Firestein, B. L. The dendritic tree and brain disorders. *Mol Cell Neurosci* **50**, 10–20 (2012).
57. Zikopoulos, B. & Barbas, H. Changes in prefrontal axons may disrupt the network in autism. *J Neurosci* **30**, 14595–14609 (2010).
58. Zikopoulos, B. & Barbas, H. Altered neural connectivity in excitatory and inhibitory cortical circuits in autism. *Front Hum Neurosci* **7**, 609 (2013).
59. Mathern, G. W., Pretorius, J. K. & Babb, T. L. Quantified patterns of mossy fiber sprouting and neuron densities in hippocampal and lesional seizures. *J Neurosurg* **82**, 211–219 (1995).

60. Proper, E. A. *et al.* Immunohistochemical characterization of mossy fibre sprouting in the hippocampus of patients with pharmaco-resistant temporal lobe epilepsy. *Brain* **123** ( Pt 1), 19–30 (2000).
61. Cavarsan, C. F., Malheiros, J., Hamani, C., Najm, I. & Covolan, L. Is Mossy Fiber Sprouting a Potential Therapeutic Target for Epilepsy? *Front Neurol* **9**, 1023 (2018).
62. Suzuki, N., Akiyama, T., Warita, H. & Aoki, M. Omics Approach to Axonal Dysfunction of Motor Neurons in Amyotrophic Lateral Sclerosis (ALS). *Front Neurosci* **14**, 194 (2020).
63. Cosker, K. E. & Eickholt, B. J. Phosphoinositide 3-kinase signalling events controlling axonal morphogenesis. *Biochemical Society Transactions* **35**, 207–210 (2007).
64. Bilimoria, P. M. & Bonni, A. Molecular Control of Axon Branching. *Neuroscientist* **19**, 16–24 (2013).
65. Armijo-Weingart, L. & Gallo, G. It takes a village to raise a branch: Cellular mechanisms of the initiation of axon collateral branches. *Molecular and Cellular Neuroscience* **84**, 36–47 (2017).
66. Hong, M. & Lee, V. M.-Y. Insulin and Insulin-like Growth Factor-1 Regulate Tau Phosphorylation in Cultured Human Neurons. *Journal of Biological Chemistry* **272**, 19547–19553 (1997).
67. Yoshimura, T. *et al.* GSK-3 $\beta$  Regulates Phosphorylation of CRMP-2 and Neuronal Polarity. *Cell* **120**, 137–149 (2005).
68. Trivedi, N., Marsh, P., Goold, R. G., Wood-Kaczmar, A. & Gordon-Weeks, P. R. Glycogen synthase kinase-3 $\beta$  phosphorylation of MAP1B at Ser1260 and Thr1265 is spatially restricted to growing axons. *Journal of Cell Science* **118**, 993–1005 (2005).
69. Zhou, F.-Q., Zhou, J., Dedhar, S., Wu, Y.-H. & Snider, W. D. NGF-Induced Axon Growth Is Mediated by Localized Inactivation of GSK-3 $\beta$  and Functions of the Microtubule Plus End Binding Protein APC. *Neuron* **42**, 897–912 (2004).
70. Schelski, M. & Bradke, F. Neuronal polarization: From spatiotemporal signaling to cytoskeletal dynamics. *Molecular and Cellular Neuroscience* **84**, 11–28 (2017).

71. Shelly, M. *et al.* Local and Long-Range Reciprocal Regulation of cAMP and cGMP in Axon/Dendrite Formation. *Science* **327**, 547–552 (2010).
72. Munoz-Llancao, P. *et al.* Exchange Protein Directly Activated by cAMP (EPAC) Regulates Neuronal Polarization through Rap1B. *Journal of Neuroscience* **35**, 11315–11329 (2015).
73. Zhou, Z. *et al.* Photoactivated adenylyl cyclase (PAC) reveals novel mechanisms underlying cAMP-dependent axonal morphogenesis. *Sci Rep* **5**, 19679 (2016).
74. Ketschek, A. & Gallo, G. Nerve growth factor induces axonal filopodia through localized microdomains of phosphoinositide 3-kinase activity that drive the formation of cytoskeletal precursors to filopodia. *J Neurosci* **30**, 12185–12197 (2010).
75. Reichardt, L. F. Neurotrophin-regulated signalling pathways. *Philos Trans R Soc Lond B Biol Sci* **361**, 1545–1564 (2006).
76. Laurino, L. *et al.* PI3K activation by IGF-1 is essential for the regulation of membrane expansion at the nerve growth cone. *J Cell Sci* **118**, 3653–3662 (2005).
77. Sosa, L. *et al.* IGF-1 receptor is essential for the establishment of hippocampal neuronal polarity. *Nat Neurosci* **9**, 993–995 (2006).
78. Scolnick, J. A. *et al.* Role of IGF Signaling in Olfactory Sensory Map Formation and Axon Guidance. *Neuron* **57**, 847–857 (2008).
79. Özdinler, P. H. & Macklis, J. D. IGF-I specifically enhances axon outgrowth of corticospinal motor neurons. *Nat Neurosci* **9**, 1371–1381 (2006).
80. Jones, D. M., Tucker, B. A., Rahimtula, M. & Mearow, K. M. The synergistic effects of NGF and IGF-1 on neurite growth in adult sensory neurons: convergence on the PI 3-kinase signaling pathway. *J Neurochem* **86**, 1116–1128 (2003).
81. Cheng, P.-L. *et al.* Self-amplifying autocrine actions of BDNF in axon development. *Proc Natl Acad Sci U S A* **108**, 18430–18435 (2011).
82. Wit, C. B. & Hiesinger, P. R. Neuronal filopodia: From stochastic dynamics to robustness of brain morphogenesis. *Seminars in Cell & Developmental Biology* S1084952122001203 (2022) doi:10.1016/j.semcdb.2022.03.038.

83. Dent, E. W. *et al.* Filopodia are required for cortical neurite initiation. *Nat Cell Biol* **9**, 1347–1359 (2007).
84. Gallo, G. Mechanisms underlying the initiation and dynamics of neuronal filopodia: from neurite formation to synaptogenesis. *Int Rev Cell Mol Biol* **301**, 95–156 (2013).
85. Heiman, M. G. & Shaham, S. Twigs into branches: how a filopodium becomes a dendrite. *Current Opinion in Neurobiology* **20**, 86–91 (2010).
86. Gallo, G. Mechanisms Underlying the Initiation and Dynamics of Neuronal Filopodia. in *International Review of Cell and Molecular Biology* vol. 301 95–156 (Elsevier, 2013).
87. Kalil, K. & Dent, E. W. Branch management: mechanisms of axon branching in the developing vertebrate CNS. *Nat Rev Neurosci* **15**, 7–18 (2014).
88. Brosig, A. *et al.* The Axonal Membrane Protein PRG2 Inhibits PTEN and Directs Growth to Branches. *Cell Reports* **29**, 2028–2040.e8 (2019).
89. Ziv, N. E. & Smith, S. J. Evidence for a Role of Dendritic Filopodia in Synaptogenesis and Spine Formation. *Neuron* **17**, 91–102 (1996).
90. Nobes, C. D. & Hall, A. Rho, Rac, and Cdc42 GTPases regulate the assembly of multimolecular focal complexes associated with actin stress fibers, lamellipodia, and filopodia. *Cell* **81**, 53–62 (1995).
91. Ellis, S. & Mellor, H. The novel Rho-family GTPase Rif regulates coordinated actin-based membrane rearrangements. *Current Biology* **10**, 1387–1390 (2000).
92. Passey, S., Pellegrin, S. & Mellor, H. What is in a filopodium? Starfish versus hedgehogs. *Biochemical Society Transactions* **32**, 1115–1117 (2004).
93. Svitkina, T. M. *et al.* Mechanism of filopodia initiation by reorganization of a dendritic network. *Journal of Cell Biology* **160**, 409–421 (2003).
94. Peng, J., Wallar, B. J., Flanders, A., Swiatek, P. J. & Alberts, A. S. Disruption of the Diaphanous-Related Formin Drf1 Gene Encoding mDia1 Reveals a Role for Drf3 as an Effector for Cdc42. *Current Biology* **13**, 534–545 (2003).
95. Krugmann, S. *et al.* Cdc42 induces filopodia by promoting the formation of an IRSp53:Mena complex. *Current Biology* **11**, 1645–1655 (2001).

96. Goh, W. I. *et al.* Rif-mDia1 Interaction Is Involved in Filopodium Formation Independent of Cdc42 and Rac Effectors. *Journal of Biological Chemistry* **286**, 13681–13694 (2011).
97. Smith, C. L. The initiation of neurite outgrowth by sympathetic neurons grown in vitro does not depend on assembly of microtubules [published erratum appears in J Cell Biol 1995 Feb;128(3):443]. *The Journal of Cell Biology* **127**, 1407–1418 (1994).
98. Higgs, V. E. & Das, R. M. Establishing neuronal polarity: microtubule regulation during neurite initiation. *Oxford Open Neuroscience* **1**, kvac007 (2022).
99. Fuchs, J. *et al.* Plasma membrane phospholipid phosphatase-related proteins as pleiotropic regulators of neuron growth and excitability. *Front. Mol. Neurosci.* **15**, 984655 (2022).
100. Waggoner, D. W., Gómez-Muñoz, A., Dewald, J. & Brindley, D. N. Phosphatidate Phosphohydrolase Catalyzes the Hydrolysis of Ceramide 1-Phosphate, Lysophosphatidate, and Sphingosine 1-Phosphate. *Journal of Biological Chemistry* **271**, 16506–16509 (1996).
101. Sigal, Y. J., McDermott, M. I. & Morris, A. J. Integral membrane lipid phosphatases/phosphotransferases: common structure and diverse functions. *Biochem J* **387**, 281–293 (2005).
102. Tong, S. *et al.* Structural Insight into Substrate Selection and Catalysis of Lipid Phosphate Phosphatase PgpB in the Cell Membrane. *Journal of Biological Chemistry* **291**, 18342–18352 (2016).
103. Coiro, P., Stoenica, L., Strauss, U. & Bräuer, A. U. Plasticity-related Gene 5 Promotes Spine Formation in Murine Hippocampal Neurons. *Journal of Biological Chemistry* **289**, 24956–24970 (2014).
104. Liu, X. *et al.* PRG-1 Regulates Synaptic Plasticity via Intracellular PP2A/β1-Integrin Signaling. *Developmental Cell* **38**, 275–290 (2016).
105. Fink, K. L., López-Giráldez, F., Kim, I.-J., Strittmatter, S. M. & Cafferty, W. B. J. Identification of Intrinsic Axon Growth Modulators for Intact CNS Neurons after Injury. *Cell Reports* **18**, 2687–2701 (2017).

106. Yu, P. *et al.* Cooperative interactions of LPPR/PRG family members in membrane localization and alteration of cellular morphology. *Journal of Cell Science* jcs.169789 (2015) doi:10.1242/jcs.169789.
107. Sigal, Y. J., Quintero, O. A., Cheney, R. E. & Morris, A. J. Cdc42 and ARP2/3-independent regulation of filopodia by an integral membrane lipid-phosphatase-related protein. *Journal of Cell Science* **120**, 340–352 (2007).
108. Broggin, T. *et al.* Plasticity Related Gene 3 (PRG3) overcomes myelin-associated growth inhibition and promotes functional recovery after spinal cord injury. *Aging* **8**, 2463–2487 (2016).
109. Cornish, J., Chamberlain, S. G., Owen, D. & Mott, H. R. Intrinsically disordered proteins and membranes: a marriage of convenience for cell signalling? *Biochem Soc Trans* **48**, 2669–2689 (2020).
110. Tokumitsu, H. *et al.* Identification and characterization of PRG-1 as a neuronal calmodulin-binding protein. *Biochemical Journal* **431**, 81–91 (2010).
111. Vogt, J. *et al.* Molecular cause and functional impact of altered synaptic lipid signaling due to a *prg-1* gene SNP. *EMBO Mol Med* **8**, 25–38 (2016).
112. DiRusso, C. J., Dashtiahangar, M. & Gilmore, T. D. Scaffold proteins as dynamic integrators of biological processes. *Journal of Biological Chemistry* **298**, 102628 (2022).
113. Deribe, Y. L., Pawson, T. & Dikic, I. Post-translational modifications in signal integration. *Nat Struct Mol Biol* **17**, 666–672 (2010).
114. Humphrey, S. J., James, D. E. & Mann, M. Protein Phosphorylation: A Major Switch Mechanism for Metabolic Regulation. *Trends in Endocrinology & Metabolism* **26**, 676–687 (2015).
115. Johnson, L. N. & Lewis, R. J. Structural Basis for Control by Phosphorylation. *Chem. Rev.* **101**, 2209–2242 (2001).
116. Álvarez-Salamero, C., Castillo-González, R. & Navarro, M. N. Lighting Up T Lymphocyte Signaling with Quantitative Phosphoproteomics. *Front. Immunol.* **8**, 938 (2017).

117. Ardito, F., Giuliani, M., Perrone, D., Troiano, G. & Lo Muzio, L. The crucial role of protein phosphorylation in cell signaling and its use as targeted therapy (Review). *Int J Mol Med* **40**, 271–280 (2017).
118. Manning, G., Whyte, D. B., Martinez, R., Hunter, T. & Sudarsanam, S. The Protein Kinase Complement of the Human Genome. *Science* **298**, 1912–1934 (2002).
119. Damle, N. P. & Köhn, M. The human DEPhOsporylation Database DEPOD: 2019 update. *Database* **2019**, baz133 (2019).
120. Meng, L. *et al.* Mini-review: Recent advances in post-translational modification site prediction based on deep learning. *Comput Struct Biotechnol J* **20**, 3522–3532 (2022).
121. Needham, E. J., Parker, B. L., Burykin, T., James, D. E. & Humphrey, S. J. Illuminating the dark phosphoproteome. *Sci. Signal.* **12**, eaau8645 (2019).
122. Iakoucheva, L. M. *et al.* The importance of intrinsic disorder for protein phosphorylation. *Nucleic Acids Res* **32**, 1037–1049 (2004).
123. Romero, P. *et al.* Sequence complexity of disordered protein. *Proteins* **42**, 38–48 (2001).
124. Trivedi, R. & Nagarajaram, H. A. Intrinsically Disordered Proteins: An Overview. *Int J Mol Sci* **23**, 14050 (2022).
125. Iakoucheva, L. M., Brown, C. J., Lawson, J. D., Obradović, Z. & Dunker, A. K. Intrinsic Disorder in Cell-signaling and Cancer-associated Proteins. *Journal of Molecular Biology* **323**, 573–584 (2002).
126. Fang, X. *et al.* Phosphorylation and inactivation of glycogen synthase kinase 3 by protein kinase A. *Proc Natl Acad Sci U S A* **97**, 11960–11965 (2000).
127. Ketschek, A. *et al.* Nerve growth factor promotes reorganization of the axonal microtubule array at sites of axon collateral branching. *Dev Neurobiol* **75**, 1441–1461 (2015).
128. Worth, D. C., Daly, C. N., Geraldo, S., Oozeer, F. & Gordon-Weeks, P. R. Drebrin contains a cryptic F-actin-bundling activity regulated by Cdk5 phosphorylation. *J Cell Biol* **202**, 793–806 (2013).

129. Yamada, H. *et al.* Possible role of cortactin phosphorylation by protein kinase C $\alpha$  in actin-bundle formation at growth cone: Cortactin phosphorylation by PKC at growth cone. *Biol. Cell* **107**, 319–330 (2015).
130. He, Q., Dent, E. W. & Meiri, K. F. Modulation of actin filament behavior by GAP-43 (neuromodulin) is dependent on the phosphorylation status of serine 41, the protein kinase C site. *J Neurosci* **17**, 3515–3524 (1997).
131. Holahan, M. R. A Shift from a Pivotal to Supporting Role for the Growth-Associated Protein (GAP-43) in the Coordination of Axonal Structural and Functional Plasticity. *Front. Cell. Neurosci.* **11**, 266 (2017).
132. Lebrand, C. *et al.* Critical Role of Ena/VASP Proteins for Filopodia Formation in Neurons and in Function Downstream of Netrin-1. *Neuron* **42**, 37–49 (2004).
133. Gomez, T. M. & Robles, E. The Great Escape. *Neuron* **42**, 1–3 (2004).
134. Lin, Y.-L., Lei, Y.-T., Hong, C.-J. & Hsueh, Y.-P. Syndecan-2 induces filopodia and dendritic spine formation via the neurofibromin–PKA–Ena/VASP pathway. *Journal of Cell Biology* **177**, 829–841 (2007).
135. Revathidevi, S. & Munirajan, A. K. Akt in cancer: Mediator and more. *Seminars in Cancer Biology* **59**, 80–91 (2019).
136. Singh, V. *et al.* Phosphorylation: Implications in Cancer. *Protein J* **36**, 1–6 (2017).
137. Bhullar, K. S. *et al.* Kinase-targeted cancer therapies: progress, challenges and future directions. *Mol Cancer* **17**, 48 (2018).
138. Neumann, M. *et al.* Ubiquitinated TDP-43 in Frontotemporal Lobar Degeneration and Amyotrophic Lateral Sclerosis. *Science* **314**, 130–133 (2006).
139. Saha, P. & Sen, N. Tauopathy: A common mechanism for neurodegeneration and brain aging. *Mech Ageing Dev* **178**, 72–79 (2019).
140. Wegmann, S., Biernat, J. & Mandelkow, E. A current view on Tau protein phosphorylation in Alzheimer’s disease. *Current Opinion in Neurobiology* **69**, 131–138 (2021).

141. Wang, L., Bharti, Kumar, R., Pavlov, P. F. & Winblad, B. Small molecule therapeutics for tauopathy in Alzheimer's disease: Walking on the path of most resistance. *European Journal of Medicinal Chemistry* **209**, 112915 (2021).
142. Alberts, B. *et al.* Membrane Proteins. *Molecular Biology of the Cell. 4th edition* (2002).
143. Ubersax, J. A. & Ferrell Jr, J. E. Mechanisms of specificity in protein phosphorylation. *Nat Rev Mol Cell Biol* **8**, 530–541 (2007).
144. 이창로, 박영하, 김연란, & Seok, Yeong-Jae. Phosphorylation-Dependent Mobility Shift of Proteins on SDS-PAGE is Due to Decreased Binding of SDS. *Bulletin of the Korean Chemical Society* **34**, 2063–2066 (2013).
145. McCabe, J. B. & Berthiaume, L. G. Functional Roles for Fatty Acylated Amino-terminal Domains in Subcellular Localization. *MBoC* **10**, 3771–3786 (1999).
146. Kinoshita, E., Kinoshita-Kikuta, E., Takiyama, K. & Koike, T. Phosphate-binding Tag, a New Tool to Visualize Phosphorylated Proteins. *Molecular & Cellular Proteomics* **5**, 749–757 (2006).
147. Kinoshita, E. *et al.* Separation of phosphoprotein isotypes having the same number of phosphate groups using phosphate-affinity SDS-PAGE. *Proteomics* **8**, 2994–3003 (2008).
148. Kinoshita, E. & Kinoshita-Kikuta, E. Improved Phos-tag SDS-PAGE under neutral pH conditions for advanced protein phosphorylation profiling. *Proteomics* **11**, 319–323 (2011).
149. Lienhard, G. E. Non-functional phosphorylations? *Trends in Biochemical Sciences* **33**, 351–352 (2008).
150. Niu, S., Wang, Z., Ge, D., Zhang, G. & Li, Y. Prediction of functional phosphorylation sites by incorporating evolutionary information. *Protein Cell* **3**, 675–690 (2012).
151. Cole, A. R. *et al.* Relative Resistance of Cdk5-phosphorylated CRMP2 to Dephosphorylation. *Journal of Biological Chemistry* **283**, 18227–18237 (2008).
152. Hof, W. V. 'T & Resh, M. D. Rapid Plasma Membrane Anchoring of Newly Synthesized p59 fyn: Selective Requirement for NH<sub>2</sub>-Terminal Myristoylation and Palmitoylation at Cysteine-3. *Journal of Cell Biology* **136**, 1023–1035 (1997).

153. Fukata, Y. & Fukata, M. Protein palmitoylation in neuronal development and synaptic plasticity. *Nat Rev Neurosci* **11**, 161–175 (2010).
154. Stepanenko, A. A. & Dmitrenko, V. V. HEK293 in cell biology and cancer research: phenotype, karyotype, tumorigenicity, and stress-induced genome-phenotype evolution. *Gene* **569**, 182–190 (2015).
155. Malik, R., Nigg, E. A. & Körner, R. Comparative conservation analysis of the human mitotic phosphoproteome. *Bioinformatics* **24**, 1426–1432 (2008).
156. Landry, C. R., Levy, E. D. & Michnick, S. W. Weak functional constraints on phosphoproteomes. *Trends in Genetics* **25**, 193–197 (2009).
157. Cioni, J.-M. *et al.* SEMA3A Signaling Controls Layer-Specific Interneuron Branching in the Cerebellum. *Current Biology* **23**, 850–861 (2013).
158. Hajka, D. *et al.* GSK3 as a Regulator of Cytoskeleton Architecture: Consequences for Health and Disease. *Cells* **10**, 2092 (2021).
159. Shah, K. & Rossie, S. Tale of the Good and the Bad Cdk5: Remodeling of the Actin Cytoskeleton in the Brain. *Mol Neurobiol* **55**, 3426–3438 (2018).
160. Pereira, S. F. F., Goss, L. & Dworkin, J. Eukaryote-Like Serine/Threonine Kinases and Phosphatases in Bacteria. *Microbiol Mol Biol Rev* **75**, 192–212 (2011).
161. Liu, S. J. *et al.* Tau Becomes a More Favorable Substrate for GSK-3 When It Is Prephosphorylated by PKA in Rat Brain. *Journal of Biological Chemistry* **279**, 50078–50088 (2004).
162. Kameritsch, P. *et al.* PKA negatively modulates the migration enhancing effect of Connexin 43. *Biochimica et Biophysica Acta (BBA) - Molecular Cell Research* **1866**, 828–838 (2019).
163. Mingorance-Le Meur, A. & O'Connor, T. P. Neurite consolidation is an active process requiring constant repression of protrusive activity. *EMBO J* **28**, 248–260 (2009).
164. Kemp, B. E., Bylund, D. B., Huang, T. S. & Krebs, E. G. Substrate specificity of the cyclic AMP-dependent protein kinase. *Proc. Natl. Acad. Sci. U.S.A.* **72**, 3448–3452 (1975).

165. Kemp, B. E., Graves, D. J., Benjamini, E. & Krebs, E. G. Role of multiple basic residues in determining the substrate specificity of cyclic AMP-dependent protein kinase. *J Biol Chem* **252**, 4888–4894 (1977).
166. Moore, M. J., Adams, J. A. & Taylor, S. S. Structural Basis for Peptide Binding in Protein Kinase A. *Journal of Biological Chemistry* **278**, 10613–10618 (2003).
167. Walsh, D. A., Perkins, J. P. & Krebs, E. G. An adenosine 3',5'-monophosphate-dependant protein kinase from rabbit skeletal muscle. *J Biol Chem* **243**, 3763–3765 (1968).
168. Ostrom, K. F. *et al.* Physiological roles of mammalian transmembrane adenylyl cyclase isoforms. *Physiological Reviews* **102**, 815–857 (2022).
169. Taylor, S. S., Ilouz, R., Zhang, P. & Kornev, A. P. Assembly of allosteric macromolecular switches: lessons from PKA. *Nat Rev Mol Cell Biol* **13**, 646–658 (2012).
170. Seamon, K. B., Padgett, W. & Daly, J. W. Forskolin: unique diterpene activator of adenylate cyclase in membranes and in intact cells. *Proc. Natl. Acad. Sci. U.S.A.* **78**, 3363–3367 (1981).
171. Meyer, R. B. & Miller, J. P. Analogs of cyclic AMP and cyclic GMP: General methods of synthesis and the relationship of structure to enzymic activity. *Life Sciences* **14**, 1019–1040 (1974).
172. Lochner, A. & Moolman, J. A. The Many Faces of H89: A Review. *Cardiovasc Drug Reviews* **24**, 261–274 (2006).
173. Ono, S. *et al.* Identification of an Actin Binding Region and a Protein Kinase C Phosphorylation Site on Human Fascin. *Journal of Biological Chemistry* **272**, 2527–2533 (1997).
174. Schmidt, J. T., Fleming, M. R. & Leu, B. Presynaptic protein kinase C controls maturation and branch dynamics of developing retinotectal arbors: Possible role in activity-driven sharpening. *J. Neurobiol.* **58**, 328–340 (2004).
175. Niedel, J. E., Kuhn, L. J. & Vandenberg, G. R. Phorbol diester receptor copurifies with protein kinase C. *Proc. Natl. Acad. Sci. U.S.A.* **80**, 36–40 (1983).

176. Gaburjakova, J., Krejciova, E. & Gaburjakova, M. Multisite phosphorylation of the cardiac ryanodine receptor: a random or coordinated event? *Pflugers Arch - Eur J Physiol* **472**, 1793–1807 (2020).
177. Frame, S. & Cohen, P. GSK3 takes centre stage more than 20 years after its discovery. *Biochemical Journal* **359**, 1–16 (2001).
178. Cole, A. R. *et al.* GSK-3 Phosphorylation of the Alzheimer Epitope within Collapsin Response Mediator Proteins Regulates Axon Elongation in Primary Neurons. *Journal of Biological Chemistry* **279**, 50176–50180 (2004).
179. Matsuda, Y. *et al.* Comparison of fixation methods for preservation of morphology, RNAs, and proteins from paraffin-embedded human cancer cell-implanted mouse models. *J Histochem Cytochem* **59**, 68–75 (2011).
180. Fraenkel-Conrat, H. & Olcott, H. S. The Reaction of Formaldehyde with Proteins. V. Cross-linking between Amino and Primary Amide or Guanidyl Groups. *J. Am. Chem. Soc.* **70**, 2673–2684 (1948).
181. Shi, S. R., Key, M. E. & Kalra, K. L. Antigen retrieval in formalin-fixed, paraffin-embedded tissues: an enhancement method for immunohistochemical staining based on microwave oven heating of tissue sections. *J Histochem Cytochem.* **39**, 741–748 (1991).
182. Krenacs, L., Krenacs, T., Stelkovich, E. & Raffeld, M. Heat-induced antigen retrieval for immunohistochemical reactions in routinely processed paraffin sections. *Methods Mol Biol* **588**, 103–119 (2010).
183. Hobro, A. J. & Smith, N. I. An evaluation of fixation methods: Spatial and compositional cellular changes observed by Raman imaging. *Vibrational Spectroscopy* **91**, 31–45 (2017).
184. Levitt, D. & King, M. Methanol fixation permits flow cytometric analysis of immunofluorescent stained intracellular antigens. *Journal of Immunological Methods* **96**, 233–237 (1987).
185. Hoetelmans, R. W. M. *et al.* Effects of Acetone, Methanol, or Paraformaldehyde on Cellular Structure, Visualized by Reflection Contrast Microscopy and Transmission and

- Scanning Electron Microscopy: *Applied Immunohistochemistry & Molecular Morphology* **9**, 346–351 (2001).
186. Pollice, A. A. *et al.* Sequential paraformaldehyde and methanol fixation for simultaneous flow cytometric analysis of DNA, cell surface proteins, and intracellular proteins. *Cytometry* **13**, 432–444 (1992).
  187. Kamiguchi, H. & Lemmon, V. Neural cell adhesion molecule L1: signaling pathways and growth cone motility. *J Neurosci Res* **49**, 1–8 (1997).
  188. Fuchs, J. & Eickholt, B. J. Precursor types predict the stability of neuronal branches. *Journal of Cell Science* **134**, jcs258983 (2021).
  189. Wellbourne-Wood, J. & Chatton, J.-Y. From Cultured Rodent Neurons to Human Brain Tissue: Model Systems for Pharmacological and Translational Neuroscience. *ACS Chem. Neurosci.* **9**, 1975–1985 (2018).
  190. Dailey, M. E. Optical Imaging of Neural Structure and Physiology: Confocal Fluorescence Microscopy in Live Brain Slices. in *Brain Mapping: The Methods* 49–76 (Elsevier, 2002). doi:10.1016/B978-012693019-1/50005-8.
  191. Roche, K. W., O'Brien, R. J., Mammen, A. L., Bernhardt, J. & Huganir, R. L. Characterization of Multiple Phosphorylation Sites on the AMPA Receptor GluR1 Subunit. *Neuron* **16**, 1179–1188 (1996).
  192. Fuchs, J. Studies on the function of PRG2/PLPPR3 in neuron morphogenesis. (2022) doi:10.17169/refubium-33236.
  193. Chung, D., Shum, A. & Caraveo, G. GAP-43 and BASP1 in Axon Regeneration: Implications for the Treatment of Neurodegenerative Diseases. *Front. Cell Dev. Biol.* **8**, 567537 (2020).
  194. Nirody, J. A., Budin, I. & Rangamani, P. ATP synthase: Evolution, energetics, and membrane interactions. *J Gen Physiol* **152**, e201912475 (2020).
  195. Fan, Y. *et al.* Histone H1 Depletion in Mammals Alters Global Chromatin Structure but Causes Specific Changes in Gene Regulation. *Cell* **123**, 1199–1212 (2005).

196. Caroni, P. NEW EMBO MEMBERS' REVIEW: Actin cytoskeleton regulation through modulation of PI(4,5)P2 rafts. *The EMBO Journal* **20**, 4332–4336 (2001).
197. Van Den Pol, A. N., Obrietan, K., Belousov, A. B., Yang, Y. & Heller, H. C. Early synaptogenesis in vitro: Role of axon target distance. *J. Comp. Neurol.* **399**, 541–560 (1998).
198. Ménard, C. *et al.* Glutamate presynaptic vesicular transporter and postsynaptic receptor levels correlate with spatial memory status in aging rat models. *Neurobiology of Aging* **36**, 1471–1482 (2015).
199. Du, X. *et al.* Research progress on the role of type I vesicular glutamate transporter (VGLUT1) in nervous system diseases. *Cell Biosci* **10**, 26 (2020).
200. Cousin, M. A. Synaptophysin-dependent synaptobrevin-2 trafficking at the presynapse- Mechanism and function. *J. Neurochem.* **159**, 78–89 (2021).
201. Bai, F. & Witzmann, F. A. Synaptosome proteomics. *Subcell Biochem* **43**, 77–98 (2007).
202. Wong, W. & Scott, J. D. AKAP signalling complexes: focal points in space and time. *Nat Rev Mol Cell Biol* **5**, 959–970 (2004).
203. Theurkauf, W. E. & Vallee, R. B. Molecular characterization of the cAMP-dependent protein kinase bound to microtubule-associated protein 2. *J Biol Chem* **257**, 3284–3290 (1982).
204. Zhong, H. *et al.* Subcellular Dynamics of Type II PKA in Neurons. *Neuron* **62**, 363–374 (2009).
205. Ilouz, R. *et al.* Isoform-specific subcellular localization and function of protein kinase A identified by mosaic imaging of mouse brain. *eLife* **6**, e17681 (2017).
206. Kennedy, E. J. & Scott, J. D. Selective disruption of the AKAP signaling complexes. *Methods Mol Biol* **1294**, 137–150 (2015).
207. Cheng, J. *et al.* Precise Somatotopic Thalamocortical Axon Guidance Depends on LPA-Mediated PRG-2/Radixin Signaling. *Neuron* **92**, 126–142 (2016).

208. Widmer, F. & Caroni, P. Identification, localization, and primary structure of CAP-23, a particle-bound cytosolic protein of early development. *Journal of Cell Biology* **111**, 3035–3047 (1990).
209. Maekawa, S., Maekawa, M., Hattori, S. & Nakamura, S. Purification and molecular cloning of a novel acidic calmodulin binding protein from rat brain. *J Biol Chem* **268**, 13703–13709 (1993).
210. Carpenter, B. *et al.* BASP1 Is a Transcriptional Cosuppressor for the Wilms' Tumor Suppressor Protein WT1. *Molecular and Cellular Biology* **24**, 537–549 (2004).
211. Uhlen, M. *et al.* A proposal for validation of antibodies. *Nat Methods* **13**, 823–827 (2016).
212. Fukui, K. *et al.* Proteomic study on neurite responses to oxidative stress: search for differentially expressed proteins in isolated neurites of N1E-115 cells. *J Clin Biochem Nutr* **64**, 36–44 (2019).
213. Zakharov, V. V. *et al.* Natural N-terminal fragments of brain abundant myristoylated protein BASP1. *Biochimica et Biophysica Acta (BBA) - General Subjects* **1622**, 14–19 (2003).
214. Frey, D., Laux, T., Xu, L., Schneider, C. & Caroni, P. Shared and unique roles of CAP23 and GAP43 in actin regulation, neurite outgrowth, and anatomical plasticity. *J Cell Biol* **149**, 1443–1454 (2000).
215. Korshunova, I. *et al.* Characterization of BASP1-mediated neurite outgrowth. *J. Neurosci. Res.* **86**, 2201–2213 (2008).
216. Park, K.-S., Mohapatra, D. P., Misonou, H. & Trimmer, J. S. Graded Regulation of the Kv2.1 Potassium Channel by Variable Phosphorylation. *Science* **313**, 976–979 (2006).
217. Voolstra, O., Beck, K., Oberegelsbacher, C., Pfannstiel, J. & Huber, A. Light-dependent phosphorylation of the drosophila transient receptor potential ion channel. *J Biol Chem* **285**, 14275–14284 (2010).
218. Voolstra, O., Bartels, J.-P., Oberegelsbacher, C., Pfannstiel, J. & Huber, A. Phosphorylation of the Drosophila transient receptor potential ion channel is regulated by

the phototransduction cascade and involves several protein kinases and phosphatases.

*PLoS One* **8**, e73787 (2013).

219. Barker, B. S. *et al.* Ion Channels. in *Conn's Translational Neuroscience* 11–43 (Elsevier, 2017). doi:10.1016/B978-0-12-802381-5.00002-6.
220. Cooper, G. M. Structure of the Plasma Membrane. *The Cell: A Molecular Approach*. 2nd edition (2000).
221. Nishi, H., Hashimoto, K. & Panchenko, A. R. Phosphorylation in protein-protein binding: effect on stability and function. *Structure* **19**, 1807–1815 (2011).
222. Kohansal-Nodehi, M., Chua, J. J., Urlaub, H., Jahn, R. & Czernik, D. Analysis of protein phosphorylation in nerve terminal reveals extensive changes in active zone proteins upon exocytosis. *eLife* **5**, e14530 (2016).
223. Laux, T. *et al.* Gap43, Marcks, and Cap23 Modulate Pi(4,5)p2 at Plasmalemmal Rafts, and Regulate Cell Cortex Actin Dynamics through a Common Mechanism. *Journal of Cell Biology* **149**, 1455–1472 (2000).
224. Wiederkehr, A., Staple, J. & Caroni, P. The Motility-Associated Proteins GAP-43, MARCKS, and CAP-23 Share Unique Targeting and Surface Activity-Inducing Properties. *Experimental Cell Research* **236**, 103–116 (1997).
225. Mosevitsky, M. I. Nerve Ending “Signal” Proteins GAP-43, MARCKS, and BASP1. in *International Review of Cytology* vol. 245 245–325 (Elsevier, 2005).
226. Forsova, O. S. & Zakharov, V. V. High-order oligomers of intrinsically disordered brain proteins BASP1 and GAP-43 preserve the structural disorder. *FEBS J* **283**, 1550–1569 (2016).
227. Hartwig, J. H. *et al.* MARCKS is an actin filament crosslinking protein regulated by protein kinase C and calcium–calmodulin. *Nature* **356**, 618–622 (1992).
228. Takasaki, A., Hayashi, N., Matsubara, M., Yamauchi, E. & Taniguchi, H. Identification of the Calmodulin-binding Domain of Neuron-specific Protein Kinase C Substrate Protein CAP-22/NAP-22. *Journal of Biological Chemistry* **274**, 11848–11853 (1999).

229. Maekawa, S., Kobayashi, Y., Morita, M. & Suzaki, T. Tight binding of NAP-22 with acidic membrane lipids. *Neuroscience Letters* **600**, 244–248 (2015).
230. Brudvig, J. J. & Weimer, J. M. X MARCKS the spot: myristoylated alanine-rich C kinase substrate in neuronal function and disease. *Front. Cell. Neurosci.* **9**, (2015).
231. Benowitz, L. I. & Routtenberg, A. GAP-43: an intrinsic determinant of neuronal development and plasticity. *Trends in Neurosciences* **20**, 84–91 (1997).
232. Caroni, P., Aigner, L. & Schneider, C. Intrinsic neuronal determinants locally regulate extrasynaptic and synaptic growth at the adult neuromuscular junction. *J Cell Biol* **136**, 679–692 (1997).
233. Iino, S., Kobayashi, S. & Maekawa, S. Immunohistochemical localization of a novel acidic calmodulin-binding protein, NAP-22, in the rat brain. *Neuroscience* **91**, 1435–1444 (1999).
234. Yamamoto, Y., Sokawa, Y. & Maekawa, S. Biochemical evidence for the presence of NAP-22, a novel acidic calmodulin binding protein, in the synaptic vesicles of rat brain. *Neuroscience Letters* **224**, 127–130 (1997).
235. Zhang, W. & Benson, D. L. Stages of Synapse Development Defined by Dependence on F-Actin. *J. Neurosci.* **21**, 5169–5181 (2001).
236. Nelson, J. C., Stavoe, A. K. H. & Colón-Ramos, D. A. The actin cytoskeleton in presynaptic assembly. *Cell Adh Migr* **7**, 379–387 (2013).
237. Chia, P. H., Chen, B., Li, P., Rosen, M. K. & Shen, K. Local F-actin network links synapse formation and axon branching. *Cell* **156**, 208–220 (2014).
238. Strittmatter, S. M., Vartanian, T. & Fishman, M. C. GAP-43 as a plasticity protein in neuronal form and repair. *J. Neurobiol.* **23**, 507–520 (1992).
239. Hens, J. J. H. *et al.* B-50/GAP-43 Binds to Actin Filaments Without Affecting Actin Polymerization and Filament Organization. *J Neurochem* **61**, 1530–1533 (1993).
240. Aderem, A. Signal transduction and the actin cytoskeleton: the roles of MARCKS and profilin. *Trends in Biochemical Sciences* **17**, 438–443 (1992).

241. Fehon, R. G., McClatchey, A. I. & Bretscher, A. Organizing the cell cortex: the role of ERM proteins. *Nat Rev Mol Cell Biol* **11**, 276–287 (2010).
242. Kim, H.-S., Bae, C.-D. & Park, J. Glutamate receptor-mediated phosphorylation of ezrin/radixin/moesin proteins is implicated in filopodial protrusion of primary cultured hippocampal neuronal cells: Glutamate-induced ERM phosphorylation in neuron. *Journal of Neurochemistry* no-no (2010) doi:10.1111/j.1471-4159.2010.06713.x.
243. Hyman, A. A., Weber, C. A. & Jülicher, F. Liquid-Liquid Phase Separation in Biology. *Annu. Rev. Cell Dev. Biol.* **30**, 39–58 (2014).
244. Milovanovic, D., Wu, Y., Bian, X. & De Camilli, P. A liquid phase of synapsin and lipid vesicles. *Science* **361**, 604–607 (2018).
245. Wu, X., Cai, Q., Feng, Z. & Zhang, M. Liquid-Liquid Phase Separation in Neuronal Development and Synaptic Signaling. *Developmental Cell* **55**, 18–29 (2020).
246. McDonald, N. A., Fetter, R. D. & Shen, K. Assembly of synaptic active zones requires phase separation of scaffold molecules. *Nature* **588**, 454–458 (2020).
247. Zeng, M. *et al.* Phase Transition in Postsynaptic Densities Underlies Formation of Synaptic Complexes and Synaptic Plasticity. *Cell* **166**, 1163-1175.e12 (2016).
248. Zeng, M. *et al.* Reconstituted Postsynaptic Density as a Molecular Platform for Understanding Synapse Formation and Plasticity. *Cell* **174**, 1172-1187.e16 (2018).
249. Chen, X., Wu, X., Wu, H. & Zhang, M. Phase separation at the synapse. *Nat Neurosci* **23**, 301–310 (2020).
250. Bai, G. & Zhang, M. Inhibitory postsynaptic density from the lens of phase separation. *Oxford Open Neuroscience* **1**, kvac003 (2022).
251. Graham, K. *et al.* Liquid-like VASP condensates drive actin polymerization and dynamic bundling. *Nat. Phys.* **19**, 574–585 (2023).
252. Povarova, O. I., Antifeeva, I. A., Fonin, A. V., Turoverov, K. K. & Kuznetsova, I. M. The Role of Liquid-Liquid Phase Separation in Actin Polymerization. *Int J Mol Sci* **24**, 3281 (2023).

253. Chen, X., Jia, B., Zhu, S. & Zhang, M. Phase separation-mediated actin bundling by the postsynaptic density condensates. *eLife* **12**, e84446 (2023).
254. Kwon, H.-B. & Sabatini, B. L. Glutamate induces de novo growth of functional spines in developing cortex. *Nature* **474**, 100–104 (2011).
255. Jiang, X., Sando, R. & Südhof, T. C. Multiple signaling pathways are essential for synapse formation induced by synaptic adhesion molecules. *Proc Natl Acad Sci U S A* **118**, e2000173118 (2021).
256. Liang, J. *et al.* Axonal CB1 Receptors Mediate Inhibitory Bouton Formation via cAMP Increase and PKA. *J. Neurosci.* **41**, 8279–8296 (2021).
257. Gomez-Castro, F. *et al.* Convergence of adenosine and GABA signaling for synapse stabilization during development. *Science* **374**, eabk2055 (2021).
258. Chevaleyre, V., Heifets, B. D., Kaeser, P. S., Südhof, T. C. & Castillo, P. E. Endocannabinoid-Mediated Long-Term Plasticity Requires cAMP/PKA Signaling and RIM1 $\alpha$ . *Neuron* **54**, 801–812 (2007).
259. Park, P. *et al.* PKA drives an increase in AMPA receptor unitary conductance during LTP in the hippocampus. *Nat Commun* **12**, 413 (2021).
260. Trudeau, L.-E., Emery, D. G. & Haydon, P. G. Direct Modulation of the Secretory Machinery Underlies PKA-Dependent Synaptic Facilitation in Hippocampal Neurons. *Neuron* **17**, 789–797 (1996).
261. Park, A. J. *et al.* A presynaptic role for PKA in synaptic tagging and memory. *Neurobiol Learn Mem* **114**, 101–112 (2014).
262. Cho, R. W. *et al.* Phosphorylation of Complexin by PKA Regulates Activity-Dependent Spontaneous Neurotransmitter Release and Structural Synaptic Plasticity. *Neuron* **88**, 749–761 (2015).
263. Sando, R. & Südhof, T. C. Latrophilin GPCR signaling mediates synapse formation. *eLife* **10**, e65717 (2021).
264. Torres-Quesada, O., Mayrhofer, J. E. & Stefan, E. The many faces of compartmentalized PKA signalosomes. *Cellular Signalling* **37**, 1–11 (2017).

265. Tao, J. & Malbon, C. C. G-protein-coupled receptor-associated A-kinase anchoring proteins AKAP5 and AKAP12: differential signaling to MAPK and GPCR recycling. *JMS* **3**, 19 (2008).
266. Bachmann, V. A. *et al.* Gpr161 anchoring of PKA consolidates GPCR and cAMP signaling. *Proc. Natl. Acad. Sci. U.S.A.* **113**, 7786–7791 (2016).
267. Hochbaum, D., Barila, G., Ribeiro-Neto, F. & Altschuler, D. L. Radixin assembles cAMP effectors Epac and PKA into a functional cAMP compartment: role in cAMP-dependent cell proliferation. *J Biol Chem* **286**, 859–866 (2011).
268. Ponuwei, G. A. A glimpse of the ERM proteins. *J Biomed Sci* **23**, 35 (2016).
269. Deming, P. B. *et al.* Anchoring of Protein Kinase A by ERM (Ezrin-Radixin-Moesin) Proteins Is Required for Proper Netrin Signaling through DCC (Deleted in Colorectal Cancer). *Journal of Biological Chemistry* **290**, 5783–5796 (2015).
270. Sassone-Corsi, P. The cyclic AMP pathway. *Cold Spring Harb Perspect Biol* **4**, a011148 (2012).
271. Cunha, R. A. How does adenosine control neuronal dysfunction and neurodegeneration? *J. Neurochem.* **139**, 1019–1055 (2016).
272. Rebola, N. *et al.* Adenosine A1 and A2A receptors are co-expressed in pyramidal neurons and co-localized in glutamatergic nerve terminals of the rat hippocampus. *Neuroscience* **133**, 79–83 (2005).
273. Hoyer, D. Serotonin receptors nomenclature. in *The Serotonin System* 63–93 (Elsevier, 2019). doi:10.1016/B978-0-12-813323-1.00004-9.
274. Howlett, A. C. & Abood, M. E. CB1 and CB2 Receptor Pharmacology. *Adv Pharmacol* **80**, 169–206 (2017).
275. Langer, I., Jeandriens, J., Couvineau, A., Sanmukh, S. & Latek, D. Signal Transduction by VIP and PACAP Receptors. *Biomedicines* **10**, 406 (2022).
276. Surmeier, D. J., Ding, J., Day, M., Wang, Z. & Shen, W. D1 and D2 dopamine-receptor modulation of striatal glutamatergic signaling in striatal medium spiny neurons. *Trends in Neurosciences* **30**, 228–235 (2007).

277. Mishra, A., Singh, S. & Shukla, S. Physiological and Functional Basis of Dopamine Receptors and Their Role in Neurogenesis: Possible Implication for Parkinson's disease. *J Exp Neurosci* **12**, 1179069518779829 (2018).
278. Martel, J. C. & Gatti McArthur, S. Dopamine Receptor Subtypes, Physiology and Pharmacology: New Ligands and Concepts in Schizophrenia. *Front Pharmacol* **11**, 1003 (2020).
279. Borroto-Escuela, D. O. *et al.* Serotonin Heteroreceptor Complexes and Their Integration of Signals in Neurons and Astroglia—Relevance for Mental Diseases. *Cells* **10**, 1902 (2021).
280. Fernandez-Duenas, V., Ferré, S. & Ciruela, F. Adenosine A2A-dopamine D2 receptor heteromers operate striatal function: impact on Parkinson's disease pharmacotherapeutics. *Neural Regen Res* **13**, 241–243 (2018).
281. So, S. S., Ngo, T., Keov, P., Smith, N. J. & Kufareva, I. Tackling the complexities of orphan GPCR ligand discovery with rationally assisted approaches. in *GPCRs* 295–334 (Elsevier, 2020). doi:10.1016/B978-0-12-816228-6.00016-7.
282. Trimbuch, T. *et al.* Synaptic PRG-1 Modulates Excitatory Transmission via Lipid Phosphate-Mediated Signaling. *Cell* **138**, 1222–1235 (2009).
283. Wang, D. *et al.* PRG5 Knockout Precipitates Late-Onset Hypersusceptibility to Pilocarpine-Induced Juvenile Seizures by Exacerbating Hippocampal Zinc Signaling-Mediated Mitochondrial Damage. *Frontiers in Neuroscience* **15**, (2021).
284. Sokolina, K. *et al.* Systematic protein-protein interaction mapping for clinically relevant human GPCRs. *Mol Syst Biol* **13**, 918 (2017).
285. Ostroumova, O. S., Schagina, L. V., Mosevitsky, M. I. & Zakharov, V. V. Ion channel activity of brain abundant protein BASP1 in planar lipid bilayers: Ion channel activity of BASP1. *FEBS Journal* **278**, 461–469 (2011).
286. Rutkowska-Wlodarczyk, I. *et al.* A Proteomic Analysis Reveals the Interaction of GluK1 Ionotropic Kainate Receptor Subunits with Go Proteins. *J. Neurosci.* **35**, 5171–5179 (2015).

287. Lerma, J. Roles and rules of kainate receptors in synaptic transmission. *Nat Rev Neurosci* **4**, 481–495 (2003).
288. Negrete-Díaz, J. V., Sihra, T. S., Flores, G. & Rodríguez-Moreno, A. Non-canonical Mechanisms of Presynaptic Kainate Receptors Controlling Glutamate Release. *Front. Mol. Neurosci.* **11**, 128 (2018).
289. Takaichi, R. *et al.* Inhibitory effect of NAP-22 on the phosphatase activity of synaptojanin-1. *J. Neurosci. Res.* **90**, 21–27 (2012).
290. Ueno, S., Miyoshi, H., Maruyama, Y., Morita, M. & Maekawa, S. Interaction of dynamin I with NAP-22, a neuronal protein enriched in the presynaptic region. *Neuroscience Letters* **675**, 59–63 (2018).
291. Choudhry, H., Aggarwal, M. & Pan, P.-Y. Mini-review: Synaptojanin 1 and its implications in membrane trafficking. *Neurosci Lett* **765**, 136288 (2021).
292. Arriagada-Díaz, J., Prado-Vega, L., Cárdenas, A. M., Ardiles, A. O. & Gonzalez-Jamett, A. M. Dynamin Superfamily at Pre- and Postsynapses: Master Regulators of Synaptic Transmission and Plasticity in Health and Disease. *Neuroscientist* **28**, 41–58 (2022).
293. Trotman, L. C. *et al.* Pten Dose Dictates Cancer Progression in the Prostate. *PLoS Biol* **1**, e59 (2003).
294. Graham, F. L. & Van Der Eb, A. J. A new technique for the assay of infectivity of human adenovirus 5 DNA. *Virology* **52**, 456–467 (1973).
295. Jiang, W. & Hunter, T. Analysis of cell-cycle profiles in transfected cells using a membrane-targeted GFP. *Biotechniques* **24**, 349–350, 352, 354 (1998).
296. Sampathkumar, C. *et al.* Loss of MeCP2 disrupts cell autonomous and autocrine BDNF signaling in mouse glutamatergic neurons. *eLife* **5**, e19374 (2016).
297. Tyanova, S., Mann, M. & Cox, J. MaxQuant for In-Depth Analysis of Large SILAC Datasets. in *Stable Isotope Labeling by Amino Acids in Cell Culture (SILAC)* (ed. Warscheid, B.) vol. 1188 351–364 (Springer New York, 2014).
298. Tyanova, S. *et al.* The Perseus computational platform for comprehensive analysis of (prote)omics data. *Nat Methods* **13**, 731–740 (2016).

299. Meijering, E. *et al.* Design and validation of a tool for neurite tracing and analysis in fluorescence microscopy images. *Cytometry* **58A**, 167–176 (2004).

## 10. List of publications

---

### Publications related to this thesis:

Fuchs, J., Bareesel, S., **Kroon, C.**, Polyzou, A., Eickholt, B. J., & Leondaritis, G. (2022). Plasma membrane phospholipid phosphatase-related proteins as pleiotropic regulators of neuron growth and excitability. *Frontiers in Molecular Neuroscience*.

Brosig, A., Fuchs, J., Ipek, F., **Kroon, C.**, Schrötter, S., Vadhvani, M., ... & Eickholt, B. J. (2019). The axonal membrane protein PRG2 inhibits PTEN and directs growth to branches. *Cell reports*, 29(7), 2028-2040.

**Kroon et al.** (2023) in preparation

### Other contributions during the course of this PhD:

**Kroon, C.**, Breuer, L., Jones, L., An, J., Akan, A., Mohamed Ali, E. A., ... & Weissgerber, T. L. (2022). Blind spots on western blots: Assessment of common problems in western blot figures and methods reporting with recommendations to improve them. *PLoS biology*, 20(9), e3001783.

Kreis, P., Gallrein, C., Rojas-Puente, E., Mack, T. G., **Kroon, C.**, Dinkel, V., ... & Eickholt, B. J. (2019). ATM phosphorylation of the actin-binding protein drebrin controls oxidation stress-resistance in mammalian neurons and *C. elegans*. *Nature communications*, 10(1), 486.